Temperature responses of microbial soil organic matter decomposition and associated respiration at various scales, ranging from exo-enzymes to populations and communities

By

Kyungjin Min

Submitted to the graduate degree program in Ecology and Evolutionary Biology and the Graduate Faculty of the University of Kansas in partial fulfillment of the requirements for the degree of Doctor of Philosophy.

Chair: Sharon Billings

Ford Ballantyne IV

Bryan Foster

Townsend Peterson

David Fowle

Date Defended: 29 March 2017

The dissertation committee for Kyungjin Min certifies that this is the approved version of the following dissertation:

Temperature responses of microbial soil organic matter decomposition and associated respiration at various scales, ranging from exo-enzymes to populations and communities

Chairperson: Sharon Billings

Date Approved: 29 March 2017

ABSTRACT

Knowledge about how temperature will influence microbial decomposition of soil organic matter and resultant CO_2 efflux from soils is of importance to understand the global C balance and more accurately project future climate. Yet, it is difficult to quantify microbial activities in their natural habitats due to inherent heterogeneity in soils. Here I investigate microbial activities in controlled experiments ranging in complexity, such that I can parse the temperature responses of multiple processes operating simultaneously in soils. Soil microbes exude exo-enzymes into the soil matrix, where they break down organic molecules into smaller substrates. Microbes assimilate these smaller substrates to grow, while respiring CO_2. In chapter 1, I demonstrate that pH can differentially influence temperature responses of distinct exo-enzyme activities relevant to C and N acquisition from soil organic matter. Expanding this, in chapter 2 I find that temperature and substrate availability can interactively influence biomass-specific respiration rates, C use efficiency (CUE), and stable isotope C discrimination from an isolated population of microbes. Enhancing the complexity again, in chapter 3 I show that temperature responses of exo-enzyme activities and respiration of natural microbial communities in soils are conserved at biomass-specific rates across diverse timescales and in spite of distinct community structures, while those at soil mass-specific rates are not. This body of work has ecological implications about microbial adaptation in a warmer world. Different temperature responses of exo-enzymes and CUE with varying environmental conditions can lead to microbial communities with distinct strategies of resource allocation to production of exo-enzymes and biomass for survival and reproduction. These inferences about microbial adaptation obtained from simplified systems can help understand driving mechanisms of apparent temperature responses and guide

parameterizations in microbially-explicit Earth-system models to better project microbial feedbacks to climate.

ACKNOWLEDGEMENTS

I dedicate this dissertation to my family and my boyfriend Joon-Young Moon. My mom, dad, brother, grandpa, and boyfriend have encouraged my study with warm heart. I always wanted to tell them good news, which turned out to be difficult. Whenever I feel my world is shaking, it was their love and support that ironed my view of life. So, thank you mom, dad, brother, grandpa, and Joon-Young for being there.

I did not fully realize that my life in Kansas would be the beginning of another chapter when I was first skyping with Sharon Billings and Ford Ballantyne. I chose to study because I was good at getting good scores. After advised by Sharon and Ford, I learned how fun it is to study. Indeed, I am in the era of the joy of being scholars. So, thank you my awesome advisors.

Most of the time, my lab mate was Christoph Lehmeier. Our interaction was sometimes rainy, cloudy, cold, but more often breezy and shiny. Before knowing him, I was always curious why all the good cars are German products. Now I do not ask why. Thank you Christoph for being a distinguished colleague.

I was also lucky to work with Kate Buckeridge. While she was here, we did not have a good relationship with instruments. Yet, with two heads, mostly only with her head, we made progress and continued science together. So thank you Kate for showing your kindness to me and instruments.

Emma Hauser is my new lab mate and she is using the cubicle Kate used before. While she was visiting Lawrence during new graduate student recruitment event, she stayed in my house. For two nights, my cat Poohy chose her over me. I trust my cat's decision and see everday how nice she is. Thank you Emma for joining our lab.

I met lots of amazing people, while working at KU. I still remember interacting with Yanjun Chen, Mitch Sellers, Samantha Elledge , Carl Heroneme, and Keelan Barger. Thank you all for your time and efforts to assist my work. People working at KBS are the most warmest, which changed my biased view about mid-west. Last, but not least, I appreciate my committee members Bryan Foster, Townsend Peterson, and David Fowle to guide me to the right direction.

TABLES OF CONTENTS

GENERAL INTRODUCTION

Soil microorganisms, although invisible to the naked eye, play a major role in controlling C cycling on Earth. They release exo-enzymes into the soil matrix to break down soil organic matter for assimilable nutrients, while respiring CO_2 into the atmosphere (Sinsabaugh et al. 1991). Because microbial respiration represents up to 90% of total soil CO_2 losses (Subke et al. 2006), they provide a positive feedback to anthropogenic increases in atmospheric CO_2 concentration and associated increasing temperature. Yet, it is uncertain how increasing temperature will influence microbial soil organic matter breakdown and subsequent CO_2 emission in a warmer world. Thus, it is essential to assess the effects of temperature on soil microorganisms for advancing our understanding of microbial roles with changing climate.

Temperature typically increases microbial process rates of soil organic matter decomposition and respiration over a timescale of hours-to-days (Arrhenius 1889). Yet, the positive relationship between temperature and microbial activities does not always hold valid in different environmental conditions. This is because confounding factors such as water and substrate availability that differ across soil type and depth typically co-vary with increasing temperature over time, making it difficult to use data derived from environmental samples to predict microbial temperature responses. These include environmental factors, such as changing soil moisture, substrate availability, and protection of soil organic matter (Knorr et al. 2005; Hartley et al. 2007; Bradford et al. 2008). In addition to these confounding factors, microorganisms can also modify their community structure and function in response to temperature, such that they can survive in new conditions. These shifts in structure and function are broadly defined as

microbial adaptation (Billings and Ballantyne 2013). Often, however, it is extremely difficult to parse microbially-driven changes in soil organic matter decomposition from abiotically-driven dynamics with warming in soils, preventing us from understanding microbial CO_2 losses in a warmer world.

Accordingly, in this dissertation I explore how temperature will modify microbial soil organic matter decomposition and associated CO_2 respiration, while minimizing the effects of confounding factors. I did this by expanding experimental scales and complexity step by step, such that I could parse out driving biological mechanisms for changing CO_2 respiration with warming. In the three chapters, I address the following goals:

(1) quantify temperature responses of purified microbial exo-enzyme activities at different pH, without microorganisms involved (chapter 1);

(2) assess how temperature and C availability influence microbial respiration, C use efficiency, and stable isotope C discrimination of an isolated microbial population in continuous culture system (chapter 2);

(3) evaluate how temperature responses of microbial function (exo-enzyme activities and respiration) and community structure vary across time in boreal forest soils (chapter 3).

Literature cited

1. Arrhenius, S. (1889). Über die Reaktionsgeschwindigkeit bei der Inversion von Rohrzucker durch S€ aurenle. *Zeitschrift fur Phys. Chemique* 4, 226–248.

2. Billings, S. A., and Ballantyne, F. (2013). How interactions between microbial resource

demands, soil organic matter stoichiometry, and substrate reactivity determine the direction and magnitude of soil respiratory responses to warming. *Glob. Chang. Biol.* 19, 90–102.

3. Bradford, M. A., Davies, C. A., Frey, S. D., Maddox, T. R., Melillo, J. M., Mohan, J. E., et al. (2008). Thermal adaptation of soil microbial respiration to elevated temperature. *Ecol. Lett.* 11, 1316–1327. doi:10.1111/j.1461-0248.2008.01251.x.

4. Hartley, I. P., Heinemeyer, A., and Ineson, P. (2007). Effects of three years of soil warming and shading on the rate of soil respiration : substrate availability and not thermal acclimation mediates observed response. *Glob. Chang. Biol.* 13, 1761–1770. doi:10.1111/j.1365-2486.2007.01373.x.

5. Knorr, W., Prentice, I. C., House, J. I., and Holland, E. A. (2005). Long-term sensitivity of soil carbon turnover to warming. *Nature* 433, 298–301.

6. Sinsabaugh, R. L., Antibus, R. K., and Linkins, A. E. (1991). An enzymic approach to the analysis of microbial activity during plant litter decomposition. *Agric. Ecosyst. Environ.* 34, 43–54. doi:http://dx.doi.org/10.1016/0167-8809(91)90092-C.

7. Subke, J., Inglima, I., and Francesca Cotrufo, M. (2006). Trends and methodological impacts in soil CO2 efflux partitioning: a metaanalytical review. *Glob. Chang. Biol.* 12, 921–943.

CHAPTER 1: Differential effects of pH on temperature sensitivity of organic carbon and nitrogen decay

ABSTRACT

Soil microorganisms release extracellular enzymes into the soil matrix to access carbon (C) and nitrogen (N) from soil organic matter (SOM). Temperature and pH are major factors governing the rates at which these enzymes decay SOM, hence influencing the availability of C and N for microbial assimilation. As temperature increases, the rate of decomposition is also expected to increase. Recent advances provide estimates of intrinsic temperature sensitivities of key decay reactions at one, circum-neutral pH, but how temperature sensitivity of enzymatic SOM degradation is influenced by pH remains unclear. Here we expand on recent work by determining specific activities of C-acquiring (β-glucosidase; BGase) and C- and N-acquiring (*N*-Acetyl-Glucosaminidase; NAGase) enzymes with purified, fluorescently labeled organic substrate at temperatures from 5 to 25°C (5°C steps) and at pH values from 3.5 to 8.5 (1 pH unit steps). Using specific activity data, we quantified temperature sensitivities of the reactions with estimates of activation energy (E_a) at each pH value. We then used E_a estimates to compute temperature-induced changes in the C:N flow ratio, which is defined as the ratio of enzymatic liberation rates of C to N from the substrates. Across all temperatures, BGase activity was generally high in the pH range of 5.5 to 8.5, while NAGase exhibited a relatively narrow

optimum between pH 5.5-6.5. Temperature sensitivity of BGase differed significantly among pH values; the strongest temperature responses were observed at pH 4.5. NAGase, in contrast, did not exhibit any significant pH-dependent changes in temperature sensitivity. The temperature increase from 5 to 25°C induced changes in the C:N flow ratio, with direction and magnitude strongly dependent on the pH. We observed a large, temperature-induced increase in C:N flow ratio at pH 4.5 and decreases in C:N flow ratio at pH >5.5 that were most pronounced at pH 7.5. Our data show that pH can induce differential effects on reaction rates and temperature sensitivity of organic C and N liberation, with consequences for changes in the relative availabilities of C and N for microbial assimilation.

INTRODUCTION

The mean surface temperature of the Earth is projected to increase by 0.3 to 4.8°C during the 21th century, primarily due to the increasing CO_2 concentration in the atmosphere (IPCC 2013). Soil respiration (total CO_2 efflux from soil surface) represents as much as half the total biogenic CO_2 production (Schimel 1995; Trumbore 2006), much of which is produced by the activity of heterotrophic microorganisms (Högberg et al. 2001). Rates of heterotrophic soil respiration often increase with temperature (MacDonald et al. 1995; Mikan et al. 2002; Fierer et al. 2006; Zhou et al. 2009), generating a positive feedback to increasing concentrations of atmospheric CO_2. However, variable, unexplained responses of heterotrophic soil respiration to temperature have been observed across ecosystems (Zhou et al. 2009; Suseela et al. 2012), highlighting our limited understanding of the drivers of this flux. Thus, a more detailed knowledge of the

mechanisms governing the response of heterotrophic soil respiration to temperature is indispensable for predicting the Earth's future atmospheric CO_2 concentrations.

Decomposition of SOM is a necessary precursor for sustaining heterotrophic soil respiration. Soil microorganisms exude enzymes into the soil matrix (extracellular enzymes) to cleave macromolecular compounds into smaller, assimilable resources. The effects of temperature on the rates of those enzymatic reactions, and ultimately heterotrophic soil CO_2 efflux, can be modeled using the biochemical and thermodynamic foundation established by van't Hoff and Arrhenius (van't Hoff 1884; Arrhenius 1889; Knorr et al. 2005; Davidson and Janssens 2006).

$$K = A \cdot e^{\frac{-E_a}{RT}} \quad (1)$$

The model describes how reaction rates (K) vary as a function of temperature (T, in Kelvin) and is parameterized by the activation energy (E_a) required for the reaction to proceed, a pre-exponential factor (A) which represents the likelihood that molecules collide in the proper orientation, and R, the ideal gas constant.

When the reaction proceeds in unconstrained conditions, unlimited by substrate, E_a reflects the intrinsic temperature sensitivity of the reaction. Relative increases in reaction rates with temperature are higher for reactions with higher E_a than for reactions with lower E_a. However, myriad environmental factors, including chemical (e.g., redox potential), physical (e.g., adsorption/desorption of extracellular enzymes and substrates on soil particles, diffusion of extracellular enzymes), and microbial (e.g., biomass, extracellular enzyme production) variables, can induce deviations from the underlying van't Hoff-Arrhenius temperature sensitivity of enzymatic decay in soils (Davidson et al. 2006; Conant et al. 2011). To quantitatively determine

the influence of such factors on SOM decay, we must first measure intrinsic temperature sensitivities (*sensu* van't Hoff-Arrhenius) for distinct enzyme-substrate pairings as reference values.

An important edaphic variable that influences SOM decomposition dynamics is the pH of the soil solution. Soil pH governs the ionization of functional groups of organic molecules, the conformation of substrates and enzymes, the degree to which extracellular enzymes adsorb to soil particles, and the solubility of co-factors essential for the enzymatic reactions (Tipton et al. 1979; Frankenberger and Johanson 1982; Tabatabai 1994; Brady and Weil 2007). Significant temporal and spatial variation in pH observed in the field (Zoltan 2008) is linked to variations in extracellular enzyme activities in diverse ecosystems (Sinsabaugh et al. 2008). Numerous studies have explored the influence of pH on extracellular enzyme kinetics, but the pH effect is often determined at a single temperature, and temperature sensitivities typically are quantified at a single pH (Deng and Tabatabai 1994; Parham and Deng 2000; Turner 2010; Lehmeier et al. 2013). As a result, it is unclear how pH influences extracellular enzyme activities across a range of temperatures.

Changes in enzymatic activities in response to temperature and pH may alter microbial resource availability and associated microbial feedbacks. Simulating the concurrent extracellular enzymatic degradation of cellulose (no N) and chitin (C:N of 8), Lehmeier et al. (2013) demonstrated that changes in temperature can affect relative rates of C and N liberation (termed the C:N flow ratio, Billings and Ballantyne 2013) solely through the different temperature sensitivities of cellulose- and chitin-cleaving reactions. Because soil microorganisms experience

stoichiometric constraints (Sterner and Elser 2002; Cleveland and Liptzin 2007), changing relative availability of C and N may directly affect microbial growth and respiration (Frey et al. 2004; Treseder 2008; Min et al. 2011). Shifting relative availability of C and N may prompt microbes to adjust relative production and exudation rates of C- and N-acquiring extracellular enzymes to balance the bioavailability of C and N (Billings and Ballantyne 2013). Given the roles of pH and temperature as fundamental determinants of reaction rates, quantifying any interactive effects of pH and temperature on extracellular enzyme activities is critical for predicting microbial feedbacks to soil respiration across diverse ecosystems.

Here, we quantify the temperature sensitivity of enzyme-catalyzed reactions using purified enzymes and organic substrates analogous to cellulose and chitin across an ecologically relevant pH range, from 3.5 to 8.5. We performed the experiments at five distinct temperatures, from 5 to 25°C with 5°C steps, and determined the temperature sensitivity of the reactions over this temperature range. We then used estimates of temperature sensitivity to assess how pH may likely influence the relative rates of C and N liberation from cellulose and chitin decay as temperature changes. We chose analog substrates for cellulose and chitin because they are two of the most abundant and globally ubiquitous substrates in soils and serve as important resources of C (cellulose) and N and C (chitin) for microbes. Our approach enables us to determine enzyme activity per unit enzyme mass with sufficient single substrate, thereby elucidating intrinsic, temperature-dependent changes in decay rates at a fundamental, biochemical level, unfettered by other confounding factors present in soils.

MATERIALS AND METHODS

Measuring reaction rates using purified extracellular enzymes and MUB-labeled substrates

We measured the specific activity of two pairs of extracellular enzymes and corresponding substrates in buffer solution at temperatures ranging from 5 to 25°C (5°C steps) and pH values from 3.5 to 8.5 (1 pH unit steps): BGase (EC 3.2.1.21; Megazyme, Ireland) with 4-Methylumbelliferyl □-D-cellobioside (MUB-BG; Sigma-aldrich, USA) and NAGase (EC 3.2.1.52; New England Biolabs, USA) with 4-Methylumbelliferyl *N*-Acetyl-Glucosaminide (MUB-NAG; Sigma-aldrich, USA). When a MUB label is cleaved from a substrate by the activity of the specific enzyme, it emits a fluorescence signal upon excitation by light (Mead et al. 1955). Aliquots of crystalline MUB-BG (273 μM), MUB-NAG (400 μM), and a MUB standard (10 μM; Sigma-Aldrich, USA) were dissolved in deionized water. Extracellular enzymes were dissolved in 0.2M of sodium acetate buffer adjusted to pH 3.5, 4.5, 5.5, 6.5, 7.5 or 8.5. The reported pH, therefore, refers to the buffer pH instead of the pH of the final reaction solution; the pH of the final reaction solution is, however, close to the pH of the buffer, given that more than 80% of the solution volume in each well was buffer and that the buffer itself inherently minimizes changes in solution pH. The amount of BGase and NAGase in one individual well of a 96-well plate were 0.024 and 0.16 units, respectively.

To perform each enzyme activity assay, we pipetted 50 μl of dissolved substrates and 200 μl of enzyme solutions into 16 wells of 96-well black microplates (Costar®, USA). In each microplate, designated wells were filled with 250 μl of three different controls (enzyme, quench, and substrate control) as well as MUB standard (Table 1). After pipetting, we transferred each

plate to a Synergy™ HT microplate reader (BioTek Instruments, Inc., USA) and recorded the evolution of fluorescence every minute for the BGase/MUB-BG (Fig. 1a). Because NAGase/MUB-NAG reactions generally proceed more slowly than BGase/MUB-BG reactions, MUB fluorescence generation by NAGase was recorded every two minutes instead of every minute. Fluorescence was measured for sufficient duration to quantify the initial linear increase in total fluorescence (i.e. the accumulation of MUB upon enzymatic cleavage), which then served to calculate specific enzyme activity rates.

Fluorescence of MUB-labeled substrate (substrate control) as well as of MUB standard can be influenced by solution age (the time since dissolving MUB-labeled substrate or MUB standard in deionized water) and by the buffer pH in the reaction solution (Niemi and Vepsäläinen 2005; DeForest 2009). To account for this, we generated fresh substrate control for every experiment, mixed the control with buffer at the same pH value as buffer used in the respective enzyme/substrate reactions, and determined the fluorescence exhibited by these solutions. Measuring the fluorescence of substrate control permitted us to correct enzymatic reactions for any fluorescence generated by phenomena other than the enzyme-specific MUB release (Table 1). After correcting reaction fluorescence with control values, the measurements of the fresh MUB standard were used to calibrate fluorescence of reactions to obtain the molar amounts of MUB-labeled substrate cleaved by the enzymes per unit time (DeForest 2009).

Controlling reaction temperatures

Because the microplate reader cannot reduce the plate temperature below ambient temperature, we performed measurements at 20°C and below differently from those at 25°C. For assays at

25°C, one plate at each pH was placed in the microplate reader. Using a default kinetic measurement mode, we recorded the accumulated fluorescence until we observed no more increase in fluorescence with time (Fig. 1a). For BGase/MUB-BG, the reaction temperature was 25°C during the assay. The actual reaction temperature for the NAGase/MUB-NAG reaction was 26°C.

For lower temperatures (5, 10, 15, and 20°C), we modified protocols from Lehmeier et al. (2013). First, all the solutions, microplates, and pipettes were kept in an incubator (VWR low temperature incubator, USA) at the desired temperature. We pipetted the solutions in the designated wells of two identical microplates (see section 2.1; Table 1), put one in the incubator, measured the fluorescence of the other plate immediately, and put this plate back into the incubator. This measurement represents t0 (Fig. 1b). For BGase/MUB-BG reactions, one minute after the solutions had been pipetted into the two microplates, the second incubating plate was measured (t1) and returned to the incubator. We continued alternating two plates to ensure that no reaction temperature was higher than that intended due to excessive time outside of the incubator. Thus, plate 1 was measured at t0, t4, t8, and t12 (i.e., 0, 4, 8, and 12 min after the solutions were pipetted into the plate), and plate 2 at t1, t5, t9 and t13. After the measurements of the first two plates, the solutions were pipetted into the other two plates and they were measured in the same, alternating way, with plate 3 measured at t2, t6, t10 and t14 and plate 4 at t3, t7, t11 and t15. For NAGase/MUB-NAG reactions, we followed a similar protocol except we conducted the measurements at two-minute intervals, as this was better suited for documenting the initial linear phase of fluorescence evolution with time for this reaction. Thus, for each BGase/MUB-BG and NAGase/MUB-NAG reaction, four microplates were used to generate one

time course at temperatures of 10, 15, and 20°C at each pH, and were treated as one replicate (Fig. 1b). For the reactions at 5°C, we expanded this method and used eight microplates, instead of four, each measured only two times. High R^2 of the initial linear phase of fluorescence accumulation across all the individual plates for one replicate time course demonstrates the suitability of this protocol.

Calculating specific enzyme activities

All enzyme assays across the whole range of pH and temperature presented in this study were performed with the same concentrations of substrates in the reaction wells: 273 µM MUB-BG and 400 µM MUB-NAG (Table 1). Preliminary experiments conducted at pH 6.5 and 25°C for MUB-BG and pH 5.5 and 26°C for MUB-NAG demonstrated that these concentrations were sufficient to saturate enzymes in these conditions (data not shown). We assumed that saturation concentrations are not higher at lower temperatures (Somero 2004; Wallenstein et al. 2010), an assumption supported by the enzyme activity data (Fig. 2).

Our calculations of enzymatic reaction rates follow DeForest (2009), but because we knew the amount of enzyme present in one well, we were able to obtain specific enzyme activity per unit enzyme mass. We equate specific enzyme activities for BGase and NAGase with intrinsic specific enzyme activities at any given temperature and pH, given the absence of confounding factors often present in soil matrices such as substrate limitation or protection from decay (Davidson et al. 2006; Conant et al. 2011).

Statistical analysis and estimating intrinsic temperature sensitivities of reactions

After log-transformation of specific enzyme activities to meet the assumptions of normality and equal variance, we determined the effects of temperature and pH on ln (specific enzyme activity) for each enzyme using two-way ANOVA. For each enzyme, we first fit a full model that included the interaction between temperature and pH, and then we used the Akaike Information Criterion (AIC) to select the most parsimonious model, which guided our comparisons of specific activity across pH and temperature. We employed Bonferroni-corrected *p*-values to conduct post-hoc, multiple comparisons of specific enzyme activities.

To assess the influence of pH on the relative temperature sensitivity of enzymatic reactions, i.e. E_a, we fit linear models with Arrhenius transformed specific activity (ln (specific enzyme activity)*R , see eq. 1) as the response, pH and enzyme type as categorical predictors, and 1/T (in Kelvin) as a covariate. Using the Arrhenius transformation as the response is standard practice when estimating E_a because slope estimates are identical to estimates of E_a. As for the analysis of specific enzyme activities, we first fit a full model and subsequently performed model selection using AIC to arrive at a reduced model, but our main interest was a direct comparison of E_a estimates across pH and enzyme type. Because we had *priori* knowledge of specific tests of ecological interest - that E_a values differ across pH for each enzyme and that E_a values differ between enzymes at each pH value -, we used pre-specified linear contrasts (Christensen, 1996). We tested for pairwise differences between slopes (E_a) for each enzyme separately (each pH value generated a different slope estimate for each enzyme) and test for slope (E_a) differences between BGase and NAGase at each pH. These comparisons were made using single-step

adjusted *p*-values to adjust for experiment-wide Type I error. All statistical analyses were performed using R v. 2.12.2 (R Core Team 2013) and SPSS (IBM SPSS Statistics ver.20), and results were considered significant when $p<0.05$.

Computing the C:N flow ratio of liberated resources

For the substrates used in this study, the C:N flow ratio (Billings and Ballantyne 2013) describes the relative release rates of C and N atoms upon enzymatic cleavage of the MUB-labeled substrates. As MUB-BG and MUB-NAG serve as proxies for cellulose (polymer of glucose) and chitin (polymer of NAG), respectively, the BGase-catalyzed liberation of one MUB molecule from MUB-BG is comparable to the release of one glucose molecule from cellulose (Sinsabaugh et al. 2008; German et al. 2012). Analogously, the NAGase-catalyzed MUB liberation from MUB-NAG is comparable to the release of one NAG molecule from chitin (Sinsabaugh et al. 2008; DeForest 2009; German et al. 2012). Because the same MUB fluorophore is liberated from both substrates, units of fluorescence can be directly converted into numbers of C and N atoms liberated (Lehmeier et al. 2013); glucose liberation generates 6 assimilable C atoms and no N, and NAG liberation generates 8 C atoms and 1 N atom. Thus, the C:N flow ratio from simultaneous decay of MUB-BG and MUB-NAG can be calculated as

$$\frac{dC}{dN} = \frac{A_{BG}}{A_{NAG}} \cdot e^{\frac{(E_{aNAG} - E_{aBG})}{RT}} \cdot 6 + 8 \qquad (2)$$

where $E_{a\mathrm{BG}}$, A_{BG}, E_{aNAG}, and A_{NAG} are estimated using the general linear model with Arrhenius transformed activity as a function of 1/T and pH for the BGase/MUB-BG and the NAGase/MUB-NAG reactions, respectively (Lehmeier et al. 2013; see section 2.4). We used

estimates of E_a, which specify relative temperature sensitivity of enzymatic MUB-BG and MUB-NAG decay across the temperature range studied here, to compute the C:N flow ratio across the specified pH range. A C:N flow ratio was considered significantly different from one if E_a of both reactions, at the same pH value, were significantly different from each other at the $p<0.05$ level.

RESULTS

Effects of temperature and pH on specific enzyme activities

We observed significant effects of temperature ($p<0.001$) and pH ($p<0.001$) for both log-transformed specific activities of BGase and log-transformed specific activities of NAGase, but a significant interaction ($p<0.001$) only for BGase. Within each temperature, log-transformed specific activities of BGase were higher at pH 5.5-8.5 than those at 4.5 (see upper case letters in Fig. 2a). At a given pH, temperature-induced increases in log-transformed specific BGase activities varied across pH value (see lower case letters in Fig. 2a). Within each temperature, NAGase activity was highest at pH 5.5 and 6.5, indicating a well-defined, optimal pH for this reaction (see Fig. 2b).

Temperature sensitivity of reactions

In this study, temperature sensitivities were defined by E_a (see eq. 1), which was computed using the entire temperature range of 5 to 25°C, and dictates how changes in temperature over this range, alter rates of reaction. The E_a of the BGase/MUB-BG reactions was significantly influenced by pH (Fig. 3a, Table 2, and Supplementary Table 1). The E_a of BGase was highest

at pH 4.5 and was significantly different from E_a values at all other pH values. The second highest E_a of BGase occurred at pH 5.5, which was significantly greater than the E_a at pH 7.5. In contrast, none of the E_a values computed for NAGase/MUB-NAG reactions were significantly different from each other among pH values (Fig. 3b, Table 2, and Supplementary Table 1). This is reflected in the near parallel slopes (E_a) of log-transformed specific activities of NAGase (Fig. 3b).

We also observed significantly higher E_a of BGase compared to NAGase at pH 4.5, and significantly lower E_a of BGase compared to NAGase at pH 7.5 (Table 2 and Supplementary Table 1). Apparent differences in E_a between BGase and NAGase at pH of 5.5, 6.5 and 8.5, although often pronounced, were not statistically significant.

Estimated C:N flow ratio

Solution pH affected the C:N flow ratio resulting from the BGase/MUB-BG and NAGase/MUB-NAG reactions. Across the temperatures and pH values tested, the C:N flow ratio was lowest at pH 4.5 and 5°C (~10:1), and exhibited a maximum value of approximately ~40:1 at pH 6.5 and 5°C (Table 3). Except at pH 5.5, where the C:N flow ratio was approximately 30:1 regardless of temperature, temperature changes induced variability in the C:N flow ratio (Table 3 and Fig. 4). At pH 4.5, the C:N flow ratio significantly increased by 21% when temperature increased from 5 to 25°C (p<0.05 for the linear contrast comparing $E_{a\mathrm{BG}}$ and E_{aNAG}; Fig. 4). In contrast, the C:N flow ratio decreased with temperature above pH 5.5, and exhibited a significant decline with increasing temperature from 5 to 25°C at pH 7.5 (as determined by p<0.05 for the linear contrast

comparing $E_{a\mathrm{BG}}$ and E_{aNAG}; Fig. 4). At pH 6.5 and 8.5, the temperature-related decreases in the C:N flow ratio were not statistically significant despite their large magnitude.

DISCUSSION

In this study, we quantified specific activities of two extracellular enzyme/substrate reactions representative of microbially-mediated decay of two important SOM compounds, cellulose and chitin, and estimated the intrinsic temperature sensitivity of these reactions. We assessed how the temperature responses of these reactions are influenced by the pH in the reaction medium, over the naturally occurring range of soil pH. As a result, we generated baseline values of intrinsic sensitivities of BGase and NAGase reactions to which measurements of apparent temperature sensitivities of cellulose and chitin decay in soils can be compared quantitatively. Thus, our work provides a means of estimating the contribution of potentially changing chemical, physical, and microbial variables with temperature to observed temperature responses of cellulose and chitin decomposition and microbial CO_2 efflux from soils.

Specific enzyme activities of BGase and NAGase

Robust activity of BGase in variable environments (Fig. 2a) is consistent with the pivotal role it plays for microbial C metabolism in cleaving a disaccharide into two hexoses. Because glucose promotes the highest yield of adenosine triphosphate and dry cell mass per molecule consumed compared to other simple C-containing compounds (Bauchop and Elsden 1960), producing BGase that remains viable across a wide range of environmental conditions may be an important feature for some microbial decomposition strategies. This is consistent with BGase activity

remaining relatively constant in environmental samples across seasons with wide pH and temperature ranges (Rastin et al. 1988; Bandick and Dick 1999; Bell and Henry 2011), apparently regardless of cellulose content in soils (German et al. 2011).

In contrast, NAGase activity declined as reaction conditions deviated from pH 5.5-6.5, at all temperatures (Fig. 2b). We know of no study reporting on the stability of NAGase across soils of different pH and temperature; further study is necessary to clarify why pH 5.5-6.5 represents an apparently optimum range for NAGase activity. However, the lower estimates of intrinsic NAGase activity relative to BGase activity reported here and elsewhere (Lehmeier et al. 2013) are not surprising, given the more critical role of BGase to central metabolism. Carbon derived from any NAG taken up by a cell must eventually be transformed to glucose intracellularly for its use in glycolysis or the tricarboxylic acid or pentose phosphate cycles, increasing the metabolic cost of its use. Nitrogen derived from NAG cleavage can be an important source of microbial N (Sinsabaugh et al. 2008), but N can also be obtained via uptake of amino acids, inorganic N, or nitrogenous monomers released via other decay reactions (Lipson and Monson 1998; Nordin et al. 2004; Schimel and Bennett 2004; Tiemann and Billings 2012).

Effects of pH on the intrinsic temperature sensitivity

Variations of temperature sensitivities (E_a) of BGase and NAGase across pH highlight how soil pH may influence SOM decay dynamics in different ecosystems. For example, despite an apparently narrow optimum at pH 5.5-6.5 (Fig. 2b), the NAGase/MUB-NAG reaction did not exhibit significantly varying temperature sensitivity across the wide range of pH values studied here (similar slopes in Fig. 3b). This suggests that temperature exerts a relatively similar,

positive influence on chitin decay in soils regardless of soil pH. Thus, all else being equal, we might predict that NAGase activity in forest and grassland soils, which typically have a pH between 4.5 and 6.5 (IGBP-DIS 1998), may experience the same degree of stimulation with increasing temperature as NAGase in desert soils, which typically have a more alkaline pH (IGBP-DIS 1998).

In contrast, the significant influence of pH on BGase temperature sensitivity, as defined by E_a, suggests that ecosystems with different soil pH may experience relatively distinct changes in the rate of BGase-mediated cellulose decay in response to temperature. For example, the lower E_a of BGase at pH 6.5, 7.5, and 8.5 compared to other pH values (Table 2 and Supplementary Table 1) and the relatively high specific activities of BGase at those pH values (Fig. 2a) may have important implications for SOM dynamics in relatively alkaline desert soils. The data suggest that BGase exuded by microbial communities in alkaline desert soils may exhibit a relatively large fraction of its maximum potential activity even with declines in temperature from relatively high day-time maximums (Whitford 2002). Traditionally, relatively low accumulation of SOM in deserts is explained by low net primary production. Recently, Stursova and Sinsabaugh (2008) argued that thermally stable oxidative enzymes, along with their apparently high optimal pH, may promote SOM decomposition in desert soils. Here, our finding suggests that the maintenance of BGase activity in alkaline conditions (Fig. 2a) across a large gradient of temperature may also limit SOM accumulation in those soils. Furthermore, the relative temperature sensitivity of BGase/MUB-BG reactions at pH 4.5 was higher than those at all other pH values (Fig. 3a, Table 2, and Supplementary Table 1). This suggests that in many of the world's forest soils, which tend to exhibit relatively low pH values, BGase-driven celluose decay

exhibits greater relative temperature sensitivity than that in more alkaline soils. Given the approximately 341 Pg C residing in such soils (estimated from Batjes 2012), our work underscores the relative vulnerability of SOC stocks residing in soils with pH of ~4.5 and subjected to decay via BGase.

Linking temperature and pH to microbially available C and N

Differential effects of pH on the temperature sensitivity of C- and N-acquiring enzymes' reactions have ecological implications for soil microbe resource availability. The C:N flow ratio provides insight into how resources assimilable to microbial communities change with temperature and pH. This concept assumes that all of the C and N atoms liberated during the simulated MUB-BG and MUB-NAG decay, our proxies for cellulose and chitin decay in soils, are readily available for microbial assimilation. As such, changes in the C:N flow ratio may prompt soil microbes to alter their resource investment in extracellular enzymes, in an effort to balance C and N demand with changing relative availability of these elements in the environment. Our study design precludes us from discerning temperature-related changes in microbial biomass or composition, substrate targets, concentration of isozymes of extracellular enzymes at different pH values, or temperature sensitivity of enzymes other than BGase and NAGase. Instead, this study illuminates how two ecologically relevant extracellular enzymes may function in different chemical environments *post* microbial exudation.

We observed a variable pattern of C:N flow ratio in response to temperature from 5 to 25°C across pH values (Table 3 and Fig. 4), largely driven by significant differences in the temperature sensitivity of BGase among pH values. The significant increase in C:N flow ratio at

pH 4.5 with increasing temperature implies that C becomes relatively more available than N as temperature increases. Across the world, highly acidic soil (≤ pH 4.5) is usually found in tundra systems, boreal forests, high-latitude peatlands, tropical forests, and tropical peatlands (FAO 2013). Among these biomes, those at high-latitude are expected to experience substantially greater SOM decay in the future, relative to systems at lower latitudes, due to the magnitude of warming projected in this region (IPCC 2013) and BGase adapted to cold temperatures (German et al. 2012). Here, we propose another explanation for why these acidic ecosystems are highly likely to undergo significant SOM decay as temperature increases: at pH of 4.5, preferentially stimulated BGase activity with temperature, relative to NAGase, could result in increasing C:N flow ratio. All else being equal, an increase in C availability tends to promote declines in microbial C use efficiency, enhancing relatively high respiratory C losses (del Giorgio and Cole 1998; Manzoni et al. 2012). This argument is supported, indirectly, by studies reporting higher temperature sensitivity of C mineralization compared to N mineralization in alpine soil slurries at pH_{CaCl2} of 3.9-4.3 and tussock tundra soil slurries at pH 4.9 (Koch et al. 2007; Wallenstein et al. 2009).

For pH values higher than 4.5, we observed both qualitative and quantitative shifts in the C:N flow ratio. At pH 5.5, the C:N flow ratio exhibited no significant change with temperature (Table 3; Fig. 4), consistent with reports of unvarying C:N mineralization with temperature in incubated soils at pH 5.9 (Nadelhoffer et al. 1991) and similar Q_{10} values of BGase and NAGase reactions at pH 5.8 (German et al. 2012). At pH 7.5, C:N flow ratios decreased significantly with temperature, with similar, but non-significant trends also evident at pH 6.5 and 8.5. These data are consistent with Lehmeier et al. (2013), who demonstrated a decreasing C:N flow ratio

from 41 to 34 at pH 6.5 as temperature increased from 7 to 25°C. Our results also are congruent with studies of arctic soils at pH of 6.1 to 7.0, in which the ratio of C:N mineralization declined with increasing temperature (Nadelhoffer et al. 1991). Analogous with potentially increasing C losses with temperature increases at pH 4.5, observations in relatively alkaline conditions highlight the potential for enhanced N loss in soils with higher pH as temperature increases. As N availability increases to a greater extent than C availability, losses may occur via ammonia volatilization and leaching of dissolved organic N (Aber et al. 1995; Bussink and Oenema 1998).

CONCLUSIONS

By quantifying intrinsic temperature sensitivities of BGase/MUB-BG and NAGase/MUB-NAG reactions at multiple pH values, we provide the baseline values describing how liberation rates of C and N from cellulose and chitin in different soils will respond to changing environments. We thus provide a point of comparison for inferring the drivers of apparent temperature sensitivities of decay, and the flows of C and N emanating from them. Our work demonstrates that pH can exert differential influences on the temperature sensitivities of BGase and NAGase. As a result, relative flows of assimilable C and N during cellulose and chitin decay may vary with pH as temperature changes. Although we do not know how C- and N-acquiring enzymes other than BGase and NAGase will influence relative C and N availability with changing temperature and pH, our study demonstrates that disparate responses of BGase and NAGase to pH and temperature dictate fluctuations in the relative availabilities of essential microbial resources, presenting a temperature-driven feedback to which microorganisms may respond by altering their decomposition strategies.

TABLES AND FIGURES

Table 1. The mixture of the assay solutions. At each pH, three different controls (enzyme, quench, and substrate) and MUB standard are assayed in the same plates for correcting and calibrating the fluorescence signal in sample wells.

Category		
Control	Enzyme	50 µl of 0.2 M NaAc Buffer + 200 µl of enzyme in buffer
	Quench	50 µl of 10 µM MUB + 200 µl of enzyme in buffer
	Substrate	50 µl of 273 µM MUB-BG or 400 µM MUB-NAG + 200 µl of 0.2 M NaAc Buffer
Standard		50 µl of 10 µM MUB + 200 µl of 0.2 M NaAc Buffer
Sample		50 µl of 273 µM MUB-BG or 400 µM MUB-NAG + 200 µl of enzyme in buffer

Table 2. Activation energies (E_a; in kJ mol^{-1}) of BGase/MUB-BG and NAGase/MUB-NAG reactions, estimated using slopes in Fig. 3. Using pre-specified linear contrasts, we tested for differences among E_a across pH and enzyme at the $p < 0.05$ level (see section 2.4). Different upper case letters denote significant differences in E_a across pH values for a given enzyme (comparing slopes within one of the panels in Fig. 3); different lower case letters denote significant differences in E_a between two enzymes at a given pH (comparing slopes across panels for a given pH in Fig. 3).

	3.5	4.5	5.5	6.5	7.5	8.5
BGase/MUB-BG						
E_a	NA	65.1	37.2	28.0	16.9	22.2
Significance		A,a	B,a	BC,a	C,a	BC,a
NAGase/MUB-NAG						
E_a	NA	28.9	39.4	36.7	45.2	33.4
Significance		A,b	A,a	A,a	A,b	A,a

NA, not applicable

Table 3. Estimated C:N flow ratios in simultaneously proceeding BGase/MUB-BG and NAGase/MUB-NAG reactions at each temperature and pH. By definition, the C:N flow ratio is the ratio of C to N atoms liberated upon substrate decay (see section 2.5). Highlighted columns represent C:N flow ratios when E_a values of BGase/MUB-BG and NAGase/MUB-NAG reactions at the same pH were significantly different from each other at the $p < 0.05$ level (see Table 2).

Temperature (°C)	pH 3.5	pH 4.5	pH 5.5	pH 6.5	pH 7.5	pH 8.5
5	NA	9.6	29.3	41.3	38.5	28.9
10	NA	9.9	29.4	39.2	34.2	26.7
15	NA	10.4	29.4	37.3	30.7	24.8
20	NA	10.9	29.5	35.5	27.7	23.2
25	NA	11.6	29.6	33.9	25.2	21.7

NA, not available

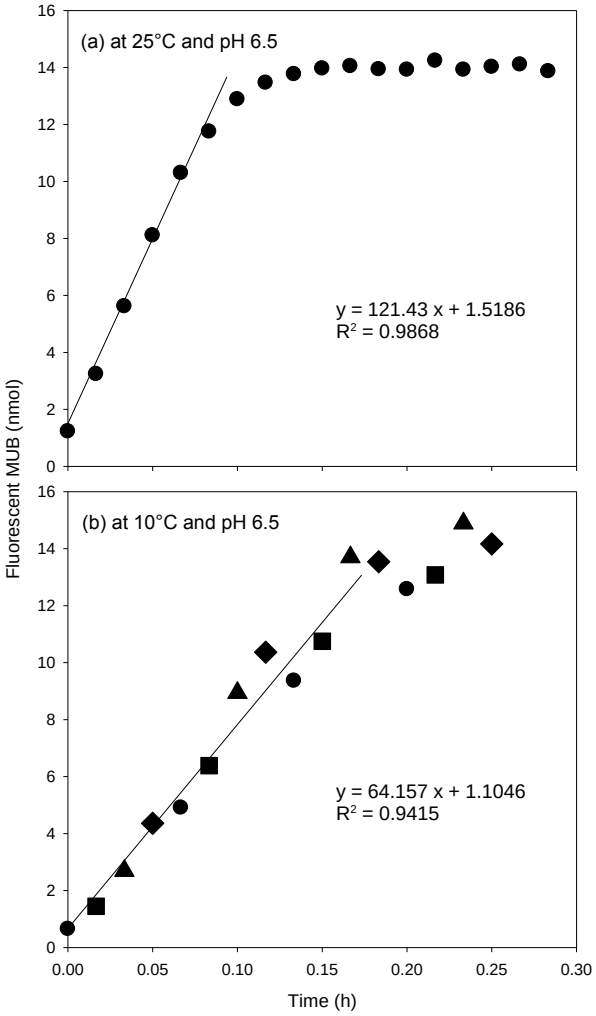

Fig. 1. Two examples of fluorescent MUB generation over incubation time as a result of BGase/MUB-BG reactions at pH 6.5 at either 25°C (a) or 10°C (b). Linear regression lines were fitted to the initial linear stage of MUB accumulation to derive BGase-mediated MUB release from MUB-BG in nmol h^{-1}. While the data points in (a) are from one 96-well plate, a total of four identical plates were alternated in (b) during the incubation period to represent one replicate (see section 2.2 for a detailed description; Circle, plate 1; square, plate 2; triangle, plate 3; diamond, plate 4)

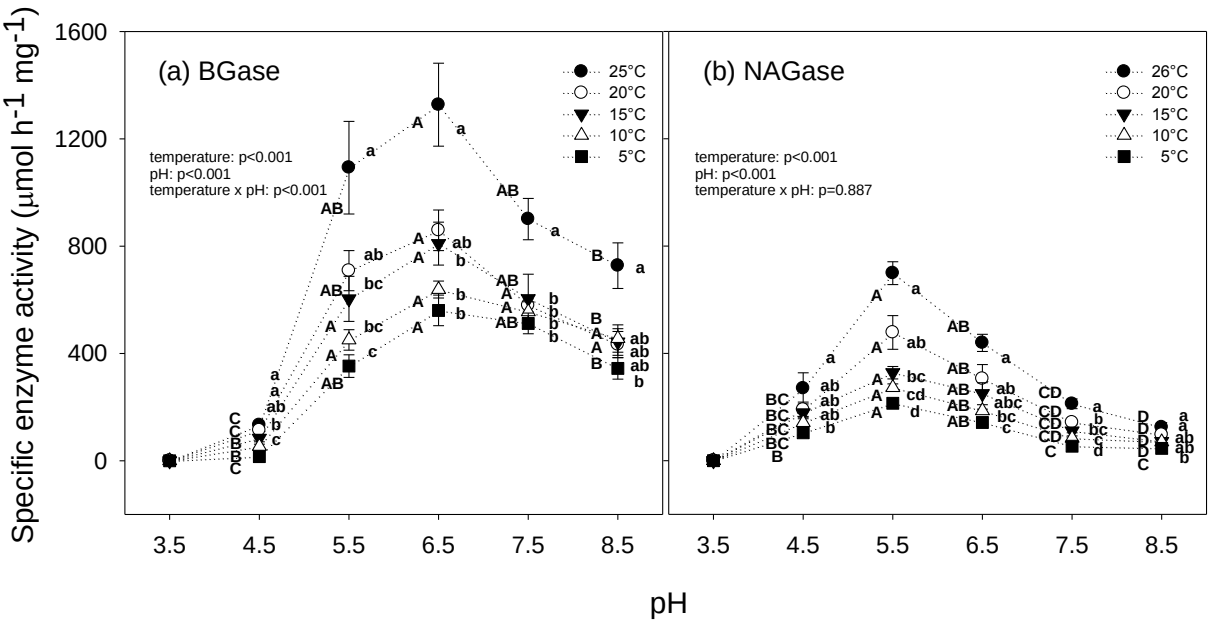

Fig. 2. Specific activities of (a) BGase and (b) NAGase (µmol h^{-1} enzyme mg^{-1}) at different temperatures as a function of pH. Error bars represent ± 1 standard error (n=4 to 8 for BGase/MUB-BG and n=3 to 4 for NAGase/MUB-NAG). Results from two-way ANOVA with temperature and pH as independent variables are included in each panel. Multiple comparisons were made across temperature within pH values, lower case letters, and across pH for particular temperature, upper case letters. We used Bonferroni corrected *p*-values to determine statistically significant comparisons at $p < 0.05$ level. Note that indicators of statistical significance reflect analyses performed using log-transformed specific activities to satisfy the assumptions of normality and equal variance

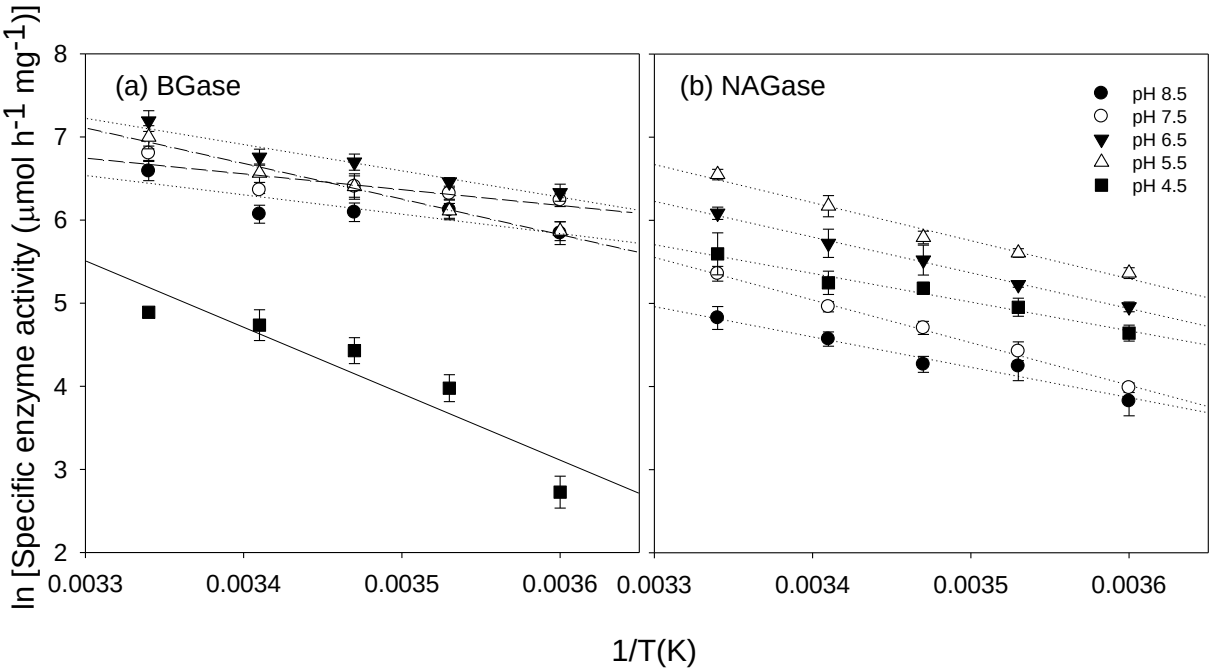

Fig. 3. Temperature sensitivities (E_a) of (a) BGase/MUB-BG and (b) NAGase/MUB-NAG reactions. To assess E_a of the reactions as detailed in eq. 1, we plot ln-transformed specific enzyme activities against 1/temperature (in K). The slopes of the linear regressions are considered equivalent to the E_a of each relevant reaction; the intercepts are values for ln (A) (see eq. 1). In (a), the slope of the solid line (pH 4.5; E_a=65.1 kJ mol^{-1}) is significantly higher than those of broken lines (see Table 2 and Supplementary Table 1 for more information). Among broken lines, the slope of the dash-dot line (—·—, pH 5.5; E_a=37.2 kJ mol^{-1}) is significantly greater than the dash-dash line (——, pH 7.5; E_a=16.9 kJ mol^{-1}; p=0.028). The slopes of NAGase/MUB-NAG reactions in (b) were not significantly different across pH values.

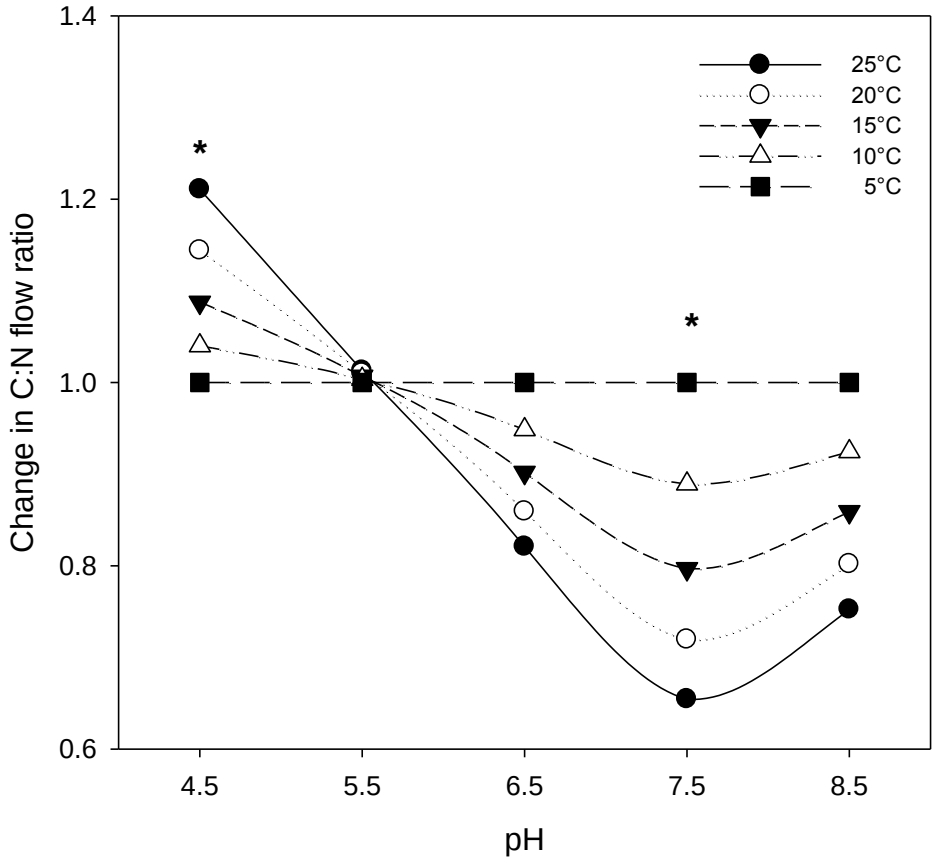

Fig. 4. C:N flow ratio of resources liberated during BGase/MUB-BG and NAGase/NAG reactions proceeding at 10, 15, 20, and 25°C relative to that at 5°C at specified pH values. This normalization represents how the relative amount of C and N potentially assimilable to microbes during decay changes as temperature increases from 5°C. See section 2.5 for a complete description of C:N flow ratio. Asterisks at pH 4.5 and 7.5 denote statistically significant changes in the C:N flow ratio as temperature increases from 5 to 25°C, as determined by significantly different E_a values of both reactions at the same pH ($p < 0.05$).

REFERENCES

Aber, J.D., Magill, A., Mcnulty, S.G., Boone, R.D., Nadelhoffer, K.J., Downs, M., Hallett, R., 1995. Forest biogeochemistry and primary production altered by nitrogen saturation. Water, Air, and Soil Pollution 85, 1665-1670.

Arrhenius, S., 1889, Über die Reaktionsgeschwindigkeit bei der Inversion von Rohrzucker durch Säuren. Zeitschrift fur Physik Chemique 4, 226-248.

Bandick, A.K., Dick, R.P., 1999. Field management effects on soil enzyme activities. Soil Biology & Biochemistry 31, 1471-1479.

Batjes, N.H., 2012. ISRIC-WISE derived soil properties on a 5 by 5 acr-minutes global grid (ver. 1.2). ISRIC Report 2012/01, Wageningen.

Bauchop, T., Elsden, S., 1960. The growth of micro-organisms in relation to their energy supply. Journal of General Microbiology 23, 457-469.

Bell, T.H., Henry, H.A., 2011. Fine scale variability in soil extracellular enzyme activity is insensitive to rain events and temperature in a mesic system. Pedobiologia 54, 141-146.

Billings, S.A., Ballantyne, F., 2013. How interactions between microbial resource demands, soil organic matter stoichiometry, and substrate reactivity determine the direction and magnitude of soil respiratory responses to warming. Global Change Biology 19, 90-102.

Brady, N., Weil, R., 2007. Nature and properties of soils, 14th ed. Prentice Hall.

Bussink, D., Oenema, O., 1998. Ammonia volatilization from dairy farming systems in temperate areas: a review. Nutrient Cycling in Agroecosystems 51, 19-33.

Christensen, R., 1996. Plane answers to complex questions: The theory of linear models. Springer.

Conant, R.T., Ryan, M.G., Ågren, G.I., Birge, H.E., Davidson, E.A., Eliasson, P.E., Evans, S.E., Frey, S.D., Giardina, C.P., Hopkins, F.M., Hyvönen, R., Kirschbaum, M.U.F., Lavallee, J.M., Leifeld, J., Parton, W.J., Steinweg, J.M., Wallenstein, M.D., Wetterstedt, J.Å.M., Bradford, M., 2011. Temperature and soil organic matter decomposition rates–synthesis of current knowledge and a way forward. Global Change Biology 17, 3392-3404.

Cleveland, C., Liptzin, D., 2007. C:N:P stoichiometry in soil: is there a "Redfield ratio" for the microbial biomass? Biogeochemistry 85, 235-252.

Davidson, E.A., Janssens, I.A., 2006. Temperature sensitivity of soil carbon decomposition and feedbacks to climate change. Nature 440, 165-173.

Davidson, E.A., Janssens, I.A., Luo, Y., 2006. On the variability of respiration in terrestrial ecosystems: moving beyond Q_{10}. Global Change Biology 12, 154-164.

DeForest, J.L., 2009. The influence of time, storage temperature, and substrate age on potential soil enzyme activity in acidic forest soils using MUB-linked substrates and L-DOPA. Soil Biology & Biochemistry 41, 1180-1186.

Deng, S.P., Tabatabai, M.A., 1994. Cellulase activity of soils. Soil Biology & Biochemistry 26, 1347-1354.

FAO. 2013. Land Resources: pH (topsoil). Retrieved 6/3/2013 from http://www.fao.org/nr/land/soils/en/.

Fierer, N., Coman, B.P., Schimel, J.P., Jackson, R.B., 2006. Predicting the temperature dependence of microbial respiration in soil: A continental-scale analysis. Global Biogeochemical Cycles 20, GB3026, doi:10.1029/2005GB002644.

Frankenberger, W., Johanson, J., 1982. Effect of pH on enzyme stability in soils. Soil Biology & Biochemistry 14, 433-437.

Frey, S.D., Knorr, M., Parrent, J.L., Simpson, R.T., 2004. Chronic nitrogen enrichment affects the structure and function of the soil microbial community in temperate hardwood and pine forests. Forest Ecology and Management 196, 159-171.

German, D.P., Chacon, S.S., Allison, S.D.,2011. Substrate concentration and enzyme allocation can affect rates of microbial decomposition. Ecology 92, 1471-1480.

German, D.P., Marcelo, K.R., Stone, M.M., Allison, S.D., 2012. The Michaelis–Menten kinetics of soil extracellular enzymes in response to temperature: a cross- latitudinal study. Global Change Biology 18, 1468-1479.

del Giorgio, P.A., Cole, J.J., 1998. Bacterial growth efficiency in natural aquatic systems. Annual Review of Ecology and Systematics 29, 503-541.

Högberg, P., Nordgren, A., Buchmann, N., Taylor, A.F., Ekblad, A., Högberg, M.N., Nyberg, G., Ottosson-Löfvenius, M., Read, D.J., 2001. Large-scale forest girdling shows that current photosynthesis drives soil respiration. Nature 411, 789-792.

IGBP-DIS, 1998. SoilData(V.0): a program for creating global soil-property databases. IGBP Global Soils Data Task, France.

IPCC, 2013. Climate Change 2013: The Physical Science Basis. Contribution of working group I to the fifth assessment report of the intergovernmental panel on climate change. Cambridge University Press, Cambridge and New York.

Knorr, W., Prentice, I., House, J., Holland, E., 2005. Long-term sensitivity of soil carbon turnover to warming. Nature 433, 298-301.

Koch, O., Tscherko, D., Kandeler, E., 2007. Temperature sensitivity of microbial respiration, nitrogen mineralization, and potential soil enzyme activities in organic alpine soils. Global Biogeochemical Cycles 21, GB4017, doi:10.1029/2007BG002983.

Lehmeier, C.A., Min, K., Niehues, N.D., Ballantyne F., Billings, S.A., 2013. Temperature-mediated changes of exoenzyme-substrate reaction rates and their consequences for the carbon to nitrogen flow ratio of liberated resources. Soil Biology & Biochemistry 57, 374-382.

Lipson, D.A., Monson, R.K., 1998. Plant-microbe competition for soil amino acids in the alpine tundra: effects of freeze-thaw and dry-rewet events. Oecologia 113, 406-414.

MacDonald, N.W., Zak, D.R., Pregitzer, K.S., 1995. Temperature effects on kinetics of microbial respiration and net nitrogen and sulfur mineralization. Soil Science Society of America Journal 59, 233-240.

Manzoni, S., Taylor, P., Richter, A., Porporato, A., Ågren, G.I., 2012. Environmental and stoichiometric controls on microbial carbon- use efficiency in soils. New Phytologist 196, 79-91.

Mead, J.A.R., Smith, J.N., Williams, R.T., 1955. Studies in detoxication. 67. Biosynthesis of the glucuronides of umbelliferone and 4-methylumbelliferone and their use in fluorimetic determination of beta-glucuronidase. Biochemical Journal 61, 569-574.

Mikan, C.J., Schimel, J.P., Doyle, A.P., 2002. Temperature controls of microbial respiration in arctic tundra soils above and below freezing. Soil Biology & Biochemistry 34, 1785-1795.

Min, K., Kang, H., Lee, D., 2011. Effects of ammonium and nitrate additions on carbon mineralization in wetland soils. Soil Biology & Biochemistry 43, 2461-2469.

Nadelhoffer, K. J., Giblin, A.E., Shaver, G.R., Laundre, J.A., 1991. Effects of Temperature and Substrate Quality on Element Mineralization in Six Arctic Soils. Ecology 72, 242-253.

Niemi, R., Vepsäläinen, M., 2005. Stability of the fluorogenic enzyme substrates and pH optima of enzyme activities in different Finnish soils. Journal of Microbiological Methods 60, 195-205.

Nordin A., Schmidt, I.K., Shaver, G.R., 2004. Nitrogen uptake by arctic soil microbes and plants in relation to soil nitrogen supply. Ecology 85, 955-962.

Parham, J., Deng, S., 2000. Detection, quantification and characterization of β-glucosaminidase activity in soil. Soil Biology & Biochemistry 32, 1183-1190.

Rastin, N., Rosenplänter, K., Hüttermann, A., 1988. Seasonal variation of enzyme activity and their dependence on certain soil factors in a beech forest soil. Soil Biology & Biochemistry 20, 637-642.

Schimel, D.S., 1995. Terrestrial ecosystems and the carbon cycle. Global Change Biology 1, 77-91.

Schimel, J.P., Bennett, J., 2004. Nitrogen mineralization: Challenges of a changing paradigm. Ecology 85, 591-602.

Sinsabaugh, R.L., Lauber,C.L., Weintraub, M.N., Ahmed, B., Allison, S.D., Crenshaw, C., Contosta, A.R., Cusack, D., Frey, S.D., Gallo, M.E., Gartner, T.B., Hobbie, S.E., Holland, K., Keeler, B.L., Powers, J.S., Stursova, M., Takacs-Vesbach, C., Waldrop, M.P., Wallenstein, M.D., Zak, D.R., Zeglin, L.H., 2008. Stoichiometry of soil enzyme activity at global scale. Ecology Letters 11, 1252-1264.

Sterner, R.W., Elser, J.J., 2002. Ecological stoichimetry: the biology of elements from molecules to the biosphere. Princeton University Press, Princeton.

Somero, G.N., 2004. Adaptation of enzymes to temperature: searching for basic "strategies". Comparative Biochemistry and Physiology Part B: Biochemistry and Molecular Biology 139, 321-333.

Stursova, M., Sinsabaugh, R.L., 2008. Stabilization of oxidative enzymes in desert soil may limit organic matter accumulation. Soil Biology & Biochemistry 40, 550-553.

Suseela, V., Conant, R.T., Wallenstein, M.D., Dukes, J.S., 2012. Effects of soil moisture on the temperature sensitivity of heterotrophic respiration vary seasonally in an old-field climate change experiment. Global Change Biology 18, 336-348.

Tabatabai, M.A., 1994. Soil enzymes. In Weaver, W., Angle, J.S., Bottomley, P.S. (Eds), Methods of soil analysis part 2. Microbiological and biological properties. Soil Science Society of America, Wisconsin, pp. 775-833.

Tiemann, L.K., Billings, S.A., 2012. Tracking C and N flows through microbial biomass with increased soil moisture variability. Soil Biology & Biochemistry 49, 11-22.

Tipton, K.F., McDonald, A., Dixon, H., 1979. Effects of pH on enzymes. In Purich, D.L. (Ed), Contemporary enzyme kinetics and mechanism. Academic Press, pp. 124-172.

Treseder, K., 2008. Nitrogen additions and microbial biomass: a meta-analysis of ecosystem studies. Ecology Letters 11, 1111-1120.

Trumbore, S., 2006. Carbon respired by terrestrial ecosystems - recent progress and challenges. Global Change Biology 12, 141-153.

Turner, B.L., 2010. Variation in pH optima of hydrolytic enzyme activities in tropical rain forest soils. Applied and Environmental Microbiology 76, 6485-6493.

van't Hoff, J.H., 1884. Etudes de dynamique chemique. Frederik Muller & Co., Amsterdam.

Wallenstein, M.D., McMahon, S.K., Schimel, J.P., 2009. Seasonal variation in enzyme activities and temperature sensitivities in Arctic tundra soils. Global Change Biology 15, 1631-1639.

Wallenstein, M.D., Allison, S.D., Ernakovich, J.E., Steinweg, J.M., Sinsabaugh, R.L., 2010. Controls on the temperature sensitivity of soil enzymes: A key driver of in situ enzyme activity rates. In Shukla, G., Varma, A. (Eds), Soil enzymology. Springer, Berlin, pp. 245-258.

Whitford, W.G., 2002. Ecology of desert systems. Academic Press.

Zoltan, S., 2008. Spatial and temporal pattern of soil pH and Eh and their impact on solute iron content in a wetland (Transdanubia, Hungary). Acta Geographica Debrecina. Landscape and Environment Series 2, 34-45.

Zhou, T., Shi, P., Hui, D., Luo, Y., 2009. Global pattern of temperature sensitivity of soil heterotrophic respiration (Q_{10}) and its implications for carbon- climate feedback. Journal of Geophysical Research 114, GO2016, doi:10.1029/2008JG000850.

CHAPTER 2: Carbon availability modifies temperature responses of heterotrophic microbial respiration, carbon uptake affinity, and stable carbon isotope discrimination

Min, K., Lehmeier, C., Ballantyne, F., Billings, S. 2016. Carbon availability modifies temperature responses of heterotrophic microbial respiration, carbon uptake affinity, and stable carbon isotope discrimination. *Frontiers in Microbiology* 7: 2083.

ABSTRACT

Microbial transformations of organic carbon (OC) generate a large flux of CO_2 into the atmosphere and influence the C balance of terrestrial and aquatic ecosystems. Yet, inherent heterogeneity in natural environments precludes direct quantification of multiple microbial C fluxes that underlie CO_2 production. Here we used a continuous flow bioreactor coupled with a stable C isotope analyzer to determine the effects of temperature and C availability (cellobiose concentration) on C fluxes and ^{13}C discrimination of a microbial population growing at steady-state in a homogeneous, well-mixed environment. We estimated C uptake affinity and C use efficiency (CUE) to characterize the physiological responses of microbes to changing environmental conditions. Temperature increased biomass-C specific respiration rate and C uptake affinity at lower C availability, but did not influence those parameters at higher C availability. CUE decreased non-linearly with increasing temperature. The non-linear, negative relationship between CUE and temperature was more pronounced under lower C availability than under relatively high C availability. We observed stable isotope fractionation between C substrate and microbial biomass C (7~12‰ depletion), and between microbial biomass and

respired CO_2 (4~10‰ depletion). Microbial discrimination against ^{13}C-containing cellobiose during C uptake was influenced by temperature and C availability, while discrimination during respiration was only influenced by C availability. Shifts in C uptake affinity with temperature and C availability may have modified uptake-induced ^{13}C fractionation. By stressing the importance of C availability on temperature responses of microbial C fluxes, C uptake affinity, CUE, and isotopic fractionation, this study contributes to a fundamental understanding of C flow through microbes. This will help guide parameterization of microbial responses to varying temperature and C availability within Earth-system models.

INTRODUCTION

Heterotrophic microorganisms break down organic carbon (OC) into assimilable molecules, which are subsequently incorporated into biomass or returned to the environment as exudates or respired CO_2. In doing so, microbes influence the quantity and biochemical composition of OC in terrestrial and aquatic systems as well as atmospheric CO_2 concentration. Because of the important role they play in regulating OC in terrestrial and aquatic systems and atmospheric CO_2, ecosystem scientists have explicitly incorporated microbial dynamics into Earth system models (Allison et al., 2010; Wieder et al., 2013; Hagerty et al., 2014; Tang and Riley, 2015). However, it remains unclear what values should be used for microbial parameters (e.g., C use efficiency (CUE), biomass-C specific respiration) and how these parameters change with environmental conditions (Luo et al., 2016). This is because heterogeneity in natural environments, especially in soils, makes it nearly impossible to empirically determine many of

these parameters in situ (Werth and Kuzyakov, 2010; Billings and Ballantyne, 2013; Billings et al., 2015).

Assessing microbial OC transformations in controlled, experimental systems can help us overcome some of the difficulties ecosystem scientists face when using natural samples to investigate microbial C flows (Billings et al., 2015). For example, chemostats, continuous flow bioreactors for the cultivation of microorganisms, have been widely employed to investigate fundamental microbial physiology during OC transformations by removing the influence of natural heterogeneity (Rhee and Gotham, 1981; Cajal-Medrano and Maske, 2005; Cotner et al., 2006; Chrzanowski and Grover, 2008; Ferenci, 2008). Recently, Lehmeier et al. (2016) used a coupled chemostat and C isotope analyzer to improve our understanding of C flows from substrate through microbial biomass and into respired CO_2, which is of great interest at multiple scales and levels of organization, from microbes to ecosystems (Blair et al., 1985; Hagström et al., 1988; Henn and Chapela, 2000; Šantrůčková et al., 2000; Henn et al., 2002; Werth and Kuzyakov, 2010; Brüggemann et al., 2011; Dijkstra et al., 2011a, 2011b; Penger et al., 2014). In particular, quantifying the effects of temperature on biomass-C specific respiration rate, CUE, and microbial ^{13}C discrimination for a ubiquitous microbe (Lehmeier et al., 2016) provides a mechanistic basis and justification for the often assumed temperature dependence of CUE in Earth-system models.

Temperature responses of microbial OC transformations in Lehmeier et al. (2016) were quantified using a single C substrate, cellobiose, at a single concentration, 10 mM. However, it remains unknown how the temperature responses of microbial respiration, CUE, and ^{13}C

discrimination may be influenced by C availability which varies among ecosystems, vertically and laterally throughout soil profiles, and as microbes' substrate landscapes shift over time (Kuzyakov, 2010; Richter and Markewitz, 2013). Furthermore, the absolute and relative abundance of readily assimilable C can also vary with temperature (Bárta et al., 2013; Lehmeier et al., 2013; Min et al., 2014), and thus can influence the temperature responses of microbial OC transformations (Rhee and Gotham, 1981; Pomeroy and Wiebe, 2001; Hall and Cotner, 2007; Manzoni et al., 2012; Billings and Ballantyne, 2013; Frey et al., 2013; Xu et al., 2014).

When C availability decreases, microorganisms can adjust their ability to take up C as a compensatory measure (Death et al., 1993; Williams et al., 1994; Ferenci, 1999; Gresham and Hong, 2015). The ability to take up C, or C uptake affinity, is often defined as the ratio of the maximum uptake rate (V_{max}) to the half-saturation concentration of C (k_m) of the Michaelis-Menten function (Healey, 1980; Aksnes and Egge, 1991; Button, 1993; Reay et al., 1999). Because C uptake affinity defined this way is equivalent to the slope of the Michaelis-Menten function at a C concentration of zero, it reflects the sensitivity of the uptake response to changing C availability at low absolute concentrations. This suggests that microbes may allocate resources to a more energetically costly, high affinity C uptake strategy at relatively low C availability (Patzer and Hantke, 1998), resulting in enhanced respiratory costs. Furthermore, changing C uptake affinity may alter ^{13}C discrimination during uptake and subsequently influence $\delta^{13}C$ of remaining OC pools, as well as downstream pools such as biomass and respired CO_2 (Lehmeier et al., 2016). Understanding any such C uptake affinity-induced shift in fractionation would be critical to correctly interpret $\delta^{13}C$ of terrestrial C pools and fluxes.

We grew *Pseudomonas fluorescens*, a cosmopolitan Gram-negative bacterium, in a chemostat system coupled to a $^{13}CO_2/^{12}CO_2$ analyzer and quantified how the sizes of C pools in the system and their C stable isotope ratios varied with temperature and C availability. Combining the measurements with a dynamic model of substrate-C and biomass-C, we estimated how C uptake and C uptake affinity varied with changing temperature (11.5 to 25.5˚C) and C availability (1 and 20 mM cellobiose). The cellobiose concentrations of 1 and 20 mM yielded medium C:N of 1 and 20, respectively, to span the observed range of C:N of bacterial biomass (5-10) reported in Cleveland and Liptzin (2007) and Nagata (1986). Our primary goal was to quantify how changing C substrate availability alters the temperature dependence of C flow through a common microbe and associated C stable isotope fractionations. As such, we asked: (1) how will temperature and C availability influence biomass-C specific respiration, C uptake affinity, and CUE during OC transformations? (2) how will changes in these microbial parameters with temperature and C availability, if any, modify ^{13}C discrimination among substrate, biomass and respired CO_2?

MATERIALS AND METHODS

The chemostat system coupled to a continuous flow $^{13}CO_2/^{12}CO_2$ gas analyzer employed in this study is described in full detail in Lehmeier et al. (2016). Here we summarize the protocol of running a chemostat experiment and expand Lehmeier et al.'s approach by providing estimates for C uptake affinity and a simple model for CUE.

Microorganisms and nutrient solution with two contrasting C concentrations

We used *Pseudomonas fluorescens* (ATCC ®13525, Carolina Biological Supply, USA), because it is one of the most common bacteria inhabiting both soil and water. As growth medium for *P. fluorescens*, we prepared nutrient solution modified from Abraham et al. (1998), containing 10 mM NH_4Cl, 1.6 mM KNO_3, 2.6 mM K_2HPO_4, 1.0 mM KH_2PO_4, 0.8 mM $MgSO_4$, 0.2 mM $CaCl_2$, 0.1 mM $CuCl_2$, 0.04 mM $FeSO_4$, 0.03 mM $MnCl_2$ and 0.02 mM $ZnSO_4$. After adjustment to pH 6.5, the nutrient solution was autoclaved and stored under UV light. We added cellobiose (Sigma-Aldrich, USA) to the sterile nutrient solution as the only organic C source, inoculated it with *P. fluorescens*, and grew cultures at 10°C. These pre-cultures of *P. fluorescens* served as inoculum for the chemostat bioreactor. The concentration of cellobiose in the nutrient solution was adjusted to either 1 or 20 mM, which corresponded to resource C to N ratios of 1 and 20, respectively. Cellobiose $\delta^{13}C$ values ranged from -24.4 to -24.9‰, depending on the lot from which the supply was issued. For each individual chemostat run, we used cellobiose derived from only one lot to ensure a constant $\delta^{13}C$ value of microbial substrate for each run (Supplementary Table 1).

Continuous flow chemostat system

The chemostat system consisted of two 1.9 L Mason jars (Ball, USA), which were connected via flexible tubing (Masterflex Tygon E-LFL tubing, Cole-Parmer, USA) and situated on stir plates in separate incubators. One jar functioned as a bioreactor, into which we poured 1 L of fresh nutrient solution and injected inoculum (5 mL of *P. fluorescens* pre-culture) at the start of each individual chemostat run; the other jar functioned as a reservoir for fresh nutrient solution and was regularly refilled during a chemostat run.

In the continuous culture mode, a peristaltic pump supplied fresh nutrient solution from the reservoir to the bioreactor at a constant rate, providing new resources to the growing microbial population. The pump simultaneously removed well-mixed bioreactor medium (including microbial cells) at the same rate as the nutrient solution supply rate via a waste line, such that the total volume of liquid in the bioreactor remained constant. The dilution rate of the chemostat bioreactor averaged 0.128 h^{-1} (Figure 1a). By definition, the dilution rate equals the growth rate of the microbial population in the chemostat reactor under steady-state conditions (Hoskisson and Hobbs, 2005; Bull, 2010). Steady-state in this sense means that the microbial population in the bioreactor reaches a state of constant size and activity under the prevailing environmental conditions, and that the number of cells leaving the bioreactor via dilution is counterbalanced by cell division.

Analogous to the continuous flow of liquid, gas also flowed continuously through the bioreactor. A $^{13}CO_2/^{12}CO_2$ analyzer (G2101-i, Picarro, USA) removed headspace air from the bioreactor at a rate of 25 mL min^{-1} on average and continuously measured the concentration and the $\delta^{13}C$ of headspace CO_2. The air volume removed was instantaneously replaced with CO_2-free air, bubbled into the nutrient solution at the same rate that the $^{13}CO_2/^{12}CO_2$ analyzer withdrew headspace air via a mass flow controller (MC-50SCCM, Alicat Scientific, USA). In this way, bioreactor headspace air pressure remained constant and the CO_2-free air provided the microbial population with oxygen.

Immediately after the inoculation and closure of the chemostat bioreactor, CO_2 concentration in the headspace air represented lab air conditions (approximately 400 ppm CO_2). Soon after

closure of the bioreactor, the CO_2 concentration approached zero because of the bubbling of CO_2-free air into the bioreactor and little microbial activity. Subsequently, the size of the microbial population and hence the rate of respiratory CO_2 production increased and after the switch to the continuous culture mode, it achieved steady state conditions. Prior to the steady state, the $^{13}CO_2/^{12}CO_2$ measurement of the headspace air did not solely reflect microbial respiration, because the bioreactor medium acted as a sink for respired CO_2 (in the form of H_2CO_3 and HCO_3^-; Stumm and Morgan, 1981; Lehmeier et al., 2016). When the microbial population reached steady state, both the CO_2 production rate and the $\delta^{13}C$ of the CO_2 became constant, indicating that chemical and isotopic equilibria of the carbonate system were achieved. However, even in the steady-state phase, not all of the respired CO_2 entering the bioreactor medium was released into the bioreactor headspace. This is because some respired CO_2 entered the carbonate system and was removed via the waste line due to dilution. We estimated that not more than 6~8% of respired CO_2 was lost from the bioreactor via dilution, hence, we may have underestimated microbial respiration rates by about 6-8%. Importantly, as both the supply rates of fresh medium and the steady-state CO_2 concentrations in the bioreactor headspace (the two most important factors determining the sink strength of the supplied fresh medium) were very similar across all chemostat runs, this error was very similar too. Therefore, we considered the headspace CO_2 representing the concentration and $\delta^{13}C$ of respired CO_2 (for more detailed information, please refer to section 2.3.1 and Supplementary Material in Lehmeier et al., 2016). We thus used measurements of bioreactor headspace air when the microbial population was at steady-state to quantify microbial respiration rates and $\delta^{13}C$ of respired CO_2, allowing us to draw conclusions about microbial behavior without concern for interactions between headspace CO_2 and inorganic C pools in the bioreactor medium.

For each cellobiose concentration, chemostat experiments were conducted at six different bioreactor temperatures, randomly ordered: at 1 mM of cellobiose, reactor temperature was maintained at 11.8, 13, 15.5, 17, 21, or 25.5°C; at 20 mM of cellobiose, it was 11.5, 13, 14.7, 17.5, 20.8 or 25.5°C. This experimental temperature range covers an ecologically relevant range of temperatures in many ecosystems. Below 11.5°C, microorganisms' steady-state growth was unsustainable at the dilution rate of 0.128 h^{-1}. This is consistent with findings in Höfle (1979), which reported that the maximum growth rate of *P. fluorescens* at 10°C is 0.13 h^{-1}. We conducted one repeated chemostat run at 17°C and 1 mM of cellobiose. We acknowledge that one replication is not enough to quantify an overall uncertainty of the measurements, but similar values of microbial OC transformations for these replicated runs, in conjunction with clear temperature-related trends (see Results), suggest that our measurements were reliable (Figures 1-4).

Quantification of microbial biomass and respiration at steady-state

At steady state, we collected and filtered the bioreactor medium from the waste line on dry, pre-weighed 0.22 μm polyethersulfone filters (Pall, USA). We dried the wet filters at 75°C for 48 hours in an oven and reweighed them to determine dry microbial biomass. Carbon and N in microbial biomass were quantified using an elemental analyzer coupled to an isotope-ratio mass spectrometer, either at the Keck Paleoenvironmental and Environmental Stable Isotope Laboratory at the University of Kansas or at the Stable Isotope Laboratory at the University of Arkansas. In both laboratories, the standard deviation of repeated lab standard measurements was a maximum of 0.2 ‰.

We calculated microbial respiration rates by multiplying the average reactor headspace CO_2 concentration measured over five hours at steady state with the molar air flow rate through the bioreactor. After steady-state CO_2 measurements at each chemostat run, we measured a laboratory standard gas, which had a CO_2 concentration of 1015 ppm and a $\delta^{13}C$ of -48.9‰ as calibrated against secondary CO_2 standards from KU's Keck Paleoenvironmental and Environmental Stable Isotope Laboratory. This served to check the concentrations and to correct the isotopic signatures of bioreactor headspace CO_2 measurements.

Carbon dynamics in the chemostat bioreactor

In a chemostat bioreactor provided with cellobiose as the sole OC substrate, there are two OC pools, cellobiose-C and biomass-C, if we assume exudation is negligible (Blair et al., 1985; Hagström et al., 1988). The temporal dynamics of the two OC pools can be described with two ordinary differential equations (Smith and Waltman, 1995).

$$\frac{dS}{dt} = (I - S)d - Bf(S) \qquad eq.1$$

$$\frac{dB}{dt} = B(f(S) - (d + \rho + \varepsilon)) \qquad eq.2$$

, where S is cellobiose-C in the chemostat bioreactor, I is cellobiose-C input to the chemostat bioreactor, d is the dilution rate (which equals the biomass-C-specific population growth rate in a steady-state chemostat; Hoskisson and Hobbs, 2005; Bull, 2010), B is biomass-C in the chemostat reactor, $f(S)$ is the function describing biomass-C specific uptake rate of cellobiose-C, ρ is the biomass-C specific respiration rate, ε is the biomass-C specific exudation rate, and t is time. At steady state, denoted by ̂, biomass-C and cellobiose-C concentrations are both constant

($\frac{dB}{dt} = \frac{dS}{dt}$ =0). This means that the biomass-C specific uptake rate, $f(\hat{S})$, equals the sum of d, ρ and ε. If we assume ε is negligible, $f(\hat{S})$ is estimated as the sum of d and ρ. The steady-state conditions in the chemostat allow biomass-C specific rates to be computed by dividing gross C fluxes by C pool sizes. For example, ρ was estimated by dividing the total rate of respiration of the bioreactor by microbial biomass-C at steady state, which we obtained via elemental analysis of dried biomass.

Estimates of C uptake affinity and CUE

Although the steady-state measurements of d and ρ allow us to estimate $f(\hat{S})$, this alone does not provide the physiological basis for a change in uptake fluxes. However, if we employ a standard assumption of $f(\hat{S})$saturating as a function of C availability (Button, 1993; Ferenci, 1999), we can begin to probe temperature-dependent physiological shifts. We can express $f(S)$, the function describing the biomass-C specific uptake rate of cellobiose-C (see eq. 1) with the standard Michaelis-Menten formulation for cellobiose-C uptake as

$$f(S) = \frac{V_{max}\, S}{S + k_m} \qquad eq.3$$

This approach allows us to relate changes in C uptake physiology, namely in V_{max} and k_m, to changing temperature, such that a change in C uptake physiology would be reflected in a change in either or both with temperature and C availability.

Assuming that ε is negligible and combining equations 2 and 3, we can express steady-state concentrations of biomass as

$$\widehat{B} = \frac{\left(I - \frac{k_m\,(d + \rho)}{V_{max} - d - \rho}\right) * d}{d + \rho} \qquad eq.4$$

We can rearrange eq. 4 to consolidate all our measurements and pre-specified quantities on the right hand side:

$$\frac{k_m}{V_{max} - d - \rho} = \frac{I}{d + \rho} - \frac{\hat{B}}{d} \qquad eq. 5$$

For convenience, we replace the right side of eq. 5 with A and rearrange terms to arrive at

$$V_{max} = \frac{k_m}{A} + d + \rho \qquad eq. 6$$

Here, *1/A* represents the slope of V_{max} over k_m and equals $\frac{V_{max}-d-\rho}{k_m}$. If we assume V_{max} is greatly larger than the sum of *d* and ρ (Schulze and Lipe 1964; Button 1985; Kovárová-Kovar and Egli, 1998), then *1/A* approaches C uptake affinity, defined as the ratio of V_{max} over k_m (Button, 1993; Nedwell, 1999; Reay et al., 1999). Thus, hereafter we refer to *1/A* as estimated cellobiose-C uptake affinity for *P. fluorescens* at steady-state. Our estimates of C uptake affinity are valuable because they provide insight to how *P. fluorescens* responds physiologically to changing temperature and C availability, without independently quantifying the kinetic parameters V_{max} and k_m.

We estimated CUE by substituting the apparently linear relationship between biomass-C specific respiration rate and temperature (see Statistics below) via eq. 7:

$$CUE_i = \frac{d}{d + \rho} = \frac{d}{d + (\alpha_i + \beta_i * T)} \qquad eq. 7$$

, where *i* corresponds to either 1 or 20 mM cellobiose concentrations in the nutrient medium, α_i is the y-intercept of the regression line relating biomass-C specific respiration rate to temperature at each C availability, and β_i is the slope of the line at each C availability. Using errors obtained from the modeled temperature-dependence of biomass-C specific respiration rates, we calculated

95% confidence envelopes surrounding these CUE estimates. Because the dilution rate of the chemostat bioreactor was relatively constant at 0.128 h^{-1}, changes in CUE estimates were driven by temperature-dependent changes in biomass-C specific respiration rates.

Statistics

We used general linear models to relate biomass-C specific respiration rate and C uptake affinity to temperature and cellobiose concentration in the nutrient solution. Both models consider temperature as a continuous covariate, and cellobiose concentration as a categorical predictor. Because biomass-C specific uptake rates and CUE were estimated using biomass-C specific respiration rates (see section 2.4 and 2.5), we did not fit separate models for these two responses to test the effects of temperature and cellobiose concentration. For the C stable isotope data, we treated temperature as a continuous covariate, and cellobiose concentration and C pool (biomass and CO_2) as categorical predictors. To correct any effect of varying $\delta^{13}C$ of cellobiose across experiments on $\delta^{13}C$ of both biomass and CO_2, we used the differences between $\delta^{13}C$ of cellobiose and $\delta^{13}C$ of biomass, and between $\delta^{13}C$ of cellobiose and $\delta^{13}C$ of CO_2, as dependent variables. We used the Akaike Information Criterion (AIC) index to inform model selection for each of the three response variables. All statistical analyses were performed with R (R version 3.1.2. R development core team).

RESULTS

Microbial biomass-C specific rates: respiration, growth, and uptake

Increasing temperature significantly enhanced biomass-C specific respiration at 1 mM of cellobiose ($p<0.001$), while temperature did not significantly influence biomass-C specific respiration at 20 mM of cellobiose (Figure 1B and Supplementary Table 2). Because our estimation of biomass-C specific uptake was calculated by summing biomass-C specific rates of growth and respiration (see section 2.4) and biomass-C specific growth rate was relatively constant across all chemostat runs (Figure 1A), temperature responses of biomass-C specific uptake rates were similar to those of biomass-C specific respiration at each C availability (Figure 1C). Biomass-C specific uptake rates at both C availabilities were similar at lower temperatures, but diverged with increasing temperature. At 25.5°C, biomass-C specific uptake rate of the microbes at 1 mM cellobiose was almost twice as high as the biomass-C specific uptake rates at 20 mM cellobiose. We calculated that *P.fluorescens* took up, on average across temperatures, 17.4 ± 1.9 and 1.3 ± 0.1 % of the cellobiose-C substrate supplied per hour at 1 and 20 mM, respectively.

Estimates of C uptake affinity and CUE

The interactive effect of temperature and C availability on biomass-C specific respiration rate influenced the estimates of C uptake affinity and CUE. As temperature increased from 11.5 to 25.5˚C, C uptake affinity increased from 1.31 to 4.01 mL h^{-1} mg^{-1} C at 1 mM of cellobiose, but temperature did not influence C uptake affinity at 20 mM of cellobiose (Figure 2 and Supplementary Table 2). Carbon uptake affinity was always higher at 1 mM of cellobiose than at

20 mM, and exhibited no convergence at the lowest temperature in contrast to the biomass-C specific uptake and respiration rates.

Microbial CUE ranged between 0.3 and 0.8, with similar maximum values for both C availabilities (Figure 3). Within the experimental temperature range, microbial CUE decreased nonlinearly with increasing temperature. The nonlinear nature of the relationship between temperature and CUE estimates (see eq.7) was much more pronounced at 1 mM of cellobiose than at 20 mM of cellobiose. This was the consequence of the much greater temperature response of biomass-C specific respiration and the associated relatively large difference between biomass-C specific respiration and growth rates at 1mM cellobiose.

δ^{13}C of C pools and isotopic fractionations

Temperature and C availability independently influenced $\delta^{13}C$ of microbial biomass and respired CO_2 (Table 1 and Supplementary Table 2). When cellobiose was incorporated into microbial biomass and eventually respired as CO_2, large fractionations were apparent at both 1 and 20 mM cellobiose (Figure 4). The value of $\delta^{13}C$ for biomass was always more negative than $\delta^{13}C$ of the cellobiose, and $\delta^{13}C$ of respired CO_2 was even more negative than $\delta^{13}C$ of the biomass at both C availabilities. The degree to which temperature increased both $\delta^{13}C$ of biomass and respired CO_2 was statistically indistinguishable for both cellobiose concentrations, as illustrated by the common slope coefficient depicted in Figure 4 (slope=0.23 ‰ increase in $\delta^{13}C$ per ˚C, p=0.007). The values of $\delta^{13}C$ of biomass and respired CO_2 were always more negative at 1 mM cellobiose than at 20 mM cellobiose. Assuming that *P.fluorescens* did not exude significant amounts of C, standard isotopic mass balance dictates that the $\delta^{13}C$ of C taken up by the bacteria must have

been more negative than the $\delta^{13}C$ of the cellobiose substrate (Supplementary Table 1). This apparent discrimination against ^{13}C-containing cellobiose molecules during uptake was influenced by temperature and C availability. More specifically, the lower the C availability and the lower the temperature, the greater the fractionation during uptake (the differences in $\delta^{13}C$ of cellobiose and $\delta^{13}C$ of microbial biomass in Figure 4). In contrast, fractionation during respiration (the differences in $\delta^{13}C$ of microbial biomass and $\delta^{13}C$ of respired CO_2) did not vary significantly with temperature, as depicted by parallel regression lines in Figure 4.

DISCUSSION

We used chemostats and stable C isotope analyses to quantify rates and isotopic signatures of C flowing from a single C substrate through microbial biomass into CO_2. Using a two C pool dynamic model for substrate and biomass coupled with measurements of pool sizes and fluxes, we estimated how microbial C uptake, C uptake affinity, and CUE change with temperature and C availability. The combination of model and measurements allowed us to infer changes with environmental conditions in underlying microbial physiology. Our results highlight how temperature and C availability influence biomass-C specific rates and microbial ^{13}C discrimination during OC transformations. Below, we discuss the underlying, inferred mechanistic basis for the observed responses to varying temperature and C availability, and implications for interpreting the isotopic signature of ecosystem respiration.

Interactive effects of temperature and C availability on C uptake affinity, biomass-C specific rates, and CUE

We compared microbial C fluxes at 1 and 20 mM cellobiose (current study) with those at 10 mM cellobiose as reported in Lehmeier et al. (2016). Microbial biomass-C specific rates, C uptake affinity, and biomass-C specific C uptake rates at 10 mM cellobiose fall between those reported here at 1 and 20 mM cellobiose, suggesting gradual changes in microbial temperature responses to C availability. The shifts in C uptake affinity and C uptake rates from 1 mM to 10mM to 20 mM are consistent with the notion that microorganisms can sense their environment and adjust their ability to acquire C as substrate availability varies (Williams et al., 1994; Ferenci, 1999; Gresham and Hong, 2015). Indeed, microorganisms possess multiple C transporter systems, each with varying affinity, and these systems' relative expression can change with environmental C concentrations (Williams et al., 1994; Schlösser and Schrempf, 1996; Ferenci, 1999; Kajikawa and Masaki, 1999; Koning et al., 2001; Gresham and Hong, 2015). It is beyond the scope of our study to investigate the exact mechanisms driving shifts in C uptake affinity. However, enhanced C uptake affinity can occur through various mechanisms, including changes in transporter density, microbial surface to volume ratio, membrane thickness, and gene expression of a suite of transporters with different affinity (Aksnes and Egge, 1991; Button, 1993; Kovárová-Kovar and Egli, 1998; Liu and Ferenci, 2001; Gresham and Hong, 2015).

Our system is different from natural systems in that one population of microorganisms grew with surplus C at steady state without interactions with other microbial populations. This distinction allows us to make multiple observations about microbial C flows with only temperature and C availability varying, which cannot be addressed directly using environmental samples. First, our

work reinforces the idea that CUE declines with rising temperature (Steinweg et al., 2008; Allison et al., 2010; Tucker et al., 2013; Wieder et al., 2013; Schindlbacher et al., 2015), which has not always been inferred in studies using environmental samples (Crowther and Bradford 2013; Hagerty et al., 2014). The maximum, convergent CUE around 0.7-0.8 in the current study and in Lehmeier et al. (2016) is consistent with inferred CUE values reported in aquatic systems (Hall and Cotner, 2007; Manzoni et al., 2012), soils (Dijkstra et al., 2011b; Manzoni et al., 2012; Frey et al., 2013; Blagodatskaya et al., 2014; Lee and Schmidt, 2014), and batch culture (Keiblinger et al., 2010). The ceiling value of CUE suggests that inherent limitations might keep microorganisms from achieving higher CUE values. At relatively low temperatures, microbial respiratory costs for growth, maintenance, and foraging are minimized (Rivkin and Legendre, 2001; Apple et al., 2006), likely yielding relatively high CUE. However, we expect that the negative relationship between CUE and temperature breaks down below a certain temperature limit: when microbes enter dormancy at extremely low temperature (i.e. growth rate is null), then CUE defined as growth rate /(growth rate + respiration rate) approaches zero. Thus, we highlight that current conceptions and estimates of CUE are well-defined only when C is flowing into microbial cells and that the negative CUE-temperature relationship may only hold true at temperatures at which microbes are growing.

Second, our results demonstrate that assuming a linear decline of CUE with temperature (Allison et al., 2010; Wieder et al., 2013) may not be appropriate. Indeed, CUE as defined here and in multiple other studies (see Manzoni et al., 2012) must decline with temperature in a nonlinear fashion if respiration increases in a linear fashion as observed in this (Fig. 1B) and a related study (Lehmeier et al. 2016). Our observation of a nonlinear temperature dependence of CUE

estimates emphasizes the need for further research to advance CUE estimates in Earth system models (Ballantyne and Billings in review).

Third, greater temperature responses of respiration and CUE at relatively low C availability, as observed in this study, support the idea that lower resource C:N may be generally linked to higher temperature sensitivity of OC transformations (Fierer et al., 2003; Rumpel and Kögel-Knabner, 2011; Billings and Ballantyne, 2013). We acknowledge that the meaning of resource C:N in our chemostat system (as determined by the ratio of cellobiose-C to mineral N) may be different from that in natural conditions, where microbes have varying access to both organic and inorganic mineral nutrients and resources can be protected physically and chemically. Furthermore, we do not know if changes in C availability caused nutrient limitation or a shift in relative nutrient limitation, common in natural conditions. However if these results are robust and are not masked by the myriad other features at play in natural systems, we would predict that environments with relatively lower C content such as deep, relatively old soil OC and fertilized soils/aquatic systems would be especially vulnerable to OC losses via microbial respiration with warming.

Temperature and C availability effects on microbial C isotope discrimination

Our isotope data suggest that C availability can significantly alter microbial uptake as well as uptake discrimination against ^{13}C-containing compounds. Bigger $\delta^{13}C$ differences between cellobiose and microbial biomass at low C availability can be partly explained by greater C uptake affinity and associated biomass-C specific uptake rates. Shifts from a low C affinity uptake system to a high C uptake affinity system at lower C availability may lead to greater

uptake fractionation, given that transport pathways with different affinities can exhibit varying degrees of C isotope fractionation (Henn and Chapela, 2000). However, even if different C uptake affinity systems have the same isotopic fractionation effect, greater uptake flux rates through a higher C uptake affinity system can enhance the magnitude of ^{13}C discrimination during protein-mediated reactions (Tcherkez et al., 2011). Although these scenarios provide potential clues explaining why stable C uptake fractionation was higher at low C availability, they cannot explain why the degree of microbial ^{13}C discrimination during uptake apparently was not influenced by changes in temperature (Figure 4). Thus, further studies need to examine the degree of coupling between changing C uptake affinity/uptake rate and uptake ^{13}C fractionation under different environmental conditions.

Contrary to Lehmeier et al. (2016), we observed similar respiratory fractionation across temperatures for both cellobiose concentrations, as illustrated by two parallel regression lines in Figure 4. If we assume that this similar respiratory fractionation can be used to interpret $\delta^{13}C$ values of microbial biomass and respired CO_2 in natural samples, our results may help tease apart the effects of multiple, confounding factors driving apparent respiratory C isotope fractionation in environmental samples. In natural samples, respiratory fractionation is a net result of kinetic isotopic effects, preferential substrate utilization, and heterogeneity in microbial community composition (Werth and Kuzyakov, 2010). By controlling the type and supply of substrate, and employing one population of microorganisms, our results approach intrinsic kinetic isotope effects as much as possible with little influence of other factors. Thus, comparison of respiratory fractionation in this study to that in natural samples can be useful for quantifying the magnitude and direction of the confounding factors influencing C isotope

fractionations during microbial C mineralization. Direct comparisons should be made with caution, because the range of respiratory ^{13}C discrimination in this study (from ~5 to ~11‰, the difference between $\delta^{13}C$ of biomass and respired CO_2) is higher than apparent respiratory ^{13}C discrimination reported in other studies of natural samples (Šantrůčková et al., 2000; Werth and Kuzyakov, 2010; Brüggemann et al., 2011). This discrepancy may arise from the relatively high C availability and decoupled C and N sources in our chemostat system. High absolute C availability in chemostats may induce microorganisms to greatly discriminate against ^{13}C during OC transformations, given reduced discrimination against heavy stable isotopes when resources are in relatively scant supply (Fry, 2006). However, our work provides baseline data describing the potential degree of discrimination against ^{13}C during microbially-induced C flows and how it may or may not change with environmental conditions.

Ecosystem scientists frequently assume that heterotrophic microbial ^{13}C discrimination during OC transformations is minimal and that the $\delta^{13}C$ value of soil-respired CO_2 closely reflects the $\delta^{13}C$ of the C source (Ehleringer et al., 2000; Bowling et al., 2008). This assumption may be valid for some scenarios. However, the results reported here demonstrate that microorganisms can discriminate substantially against ^{13}C during uptake and respiration, and that the degree of discrimination during OC uptake may change with C availability and temperature. This is relevant for interpretations of $\delta^{13}C$ of OC substrates in natural environments, microorganisms themselves (their live biomass, and their necromass' contribution to OC), and respired CO_2. These data serve as a cautionary tale for those using $\delta^{13}C$ signatures to infer underlying mechanisms driving those values, or those projecting ecosystem C pools and fluxes.

TABLES AND FIGURES

Table 1. Analysis of covariance results to test the effects of microbial C pools, temperature, and C availability on $\delta^{13}C$ of cellobiose, biomass, and respired CO_2 during cellobiose transformation. Microbial C pools represent biomass and respired CO_2. Significant effects are highlighted in bold.

	df	SS	MS	F value	P value
C pool	1	365.11	365.11	111.6171	**<0.001**
Temperature	1	27.26	27.26	8.3337	**0.007**
C availability	1	54.77	54.77	16.7443	**<0.001**
residuals	22	66.05	3.00		

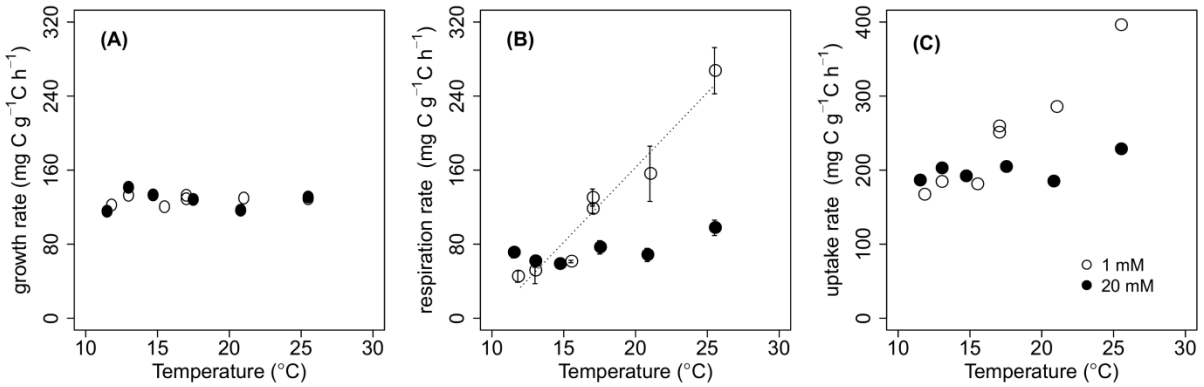

Figure 1. Biomass-C specific rates of growth (A), respiration (B), and uptake (C) with varying temperature for *P. fluorescens* grown in chemostats with cellobiose concentrations in the nutrient solution of either 1 mM (open circles) or 20 mM (closed circles). We imposed a regression line on data points when there was a significant temperature effect on rates (see Supplementary Table 2). Error bars in (B) represent ± 1SE.

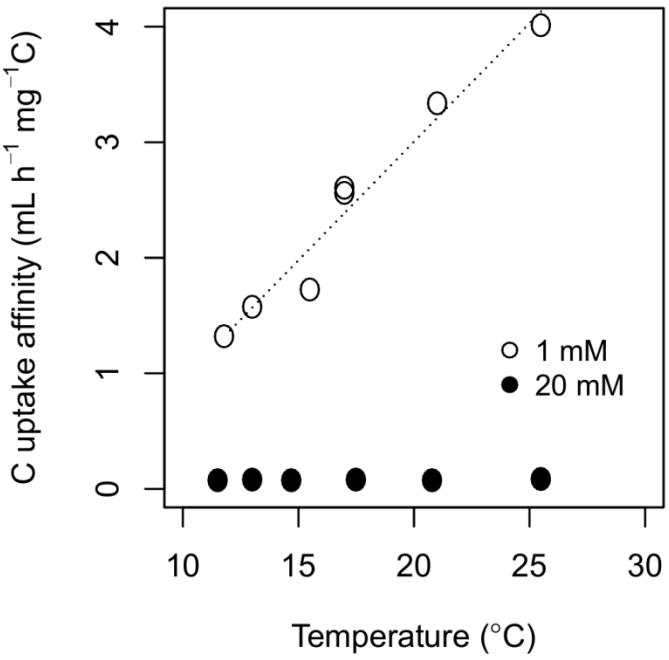

Figure 2. Temperature responses of C uptake affinity, the slope of V_{max} over k_m (see section 2.5.), estimated from the two-pool model of *P. fluorescens* grown in chemostats with cellobiose concentrations in the nutrient solution of either 1 mM (open circles) or 20 mM (closed circles). Model parameters are available in Supplementary Table 2.

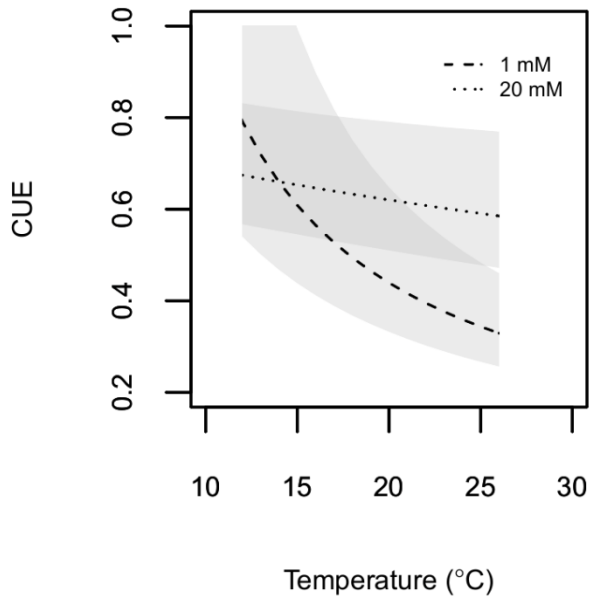

Figure 3. Estimated microbial CUE is plotted as a function of temperature. *P. fluorescens* was grown in chemostats with cellobiose concentrations in the nutrient solution of either1 mM (dashed line) or 20 mM (dotted line). Shaded areas represent 95% confidence envelopes of estimated CUE.

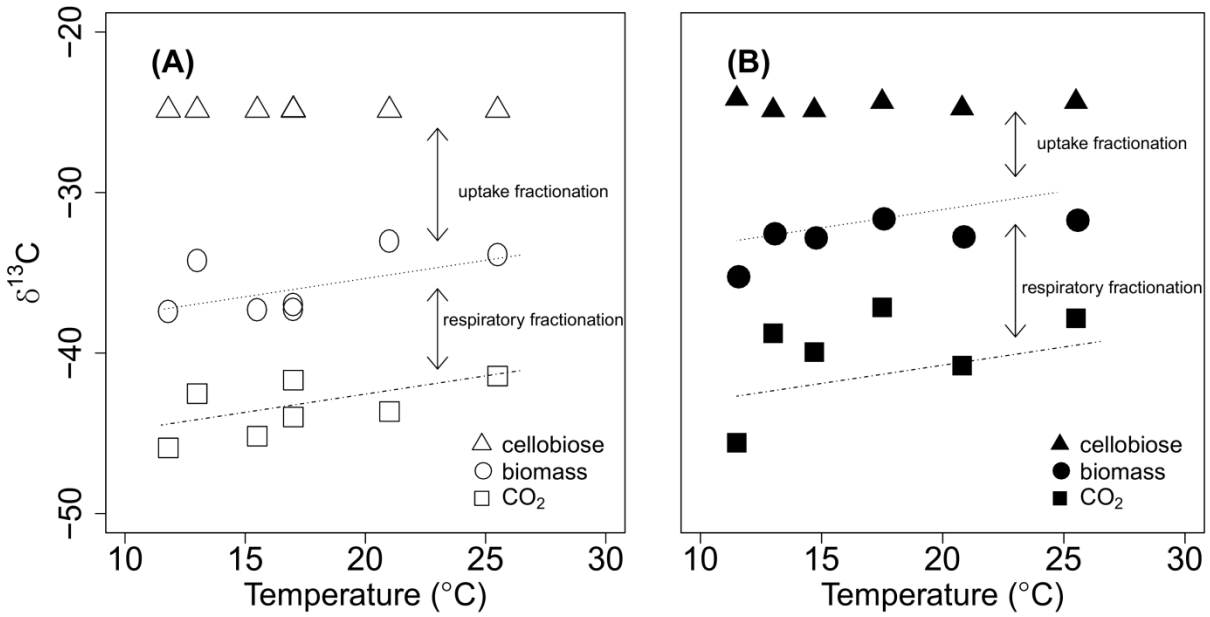

Figure 4. $\delta^{13}C$ values of provided cellobiose (the sole OC source in the system; triangles), and of microbial biomass (circles), and respired CO_2 (squares) of *P. fluorescens* in chemostats with cellobiose concentrations in the nutrient solution of either 1 mM (A) or 20 mM (B) are plotted against bioreactor temperature. Regression lines represent statistically significant, common temperature effects on $\delta^{13}C$ of microbial biomass and respired CO_2 (see Supplementary Table 2). As indicated by arrows, uptake fractionation is the difference in $\delta^{13}C$ values between cellobiose and biomass, and respiratory fractionation is the difference in $\delta^{13}C$ values between biomass and respired CO_2.

REFERENCES

Abraham,W.R., Hesse, C., and Pelz, O. (1998). Ratios of carbon isotopes in microbial lipids as an indicator of substrate usage. *Appl. Envrn. Microb*. 64, 4202–4209.

Aksnes, D. L., and Egge, J. K. (1991). A theoretical model for nutrient uptake in phytoplankton. *Mar. Ecol. Prog. Ser.* 70, 65–72. doi:10.3354/meps070065.

Allison, S. D., Wallenstein, M. D., and Bradford, M. A. (2010). Soil-carbon response to warming dependent on microbial physiology. *Nat. Geosci.* 3, 336–340.

Apple, J.K., del Giorgio, P.A., Kemp, W.M. (2006). Temperature regulation of bacterial production, respiration, and growth efficiency in a temperate salt-marsh estuary. *Aquat. Microb. Ecol.* 43, 243-254.

Bárta, J., Šlajsová, P., Tahovská, K., Picek, T., and Šantrůčková, H. (2013). Different temperature sensitivity and kinetics of soil enzymes indicate seasonal shifts in C, N and P nutrient stoichiometry in acid forest soil. *Biogeochemistry* 117, 525–537. doi:10.1007/s10533-013-9898-1.

Billings, S. A., and Ballantyne, F. (2013). How interactions between microbial resource demands, soil organic matter stoichiometry, and substrate reactivity determine the direction and magnitude of soil respiratory responses to warming. *Glob. Chang. Biol.* 19, 90–102.

Billings, S. A., Tiemann, L. K., Ballantyne IV, F., Lehmeier, C. A., and Min, K. (2015). Investigating microbial transformations of soil organic matter: synthesizing knowledge from disparate fields to guide new experimentation. *Soil* 1, 313–330. doi:10.5194/soil-1-313-2015.

Blagodatskaya, E., Blagodatsky, S., Anderson, T. H., and Kuzyakov, Y. (2014). Microbial

growth and carbon use efficiency in the rhizosphere and root-free soil. *PLoS One* 9. doi:10.1371/journal.pone.0093282.

Blair, N., Leu, A., Muñoz, E., Olsen, J., Kwong, E., and Des Marais, D. (1985). Carbon isotopic fractionation in heterotrophic microbial metabolism. *Appl. Environ. Microbiol.* 50, 996–1001.

Bowling, D.R., Pataki, D.E., and Randerson, J.T. (2008) Carbon isotopes in terrestrial ecosystem pools and CO_2 fluxes. *New Phytol.* 178, 24-40.

Brüggemann, N., Gessler, A., Kayler, Z., Keel, S. G., Badeck, F., Barthel, M., et al. (2011). Carbon allocation and carbon isotope fluxes in the plant-soil-atmosphere continuum: A review. *Biogeosciences* 8, 3457–3489. doi:10.5194/bg-8-3457-2011.

Bull, A. T. (2010). The renaissance of continuous culture in the post-genomics age. *J. Ind. Microbiol. Biotechnol.* 37, 993–1021. doi:10.1007/s10295-010-0816-4.

Button, D. (1985). Kinetics of nutrient-limited transport and microbial growth. *Microbiol.Rev.* 49, 270-297.

Button, D. (1993). Nutrient-limited microbial growth kinetics: overview and recent advances. *Antonie Van Leeuwenhoek* 63, 225–35. doi:10.1007/BF00871220.

Cajal-Medrano, R., and Maske, H. (2005). Growth efficiency and respiration at different growth rates in glucose-limited chemostats with natural marine bacteria populations. *Aquat. Microb. Ecol.* 38, 125–133. doi:10.3354/ame038125.

Chrzanowski, T. H., and Grover, J. P. (2008). Element content of Pseudomonas fluorescens varies with growth rate and temperature: A replicated chemostat study addressing ecological stoichiometry. *Limnol. Oceanogr.* 53, 1242–1251.

Cleveland, C.C., and Liptzin, D. (2007). C:N:P stoichiometry in soils: is there a “Redfield ratio”

for the microbial biomass? *Biogeochemistry 85, 235-252*

Cotner, J. B., Makino, W., and Biddanda, B. (2006). Temperature affects stoichiometry and biochemical composition of Escherichia coli. *Microb. Ecol.* 52, 26–33. doi:10.1007/s00248-006-9040-1.

Crowther, T. W., and Bradford, M.A. (2013). Thermal acclimation in widespread heterotrophic soil microbes. *Ecol. Lett.* 16, 469-477.

Death, A., Notley, L., and Ferenci, T. (1993). Derepression of LamB protein facilitates outer membrane permeation of carbohydrates into Escherichia coli under conditions of nutrient stress. *J. Bacteriol.* 175, 1475–1483.

Dijkstra, P., Blankinship, J. C., Selmants, P. C., Hart, S. C., Koch, G. W., Schwartz, E., et al. (2011a). Probing carbon flux patterns through soil microbial metabolic networks using parallel position-specific tracer labeling. *Soil Biol. Biochem.* 43, 126–132. doi:10.1016/j.soilbio.2010.09.022.

Dijkstra, P., Thomas, S. C., Heinrich, P. L., Koch, G. W., Schwartz, E., and Hungate, B. A. (2011b). Effect of temperature on metabolic activity of intact microbial communities: Evidence for altered metabolic pathway activity but not for increased maintenance respiration and reduced carbon use efficiency. *Soil Biol. Biochem.* 43, 2023–2031. doi:10.1016/j.soilbio.2011.05.018.

Ehleringer, J.R., Buchmann, N., and Flanagan, L.B. (2000) Carbon isotope ratios in belowground carbon cycle processes. *Ecol. Appl.* 10, 412-422l.

Ferenci, T. (1999). "Growth of bacterial cultures" 50 years on: Towards an uncertainty principle instead of constants in bacterial growth kinetics. *Res. Microbiol.* 150, 431–438. doi:10.1016/S0923-2508(99)00114-X.

Ferenci, T. (2008). Bacterial physiology, regulation and mutational adaptation in a chemostat environment. *Adv. Microb. Physiol.* 53, 169–229. doi:10.1016/S0065-2911(07)53003-1.

Fierer, N., Allen, A. S., Schimel, J. P., and Holden, P. (2003). Controls on microbial CO2 production: A comparison of surface and subsurface soil horizons. *Glob. Chang. Biol.* 9, 1322–1332. doi:10.1046/j.1365-2486.2003.00663.x.

Frey, S. D., Lee, J., Melillo, J. M., and Six, J. (2013). The temperature response of soil microbial efficiency and its feedback to climate. *Nat. Clim. Chang.* 3, 395–398. doi:10.1038/nclimate1796.

Fry, B. (2006). *Stable isotope ecology*. New York: Springer.

Gresham, D., and Hong, J. (2015). The Functional Basis of Adaptive Evolution in Chemostats. *FEMS Microbiol. Rev.* 39, 2–16. doi:10.1111/1574-6976.12082.

Hagerty, S. B., van Groenigen, K. J., Allison, S. D., Hungate, B. a., Schwartz, E., Koch, G. W., et al. (2014). Accelerated microbial turnover but constant growth efficiency with warming in soil. *Nat. Clim. Chang.* 4, 3–6. doi:10.1038/nclimate2361.

Hagström, Å., Azam, F., Andersson, A., Wikner, J., and Rassoulzadegan, F. (1988). Microbial loop in an oligotrophic pelagic marine ecosystem: possible roles of cyanobacteria and nanoflagellates in the organic fluxes. *Mar. Ecol. Prog. Ser.* 49, 171–178. doi:10.3354/meps049171.

Hall, E. K., and Cotner, J. B. (2007). Interactive effect of temperature and resources on carbon cycling by freshwater bacterioplankton communities. *Aquat. Microb. Ecol.* 49, 35–45. doi:10.3354/ame01124.

Healey, F. P. (1980). Slope of the Monod equation as an indicator of advantage in nutrient competition. *Microb. Ecol.* 5, 281–286.

Henn, M. R., and Chapela, I. H. (2000). Differential C isotope discrimination by fungi during decomposition of C(3)- and C(4)-derived sucrose. *Appl. Environ. Microbiol.* 66, 4180–4186.

Henn, M. R., Gleixner, G., and Chapela, I. H. (2002). Growth-Dependent Stable Carbon Isotope Fractionation by Basidiomycete Fungi : del13 C Pattern and Physiological Process. 68, 4956–4964. doi:10.1128/AEM.68.10.4956.

Höfle, M. G. (1979). Effects of sudden temperature shifts on pure cultures of four strains of freshwater bacteria. *Microb. Ecol.* 5, 17–26.

Hoskisson, P., and Hobbs, G. (2005). Continuous culture--making a comeback? *Microbiology* 151, 3153–3159. doi:10.1099/mic.0.27924-0.

Kajikawa, H., and Masaki, S. (1999). Cellobiose transport by mixed ruminal bacteria from a Cow. *Appl. Environ. Microbiol.* 65, 2565–2569.

Keiblinger, K. M., Hall, E. K., Wanek, W., Szukics, U., Hammerle, I., Ellersdorfer, G., et al. (2010). The effect of resource quantity and resource stoichiometry on microbial carbon-use-efficiency. *FEMS Microbiol. Ecol.* 73, 430–440. doi:10.1111/j.1574-6941.2010.00912.x.

Koning, S. M., Koning, S. M., Elferink, M. G. L., Elferink, M. G. L., Driessen, A. J. M., and Driessen, A. J. M. (2001). Cellobiose Uptake in the Hyperthermophilic Archaeon. *Microbiology* 183, 4979–4984. doi:10.1128/JB.183.17.4979.

Kovárová-Kovar, K., and Egli, T. (1998). Growth kinetics of suspended microbial cells : From single-substrate-controlled growth to mixed-substrate kinetics. *Microbiol. Mol. Biol. Rev.* 62, 646–666.

Kuzyakov, Y. (2010). Priming effects: Interactions between living and dead organic matter. *Soil Biol. Biochem.* 42, 1363–1371. doi:10.1016/j.soilbio.2010.04.003.

Lee, Z. M., and Schmidt, T. M. (2014). Bacterial growth efficiency varies in soils under different land management practices. *Soil Biol. Biochem.* 69, 282–290. doi:10.1016/j.soilbio.2013.11.012.

Lehmeier, C. A., Ballantyne IV, F., Min, K., and Billings, S. A. (2016). Temperature-mediated changes in microbial carbon use efficiency and 13C discrimination. *Biogeosciences* 13, 3319–3329. doi:10.5194/bgd-12-17367-2015.

Lehmeier, C. A., Min, K., Niehues, N. D., Ballantyne IV, F., and Billings, S. A. (2013). Temperature-mediated changes of exoenzyme-substrate reaction rates and their consequences for the carbon to nitrogen flow ratio of liberated resources. *Soil Biol. Biochem.* 57, 374–382.

Liu, X., and Ferenci, T. (2001). An analysis of multifactorial influences on the transcriptional control of ompF and ompC porin expression under nutrient limitation. *Microbiology* 147, 2981–2989.

Luo, Y., Ahlstrőm A. et al. (2016) Toward more realistic projections of soil carbon dynamics by Earth system models. *Glob. Biogeochem. Cy.* 30, 40-56

Manzoni, S., Taylor, P., Richter, A., Porporato, A., and Ågren, G. I. (2012). Environmental and stoichiometric controls on microbial carbon use efficiency in soils. *New Phytol.* 196, 79–91.

Min, K., Lehmeier, C. A., Ballantyne, F., Tatarko, A., and Billings, S. A. (2014). Differential effects of pH on temperature sensitivity of organic carbon and nitrogen decay. *Soil Biol. Biochem.* 76, 193–200.

Nagata, T. (1986). Carbon and nitrogen content of natural planktonic bacteria. *Appl. Environ. Microbiol.* 52, 28-32.

Nedwell, D. (1999). Effect of low temperature on microbial growth: lowered affinity for

substrates limits growth at low temperature. *FEMS Microbiol. Ecol.* 30, 101–111. doi:10.1111/j.1574-6941.1999.tb00639.x.

Patzer, S. I., and Hantke, K. (1998). The ZnuABC high-affinity zinc uptake system and its regulator Zur in Escherichia coli. *Mol. Microbiol.* 28, 1199–1210. doi:10.1046/j.1365-2958.1998.00883.x.

Penger, J., Conrad, R., and Blaser, M. (2014). Stable carbon isotope fractionation of six strongly fractionating microorganisms is not affected by growth temperature under laboratory conditions. *Geochim. Cosmochim. Acta* 140, 95–105. doi:10.1016/j.gca.2014.05.015.

Pomeroy, L. R., and Wiebe, W. J. (2001). Temperature and substrates as interactive limiting factors for marine heterotrophic bacteria. *Aquat. Microb. Ecol.* 23, 187–204. doi:10.3354/ame023187.

Reay, D. S., Nedwell, D. B., Priddle, J., and Ellis-Evans, J. C. (1999). Temperature dependence of inorganic nitrogen uptake: Reduced affinity for nitrate at suboptimal temperatures in both algae and bacteria. *Appl. Environ. Microbiol.* 65, 2577–2584.

Rhee, G., and Gotham, I. J. (1981). The effect of environmental factors on phytoplankton growth : Temperature and the interactions of temperature with nutrient limitation. *Limnol. Oceanogr*. 26, 635–648.

Richter, D. D., and Markewitz, D. (2013). How deep is soil? *Bioscience* 45, 600–609.

Rivkin, R.B., and Legendre, L. (2001). Biogenic carbon cycling in the upper ocean: effects of microbial respiration. *Science* 291, 2398-2400.

Rumpel, C., and Kögel-Knabner, I. (2011). Deep soil organic matter-a key but poorly understood component of terrestrial C cycle. *Plant Soil* 338, 143–158. doi:10.1007/s11104-010-0391-5.

Šantrůčková, H., Bird, M. I., and Lloyd, J. (2000). Microbial processes and carbon-isotope

fractionation in tropical and temperate grassland soils. *Funct. Ecol.* 14, 108–114. doi:10.1046/j.1365-2435.2000.00402.x.

Schindlbacher, A., Schnecker. J., Takriti, M., Borken, W., and Wanek, W. (2015). Microbial physioloby and soil CO2 efflux after 9 years of soil warming in a temperate forest – no indications for thermal adaptations. *Glob. Chang. Biol.* 21, 4265-4277.

Schlösser, A., and Schrempf, H. (1996). A lipid-anchored binding protein is a component of an ATP-dependent cellobiose/cellotriose-transport system from the cellulose degrader Streptomyces reticuli. *Eur. J. Biochem.* 242, 332–338.

Schulze., K.L., and Lipe, R.S. (1964). Relationship between substrate concentration, growth rate, and respiration rate of Escherichia coli in continuous culture. *Archiv. Mikrobiol.* 48. 1-20.

Smith, H. L., and Waltman, P. (1995). *The theory of the chemostat: Dynamics of microbial competition*. Cambridge University Press.

Steinweg, J.M., Plante, A.F., Conant, R.T., Paul, E.A., and Tanaka, D.L. (2008). Patterns of substrate utilization during long-term incubations at different temperatures. *Soil Biol. Biochem.* 40, 2722-2728.

Stumm, W., and Morgan, J. J. (1981). *Aquatic chemistry: an introduction emphasizing chemical equilibria in natural waters*. New York: John Wiley & Sons.

Tang, J., and Riley, W. J. (2015). Weaker soil carbon–climate feedbacks resulting from microbial and abiotic interactions. *Nat. Clim. Chang.* 5, 56–60. doi:10.1038/nclimate2438.

Tcherkez, G., Mahe, A., and Hodges, M. (2011). 12C/13C fractionations in plant primary metabolism. *Trends Plant Sci.* 16, 499–506. doi:10.1016/j.tplants.2011.05.010.

Tucker, C.L., Bell, J., Pendall, E., and Ogle, K. (2013). Does declining carbon-use efficiency explain thermal acclimation of soil respiration with warming? *Glob. Chang. Biol.* 19, 252-

263.

Werth, M., and Kuzyakov, Y. (2010). 13C fractionation at the root-microorganisms-soil interface: A review and outlook for partitioning studies. *Soil Biol. Biochem.* 42, 1372–1384. doi:10.1016/j.soilbio.2010.04.009.

Wieder, W. R., Bonan, G. B., and Allison, S. D. (2013). Global soil carbon projections are improved by modelling microbial processes. *Nat. Clim. Chang.* 3, 909–912. doi:10.1038/nclimate1951.

Williams, S. G., Greenwood, J. A., and Jones, C. W. (1994). The effect of nutrient limitation on glycerol uptake and metabolism in continuous cultures of Pseudomonas aeruginosa. *Microbiology* 140, 2961–2569.

Xu, X., Schimel, J. P., Thornton, P. E., Song, X., Yuan, F., and Goswami, S. (2014). Substrate and environmental controls on microbial assimilation of soil organic carbon: a framework for Earth system models. *Ecol. Lett.* 17, 547–555. doi:10.1111/ele.12254.

CHAPTER 3: Temperature sensitivity of microbial exo-enzyme activities and respiration across diverse timescales

ABSTRACT

Understanding how temperature sensitivities of soil microbial activities will vary across time is critical for accurate projections of climate. Here we explore the resistance, resilience, and susceptibility of temperature sensitivities of microbial exo-enzyme activities and respiration across diverse timescales, and assess potential mechanisms driving these patterns. All biomass-specific rates exhibited resistant temperature sensitivities across time, while those expressed as soil mass-specific rates exhibited resistance or resilience depending on the flux rate assessed. Bacterial and fungal community composition all differed across short- and long-term exposure to different temperature regimes, regardless of microbial functional responses. Resistant temperature sensitivities of biomass-specific rates in spite of distinct community composition imply invariant microbial temperature responses at a fundamental level. Our results also highlight how the unit of observation can drive the diverse narratives describing microbial temperature responses.

INTRODUCTION

Microbial decomposition of soil organic matter and subsequent CO_2 losses is one of the key components of carbon (C) cycling in terrestrial ecosystems (Schimel 1995; Subke *et al.* 2006). Increasing temperature promotes these microbial activities (Zogg *et al.* 1997; Baldrian *et al.* 2013; Lehmeier *et al.* 2013, 2016), accelerating anthropogenic increases in atmospheric CO_2 and associated climate change. Earth-system models often employ a fixed value of temperature sensitivity (the relative enhancement in process rates to temperature, E_a or Q_{10}) of microbial activities to project microbial contribution to the future climate (Sihi *et al.* 2016). However, evidence indicates that temperature sensitivity of soil respiration, comprised of plant- and microbial respiration, can vary with the duration of warming (Luo *et al.* 2001; Knorr *et al.* 2005; Craine *et al.* 2013), questining the stability of temperature sensitivity of microbial activities in a warmer world. We, therefore, assess time-dependent features in the temperature sensitivity of microbial activities and potential biological mechanisms driving these patterns.

We use the concepts of resistance, resilience, and susceptibility to explore temperature sensitivity of microbial exo-enzyme activities and CO_2 losses across time. Dynamic ecosystem models consider a system to express one of these phenomena in response to disturbance (Pimm 1984; Shade *et al.* 2012). Here, we consider changing temperature regime as a disturbance for soil microbial communities, and temperature sensitivity of microbial activities as a parameter of interest. We define a resistant system as maintaining a consistent temperature sensitivity of microbial activities to disturbance across time (Fig. 1 a), a resilient system as changing its temperature sensitivities but returning to its original state at some later time (Fig. 1 b), and a

susceptible system as one in which microbial temperature sensitivities change in response to disturbance but exhibit no tendency to return to the original state (Fig. 1 c). These concepts of temperature sensitivity can be investigated by invoking Arrhenius plots (log transformed activity vs the inverse of the temperature at which the reaction proceeds; Fig. 1 d-f). Arrhenius plot is a common means of exploring temperature responses of ecosystem functions of interest (Davidson & Janssens 2006; Sierra 2011; Lehmeier *et al.* 2013; Min *et al.* 2014), because the slope in an Arrhenius plot represents an estimate of the temperature sensitivity of the reaction. Unlike most warming studies focusing on the *absolute rates* of CO_2 losses between control and warmed plots (Rustad *et al.* 2001; Hartley *et al.* 2007; Bradford *et al.* 2008; Romero-olivares *et al.* 2017), our study, thus, highlights how *temperature sensitivities* of multiple microbial activities change across diverse timescales in Arrhenius plots.

Resistance of temperature sensitivity across time is expressed via similar Arrhenius plot slopes (Fig. 1 d). This may occur when there is no change in microbial functional responses to temperature or community composition across the duration of altered temperature regime, or when distinct microbial communities have redundant functional responses (Allison & Martiny 2008; Schimel & Schaeffer 2012; Graham *et al.* 2016). Resilient temperature sensitivity of microbial activities is illustrated via similar Arrhenius plot slopes at initial and final time points, but a different slope at an intermediate time point (Fig. 1 e). Plasticity of microbial physiology can endow microbial communities with great ability to cope with environmental changes (Shade *et al.* 2012), potentially prompting the "bouncing" patterns in Arrhenius plots. Or, microbial resilience can accompany shifts in community composition, with initial and final microbial

communities exhibiting similar functional traits (Allison & Martiny 2008; Schimel & Schaeffer 2012; Graham *et al.* 2016).

Microbial communities with susceptible temperature sensitivities would exhibit distinct slopes of Arrhenius plots at initial and final time points (Fig. 1 f). Susceptibility of temperature sensitivities of microbial activities might be explained by changes in substrate availability, total microbial biomass, biomass-specific responses, or microbial community composition (Joergensen *et al.* 1990; Kirschbaum 2004; Hartley *et al.* 2007; Schimel & Schaeffer 2012; Bradford 2013). Note that we must interpret data suggesting one type of temporal pattern in microbial temperature sensitivity cautiously, because we cannot assume that the study's duration and the frequency of measurement is sufficient to capture any potential change in the microbial activities with time. For example, susceptible microbial temperature sensitivity may be resilient over longer time frames. Indeed, it is difficult to design studies that assess how microbial communities respond to long-term environmental changes with enough observation frequency.

We devised an experiment to test resistance, resilience, and susceptibility of the temperature sensitivity of soil microbial C cycling across diverse timescales. We used soils along a climate transect where soil microbial communities were subjected to long-term temperature regime differences (timescales of centuries), and exposed these soils to short-term temperature manipulation (timescales of days to months). In this way, we could quantify whether temperature sensitivity of these soils' microbial C cycling was resistant, resilient or susceptible to incubation temperature regime change, both across incubation timescales and across longer timescales of exposure *in situ*. Previous works at the same sites reported that temperature sensitivity of

microbial CO_2 losses did not change (Laganière *et al.* 2015) or increased in soils with warmer temperature regime across the climate transect (Podrebarac *et al.* 2016). Because these studies employed *cumulative* CO_2 losses, it remains still unclear how microbial process rates related to C cycling and their temperature sensitivity will change with time, and what mechanisms contribute to the apparent temperature sensitivity of microbial respiration. Thus, we assess the stability of temperature sensitivity of microbial C cycling rates and potential mechanisms driving microbial temperature responses across time. We minimize the effects of substrate availability on microbial temperature responses and focus on biological mechanisms in the context of biomass and community composition. We address the following questions:

1) across diverse timescales, how do temperature sensitivities of multiple microbial process rates change in a system where substrate availability is likely not limiting?
2) are any changes in temperature sensitivities of microbial C cycling rates across time associated with modified total microbial biomass, biomass-specific responses, or community composition?

MATERIALS AND METHODS

Exploiting in situ and laboratory approaches to investigate diverse timescales of temperature responses

We explore diverse timescales of microbial temperature responses by employing a latitudinal gradient in Eastern Canada's boreal forests and laboratory incubations of soils from these forests at three different temperatures. Our laboratory incubations provided an experimental timescale of days (9, 34, 55, and 84 days), which we labeled as t_9, t_{34}, t_{55}, and t_{84}, respectively. Because forests along the gradient experience similar environmental factors except for a mean annual temperature (MAT) difference of ~5°C (Ziegler *et al.* 2017), we invoked space-for-time substitution; we considered latitudinal regions along the gradient as a long-term experiment during which ecosystems and their microbial communities have been exposed to distinct temperature regimes (timescales of centuries). We assigned the northern-most region the identifier T_1, those from the intermediate latitude T_2, and those from the southern-most region T_3, such that increasing number represents higher temperature regime. Thus, by combining the incubation time with distinct *in situ* temperature regimes, we can assess the temporal dynamics of microbial temperature sensitivities across both short- and longer timescales.

Study site, soil collection, incubation

The Newfoundland and Labrador Boreal Ecosystem Latitude Transect spans 6° of latitude (47°51'N ~ 53°42'N, 57°02'W ~ 59°15'W), along which three experimental regions exposed to distinct MAT have been established (Table S1). Greater mean annual precipitation and rates of

litterfall in the southern-most region are balanced by higher potential evapotranspiration and losses of soil C, generating similar conditions of water availability and soil organic C content across the entire transect (Ziegler *et al.* 2017). All regions possess mesic, organic-rich soils (Spodosols) and are dominated by balsam fir (*Abies balsamea* (L.) Mill.). We collected soils from three replicated forests within each region in June-July 2014. During the field campaign, we moved from south to north such that soil collections took place at approximately similar ecological times of the growing season. In each forest, we set up a 40 m transect, along which we collected the top 20 cm of the organic horizon every 10 m. Soils were shipped to the University of Kansas in a cooler and maintained at 4°C until initiating the incubation.

After removing visible plant roots, we separated each sample into the O_i and O_{ea} sub-horizons. The five samples of O_i and O_{ea} from the 40 m transect were homogenized individually and pooled to produce one O_i and one O_{ea} horizon for each forest. We rebuilt soil cores in 15 ml conical tubes by overlaying O_i onto O_{ea} at 1:5 (w/w), the same ratio found in the field (Podrebarac *et al.* 2016). We prepared 8 tubes in a jar at a given forest and incubation temperature to allow destructive sampling of the tubes over time. We incubated these jars containing 8 tubes each, at 5, 15, and 25°C for a maximum of 84 days (3 regions x 3 replicate forests x 3 incubation temperatures = 27 jars). During the incubation, water content of soil in each tube was maintained at 70% of water holding capacity and the jars were covered with parafilm to minimize water loss while allowing gas movement.

Microbial respiration, exo-enzyme activities, and biomass-C

We determined microbial CO_2 respiration, exo-enzyme activities, and microbial biomass-C four times during the incubation (on days 9, 34, 55, and 84 of the incubation). On each sampling date, we quantified microbial CO_2 loss and then removed two rebuilt soil cores (tubes) from each jar, one for exo-enzyme activity assays and the other for quantifying microbial biomass-C. Rates of respiration and exo-enzyme activities were determined at soil mass-specific (process rate per g dry soil) and biomass-specific rates (process rate per g C microbial biomass).

To quantify microbial respiration, we collected 14 ml of headspace gas prior to and 3 h after closing jars with gas-tight lids, and injected the gas samples into pre-evacuated vials capped with gas-tight septa. CO_2 concentrations were determined using a thermal conductivity detector on a gas chromatograph (Varian CP3800, Agilent, Santa Clara, USA) and the differences in CO_2 concentrations between initial and 3 h-later samples were employed to calculate microbial respiration rates.

Five hydrolytic exo-enzyme activities were determined in this study (see Supplementary Information 1 for details): β-glucosidase (BG), N-acetyl-β-D-glucosaminidase (NAG), leucine amino peptidase (LAP), acid phosphatase (AP), and cellobiohydrolase (CB). At each sampling time point, microplates containing samples, controls, and corresponding standards were incubated at 5, 15, and 25°C and monitored for fluorescence emission four times across 1.5 h to quantify a linear increase in enzyme-catalyzed fluorescence emission with time (Synergy HT, Biotek, Winooski, USA).

To permit calculations of microbial process rates per unit microbial biomass-C, we subjected soil samples to chloroform extraction method modified from Vance *et al*. (1987). We mixed two 1 g sub-samples (one control and one chloroform extracted) with 5 ml of 0.5 M K_2SO_4 and added 60 µl of amelyne-stabilized liquid chloroform to the chloroform samples. After shaking at 200 rpm for 4 h, subsamples were filtered using 1.5 µm pore-size glass microfiber filters (Sartorius, Göttingen, Germany). Extract C was converted to inorganic C after alkaline persulfate digestion and analyzed on a flow injection analyzer (Lachat, Hach, Loveland, USA). The difference in extractable inorganic C between the control and the chloroform treatment was considered extractable microbial biomass-C (hereafter, called microbial biomass).

Microbial community composition

Microbial community composition was assessed three times: once prior to the incubation and twice during the incubation (days 9 and 84) for each region's three forests. Field DNA samples were extracted from Lifeguard-fixed soils, collected from the full depth of the organic horizon (Qiagen, Carlsbad, USA). Microbial DNA during the incubation was extracted from 0.25 g of each well-mixed soil sub-sample using the MoBio Power Soil Kit (Qiagen, Carlsbad, USA). We amplified bacterial 16S rRNA (V3-V4 region) and fungal ITS2 region (see SI 2) and sequenced resulting samples on an Illumina MiSeq sequencer (Illumina, San Diego, USA) at the Integrated Genomic Facility at Kansas State University.

Data analysis

We fit the Arrhenius model ($V=A*e^{Ea/RT}$) to exo-enzyme activities and respiration to assess temperature sensitivities of these process rates over time. In the model, *V* stands for microbial

process rates, A for pre-exponential factor, E_a for temperature sensitivity of the reaction, R for gas constant, and T for reaction temperature in Kelvin. To compare temperature sensitivities of exo-enzyme activities and respiration across time, we used a mixed-effects model. First, we fit a full model with log transformed values as dependent variables, region and incubation time as independent variables, jar index as a random effect, and incubation temperature as a covariate. Then, we selected the most parsimonious model generating the lowest Akaike Information Criteria (AIC). When the most parsimonious model included a significant three-way interaction (region x incubation time x incubation temperature), an indicator that at least one slope of the Arrhenius plot is different from other slopes, we used R's general linear hypothesis test function to compare slopes of the Arrhenius models. To obtain ecologically relevant meaning, we only compared slopes of the Arrhenius models within region with different incubation time, and across regions with the same incubation time. After log-transforming microbial biomass to meet the assumption of a normal distribution, we fit a full mixed effect model with biomass as a dependent variable, region, incubation time, and incubation temperature as independent variables, and jar index as a random effect. The most parsimonious model was selected for biomass data using AIC index. Statistical analyses were performed in R at α of 0.05 (R 3.1.2. R development core team).

After checking sequenced data for quality (SI 3), we calculated both weighted and unweighted UniFrac distance for bacteria and Bray Curtis distance for fungi to compare community composition across region, incubation time, and incubation temperature. After collapsing replicated forest samples, we performed PERMANOVA and visualized the distance matrix using

Canonical Analysis of Principal Coordinates (Anderson & Willis 2003) in PRIMER 7 (version 7.0.5) and the PERMANOVA+ add on (version 1.0.3).

RESULTS

Respiration as biomass-specific and soil mass-specific rates

There was no significant interaction effect of region, incubation time, and incubation temperature on microbial respiration regardless of the unit of measure, implying resistant temperature sensitivities (Table S2-3). The E_a for biomass- and soil mass-specific respiration rates did not significantly vary across diverse timescales (Fig. 2 a-b). When we pooled all data, mean values of E_a for biomass- and soil mass-specific respiration rates were 74 ± 13 and 53 ± 11 kJ mol^{-1}, respectively. Such resistance of temperature sensitivities is illustrated by common regression slopes in the Arrhenius plots (Fig. 2 c-d).

Exo-enzyme activities

The three-way interaction among region, incubation time, and incubation temperature did not exert a significant influence on biomass-specific rates of exo-enzymes, either (Table S4-8). The values of E_a for biomass-specific activities were resistant across time, yielding a mean of 70 ± 7, 67 ± 7, 42 ± 13, 57 ± 7, and 82 ± 9 kJ mol^{-1} for BG, NAG, LAP, AP, and CB, respectively (Fig. 3 a-e). At a given exo-enzyme, the slopes of Arrhenius plots were statistically not different each other when expressed as biomass-specific rates (Fig. 3 f-j).

In contrast with the apparently resistant temperature sensitivities of biomass-specific exo-enzyme activities, those expressed on a per g soil basis exhibited both resistance and resilience (Fig. 4). Exo-enzymes BG, NAG, LAP, and AP exhibited resistant temperature sensitivities regardless of the timescale of inquiry: we found no significant three-way interaction of region, incubation time, and incubation temperature for BG, NAG, LAP, and AP, indicating statistically identical temperature sensitivities across incubation time and regions (i.e. resistance; 53 ± 4, 50 ± 4, 24 ± 12, and 38 ± 5 kJ mol^{-1}, respectively, Fig. 4 a-d, Table S9-12). The Arrhenius plots for soil mass-specific BG, NAG, LAP, and AP rates yielded common regression slopes (Fig. 4 f-i), demonstrating resistance. Though the three-way interaction among region, incubation time, and incubation temperature was not significant for NAG, this interaction was marginally significant (P=0.053); general linear hypothesis testing suggests that the slope in the mid-latitude at day 34 was different from that at day 84 (P<0.01).

However, temperature sensitivity of CB activities on a per g soil basis exhibited resilience (Fig. 4 e). The three-way interaction among region, incubation time, and incubation temperature significantly influenced soil mass-specific CB activities (p=0.006, Table S13). The values of E_a significantly changed during the short-term incubation time in the mid-latitude region (T_2). Temperature sensitivity of soil mass-specific CB activities at T_2t_{84} (11 ± 23 kJ mol^{-1}; green diamond in Fig. 4 e) was significantly lower than those at T_2t_{34} (93 ± 14 kJ mol^{-1}, p<0.001, green circle in Fig. 4 e). Also, the E_a values for CB changed across regions at the incubation day of 84 days (t_{84}). Temperature sensitivity of soil mass-specific CB activities at T_1t_{84} (91 ± 11 kJ mol^{-1}, p=0.001, blue diamond in Fig. 4 e) was significantly higher than those at T_2t_{84} (11 ± 23 kJ mol^{-1};

green diamond in Fig. 4 e). In the Arrhenius plots, significant differences in the slopes across time were highlighted in insets (Fig. 4 j).

Microbial biomass and community composition

Microbial biomass was significantly influenced by region ($p=0.001$), incubation temperature ($p<0.001$), and incubation time ($p<0.001$; Table 1). Microbial biomass in the northern-most latitude was greater than that in the mid-($p<0.001$) and southern-most latitude ($p=0.031$). At incubation temperature of 25°C, microbial biomass was lower than that at 5 ($p=0.032$) and 15°C ($p=0.014$). Microbial biomass did not vary significantly during the initial three incubation time (t_9, t_{34}, t_{55}) but at the end of incubation (t_{84}) it significantly decreased compared to t_9 ($p<0.001$), t_{34} ($p=0.005$), and t_{55} ($p=0.020$).

Both bacterial and fungal communities varied in community composition across regions and incubation time (Fig. 5). Regions with distinct temperature regime harbored significantly different bacterial ($p= 0.001$) and fungal communities ($p<0.001$), as illustrated by the cluster of the same color in Fig.5. Within regions, incubation time changed bacterial ($p<0.01$ for southern-most and northern-most regions, $p=0.79$ for mid-latitude region) and fungal community composition ($p<0.01$ for northern-most and southern-most regions, $p=0.2023$ for mid-latitude region). Incubation temperature did not significantly influence microbial community composition. The relative abundance of dominant phyla (>0.1% of total reads) varied across regions and incubation time (Fig. S1).

DISCUSSION

Improving our understanding of microbial temperature responses across time is key to reducing uncertainty in model projections of terrestrial feedback to climate change. Here we invoke the concepts of resistance, resilience, and susceptibility and integrate these concepts with Arrhenius plots to describe changes across time in soil microbial C cycling. This study advances our knowledge about temperature response of microbial C cycling in two ways. First, we demonstrate resistant temperature sensitivities of biomass-specific microbial activities in boreal forest soils across diverse timescales. If robust across ecosystems, this finding may be important for those attempting to incorporate temporal variation in microbial responses into microbial modules in Earth system models. Second, we find that two commonly used units of observation for microbial C cycling flux rates result in contrasting interpretations of temporal dynamics of temperature sensitivities. This finding stresses that any discrepancy between the stories revealed by the units of observation can help us unravel the mechanisms behind the apparent temperature responses of microbial activities.

Resistant temperature sensitivities of diverse microbial functions per unit biomass

Distinct microbial communities expressed similar temperature sensitivities of key biomass-specific process rates across diverse timescales, when substrate availability was not likely limiting. This finding indicates that, regardless of the timescale of exposure to distinct temperature regimes and distinct communities, microbial temperature sensitivities exhibit common slopes in Arrhenius plots. Such resistance in temperature sensitivity is also observed in

other studies of respiration, both plant and microbial. Heskel *et al.* (2016) recently demonstrated that temperature responses of leaf respiration expressed as a dry-mass basis are universal across biomes. Similarly, temperature responses of microbial respiration appear resistant in both short- and long-term warming studies. For example, short-term warming of days to months did not change temperature sensitivity of microbial respiration on a per unit biomass (Malcolm *et al.* 2009; Bradford *et al.* 2010). Schindlbacher *et al.* (2015) report that temperature sensitivity of biomass-specific microbial respiration did not differ between control and 9 years of warmed temperate forest soils. Our work thus adds to a growing body of evidence that temperature responses of microbial resource allocation to exo-enzymes and CO_2 loss are conserved at a fundamental, cellular level across timescales of days to centuries. If resistant temperature sensitivity of microbial C cycling is robust across ecosystems, an invariant temperature response of microbial CO_2 release for microbially-explicit Earth-system models may be reasonable.

Observations in the current study suggest that these microbial communities may be functionally redundant (Allison & Martiny 2008) in their temperature responses. Indeed, incorporating microbial community structure improves model prediction of ecosystem processes in only 29% of datasets (Graham *et al.* 2016), and community structure only influences functions when microbes vary in functional type and times of activity (Schimel & Schaeffer 2012). Resistant temperature sensitivity in spite of distinct microbial community compositions may derive from microbes' widely distributed ability to produce common exo-enzymes and to respire CO_2 (Graham *et al.* 2016), and from the wide temperature range (diel, seasonal) that soil microbial communities typically experience (Wallenstein & Hall 2012). In this study, we chose exo-enzymes commonly used for the exploration of microbial potential decomposition of soil organic

matter (German *et al.* 2012; Jing *et al.* 2014). Given ubiquitous microbial demand for nutrients, it is feasible that distinct microbial communities produce exo-enzymes with convergent temperature responses. Further, incubation temperatures in the current study encompassed temperatures experienced by microbes in these soils *in situ*; soils at our study sites all experience monthly average temperature highs during the growing season of ~18°C (http://climate.weather.gc.ca), roughly similar to our mid- to high incubation temperatures (15 and 25°C). Thus, microbial communities may already have adapted to temperature range in this study and respond to the incubation temperatures in a similar way. Considering the ubiquity of microbial nutrient demands and the cosmopolitan nature of the exo-enzymes we assessed, as well as the field-relevant temperature range of our incubation experiment, it is perhaps not surprising that we observed convergent temperature responses of these biogeochemical processes in soils.

Yet, resistant temperature sensitivity of multiple microbial activities should not be interpreted to mean that microbial C cycling in a warmer world will be easily predictable using one Arrhenius plot. This becomes evident when we consider the complex interactions within any ecosystem. For example, an important feature not considered here is that prolonged warming can modify substrate availability in the field. This can occur via changes in the duration of the growing season, plant productivity and, over the long-term, types of vegetation (Kirschbaum 2004; Knorr *et al.* 2005; Hartley *et al.* 2007). Indeed, across our latitudinal study sites the rates of mean annual litter input differ substantially in spite of the similar soil C content (Ziegler *et al.* 2017). Also, *in situ* soil respiration at these sites exhibits different temperature sensitivities (Podrebarac *et al.* 2016). Though the current study suggests that microbial modules in Earth-system models may consider temperature sensitivity of multiple microbial processes to be constant across time,

we need to be cautious when up-scaling microbial process rates to the ecosystem level, given complex feedbacks among plants, microbes, and climate.

Observation units drive our interpretation of the temperature sensitivity of microbial C cycling

The soil mass-specific vs. biomass-specific units employed in this study convey distinct ecological messages. The soil mass-specific rate is a particularly useful approach when comparing temperature responses of microbial process rates across different ecosystems (Wallenstein *et al.* 2009; German *et al.* 2012; Machmuller *et al.* 2016; Robinson *et al.* 2017). Soil mass-specific rates reveal ecosystems' aggregated responses while integrating any changes in microbial biomass size. In contrast, biomass-specific rates enable us to explore more fundamental temperature responses of microbial behavior (Malcolm *et al.* 2009; Bradford *et al.* 2010; Schindlbacher *et al.* 2015). As such, when the two units have different temperature responses, we can begin to explore the mechanistic contributors to any discrepancies in apparent temperature responses of microbial activities.

In literature, the observational unit seems to influence the interpretation of microbial temperature sensitivity over time, although no studies employed the two units simultaneously. At soil mass-specific rates, temperature sensitivity of microbial exo-enzyme activities and respiration appeared to be resistant (German *et al.* 2012), resilient (Machmuller *et al.* 2016), or susceptible (Wallenstein *et al.* 2009; German *et al.* 2012; Machmuller *et al.* 2016; Robinson *et al.* 2017) across time. In contrast, temperature sensitivity of biomass-specific respiration seemed resistant in many studies (Malcolm *et al.* 2009; Bradford *et al.* 2010; Schindlbacher *et al.* 2015). This

suggests that temperature response of microbial biomass across time can offer insight for apparent temperature sensitivity of microbial C fluxes.

We demonstrated that soil mass-and biomass-specific units exhibit different temporal patterns in temperature sensitivity of a key C-releasing exo-enzyme (CB), and potentially an exo-enzyme linked to N availability (NAG) as well. In contrast, temperature sensitivities of all other exo-enzymes and CO_2 loss rates exhibited resistance regardless of which unit we used. Differences in microbial biomass or community composition across time cannot explain the apparent resilience of CB and NAG temperature sensitivity across time. If changes in total biomass or community composition had influenced the observed pattern of resilience at soil mass-specific rates and resistance at biomass-specific rates of CB and NAG, then we would have observed the same pattern for all other enzymes and respiration, which was not the case. The data imply that microbes in the middle latitude forests produced more of these two exo-enzymes to meet their C and N demand at relatively cold incubation temperatures, for reasons that remain unclear. We suggest that explicit inquiry into microbial resource allocation to CB, NAG, and their isozymes as temperature varies may be fruitful for understanding ecosystem-scale microbial functioning (Davidson & Janssens 2006; Wallenstein *et al.* 2009; Khalili *et al.* 2011). By explicitly contrasting these two observational units within the same experiment, we highlight some microbial exo-enzymes likely important for understanding how microbial resource allocation may shift across time with varying temperature.

CONCLUSIONS

This study demonstrates how Arrhenius plots can be used to explore soil microbial communities' resistance, resilience, or susceptibility of temperature sensitivity over diverse timescales. Soil mass-specific rates revealed both resilience and resistance of temperature sensitivities of exo-enzyme activities, and resistance of temperature sensitivity of CO_2 loss rates. These responses differed from temperature responses expressed at biomass-specific rates, which demonstrated a resistant or invariant relationship between temperature and microbial production of five key enzymes and CO_2 efflux. This resistance in temperature sensitivity, expressed across timescales of months to centuries, occurred in spite of distinct composition of microbial communities. We suggest that microbial process modelers can invoke time-independent temperature responses of key microbial exo-enzymes and CO_2 losses, particularly when employing biomass-specific rates. We also suggest that empiricists pursuing investigations of microbial process rates relevant to terrestrial C cycling employ biomass-specific flux rates to promote an understanding of fundamental microbial responses to temperature. Such work can construct needed scaffolding on which we can build projections of terrestrial feedbacks to climate.

TABLES AND FIGURES

Table 1. We performed a mixed effect model with log-transformed microbial biomass as response variable, incubation temperature, region, and incubation time as independent variables, and jar index as a random effect. The most parsimonious model was selected using the Akaike Information Criterion.

	df	F value	P value
incubation temperature	2	10.412	<0.001
region	2	7.309	0.001
incubation time	3	28.282	<0.001
incubation temperature * incubation time	6	3.097	0.008
residuals	92		

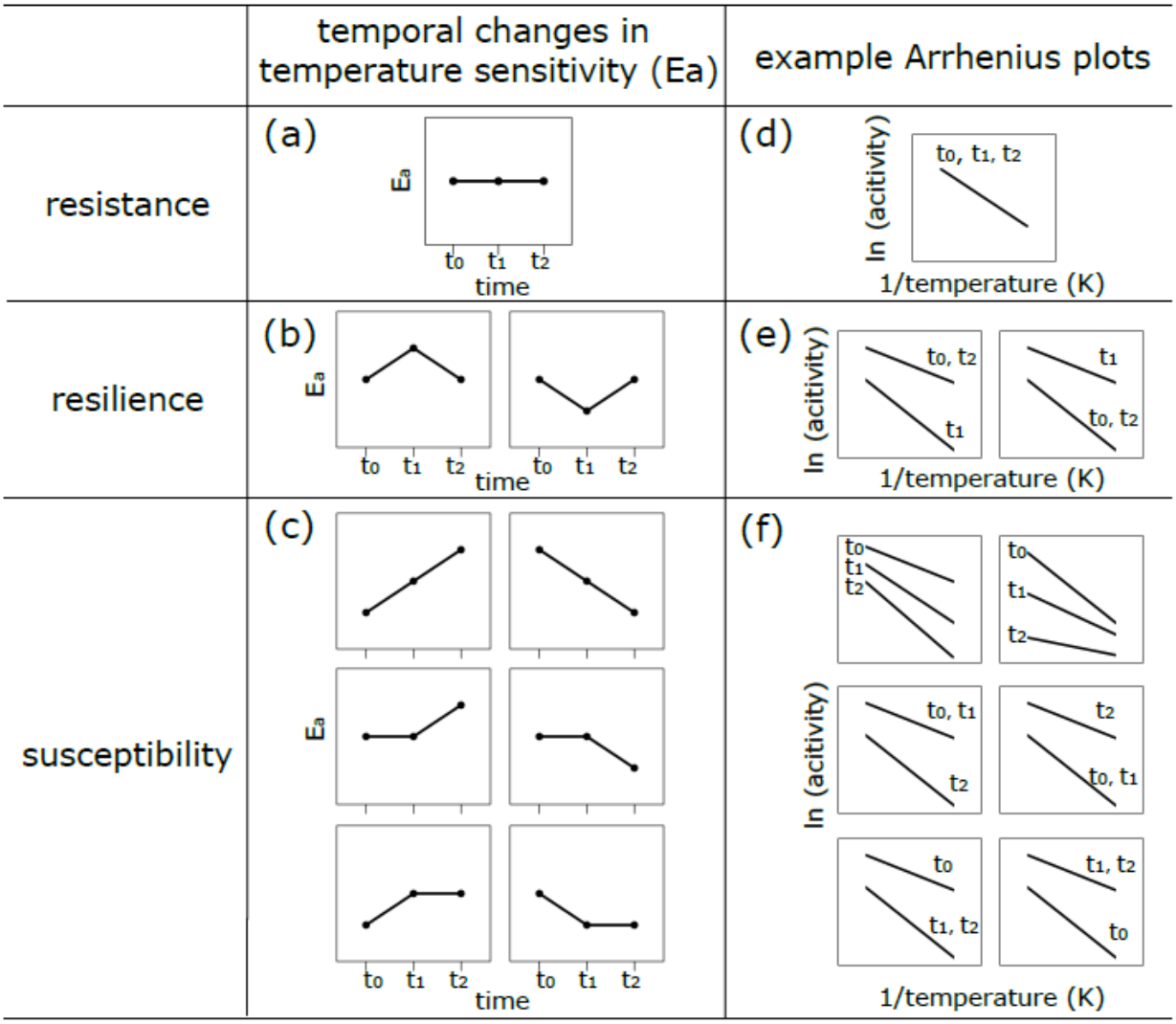

Figure 1. Three types of temporal responses of temperature sensitivity (resistance, resilience, and susceptibility) and their example Arrhenius plots. Temperature sensitivity (E_a) of process rates (second column) corresponds to the slope of the Arrhenius plot in the third column, where log transformed process rates are plotted against inverse temperature. As warming continues from t_0 to t_1 to t_2, temperature sensitivity can exhibit resistance (a), which can be detected by the constant slopes in the Arrhenius plots (b). When microbial communities show resilient temperature sensitivity (c), the slopes of initial and final time points (t_0 and t_2) are the same, while the slope of middle time point differs (t_1) in the Arrhenius plots (d). Microbial

communities can also exhibit susceptible temperature sensitivity (e), where the slopes of initial and final time points (t_0 and t_2) differ (f). In all cases, the y-intercepts of the Arrhenius plots do not influence temperature sensitivity of process rates.

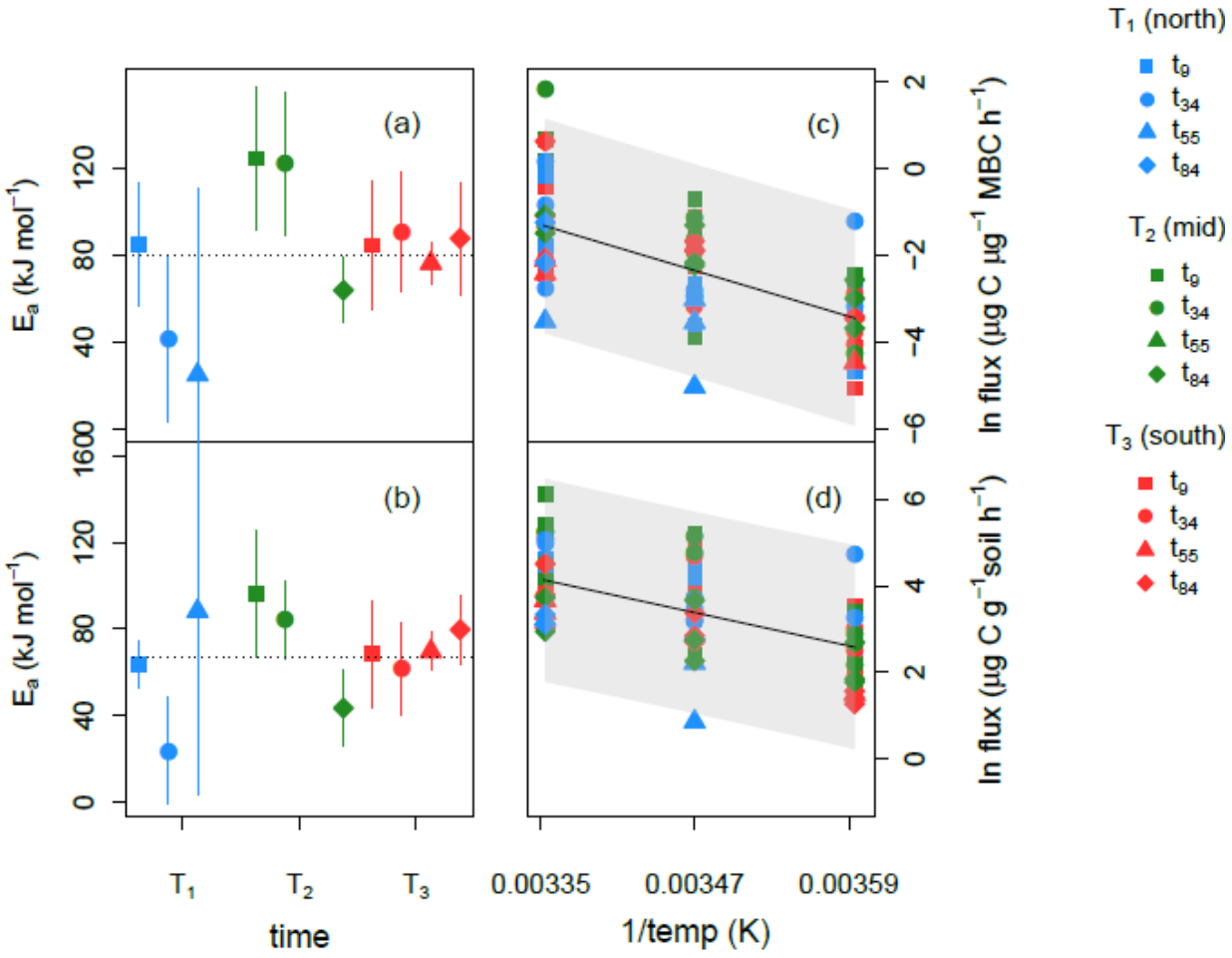

Figure 2. Temperature sensitivity (left) and the Arrhenius plot (right) for biomass-specific (upper) and soil mass-specific (lower) CO_2 respiration. Note that T_1-T_3 represents regions along the climate gradient with distinct temperature regime and t_9, t_{34}, t_{55}, and t_{84} indicate incubation time of day 9, 34, 55, and 84. Temperature sensitivity (E_a) was presented with ± 1SE across diverse timescales in left column. In the Arrhenius plot, a common regression line was overlaid on data, when there is no difference in temperature responses across time (thus, resistance).

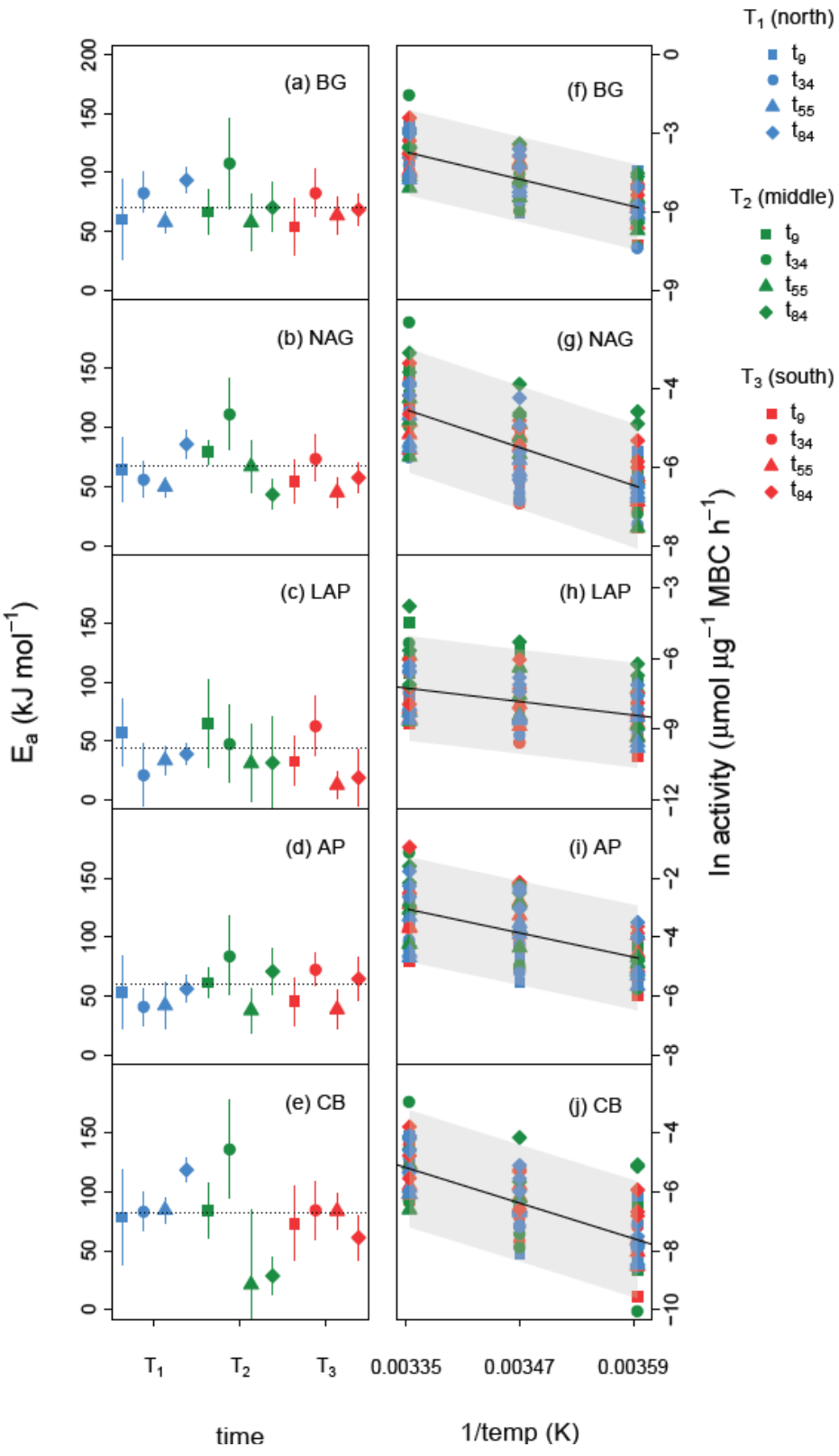
(a) BG
(b) NAG
(c) LAP
(d) AP
(e) CB
(f) BG
(g) NAG
(h) LAP
(i) AP
(j) CB
E_a (kJ mol^{-1})
ln activity (µmol µg^{-1} MBC h^{-1})
T_1 (north)
t_9
t_{34}
t_{55}
t_{84}
T_2 (middle)
t_9
t_{34}
t_{55}
t_{84}
T_3 (south)
t_9
t_{34}
t_{55}
t_{84}
T_1
T_2
T_3
time
0.00335
0.00347
0.00359
1/temp (K)

Figure 3. Temperature sensitivity (left) and the Arrhenius plot (right) for biomass-specific exo-enzyme activities (BG, β-glucosidase; NAG, N-acetyl-β-D-glucosaminidase; LAP, leucine amino peptidase; AP, acid phosphatase; CB, cellobiohydrolase). Note that T_1-T_3 represents regions along the climate gradient with distinct temperature regime and t_9, t_{34}, t_{55}, and t_{84} indicate incubation time of day 9, 34, 55, and 84. Temperature sensitivity (E_a) was presented with ± 1SE across diverse timescales in left column. In the Arrhenius plot, a common regression line was overlaid on data, when there is no difference in temperature responses across time (thus, resistance).

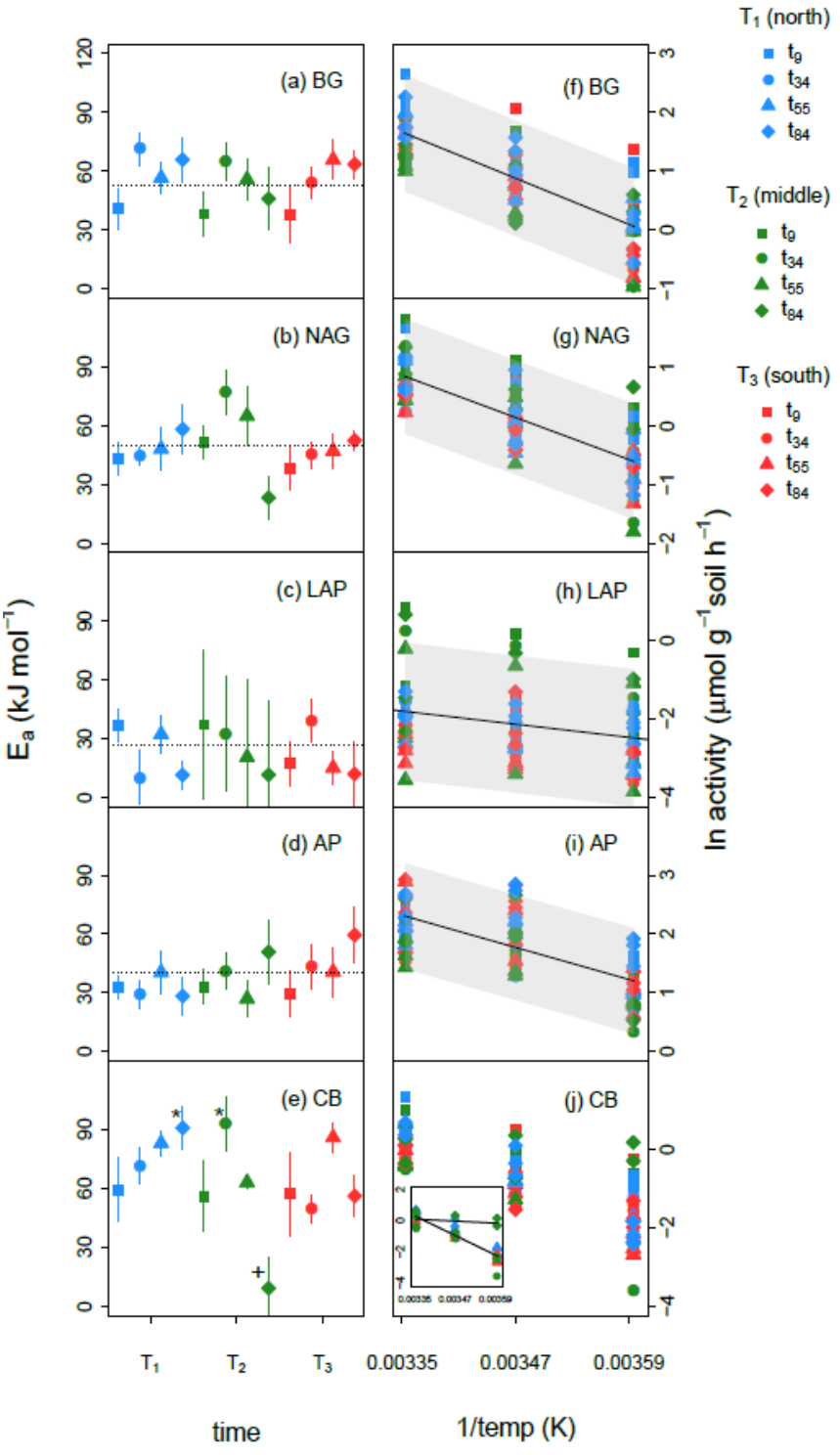
(a) BG
(b) NAG
(c) LAP
(d) AP
(e) CB
(f) BG
(g) NAG
(h) LAP
(i) AP
(j) CB
E_a (kJ mol^{-1})
ln activity (µmol g^{-1}soil h^{-1})
T_1 (north)
t_9
t_{34}
t_{55}
t_{84}
T_2 (middle)
t_9
t_{34}
t_{55}
t_{84}
T_3 (south)
t_9
t_{34}
t_{55}
t_{84}
T_1
T_2
T_3
time
0.00335
0.00347
0.00359
1/temp (K)

Figure 4. Temperature sensitivity (left) and the Arrhenius plot (right) for soil mass-specific exo-enzyme activities (BG, β-glucosidase; NAG, N-acetyl-β-D-glucosaminidase; LAP, leucine amino peptidase; AP, acid phosphatase; CB, cellobiohydrolase). Note that T_1-T_3 represents regions along the climate gradient with distinct temperature regime and t_9, t_{34}, t_{55}, and t_{84} indicate incubation time of day 9, 34, 55, and 84. Temperature sensitivity (E_a) was presented with ± 1SE across diverse timescales in left column. Different symbols (* and +) represent significantly different values at $p<0.05$. In the Arrhenius plot, a common regression line was overlaid on data, when there is no difference in temperature responses across time (thus, resistance). For CB, where significant differences in the slopes were found across time, we put insets to highlight the differences in the temperature responses.

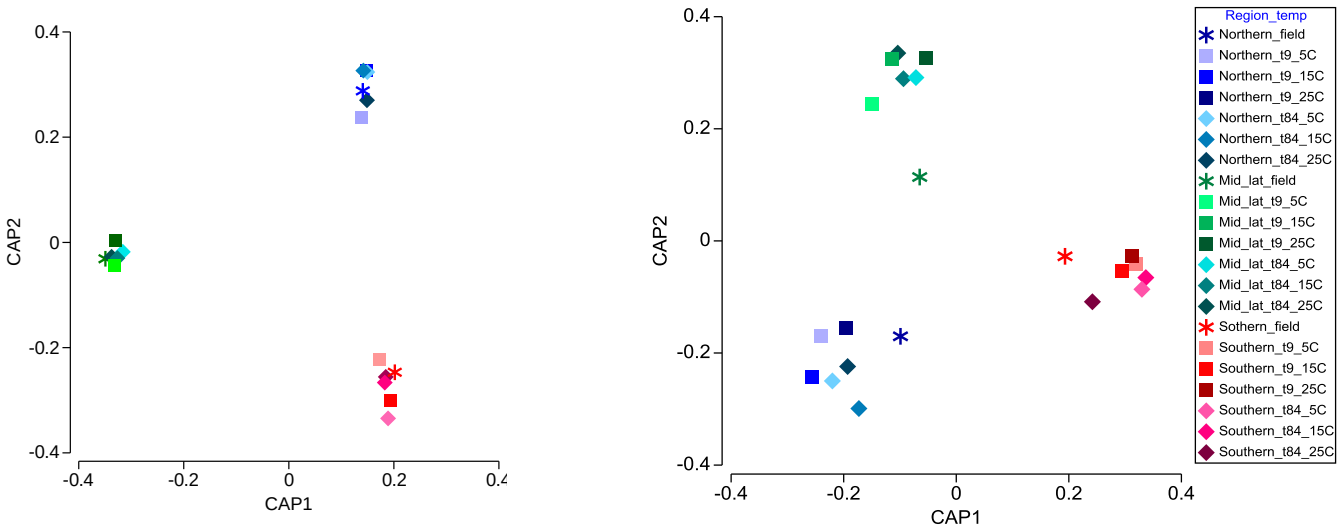

Figure 5. Canonical Analysis of Principal Coordinates (CAP) for bacterial community (a) and fungal community (b) based on unweighted UniFrac distance and Bray Curtis distance, respectively. Microbial community composition was assessed three times, one prior to the incubation (field condition) and two during the incubation for each region. Blue represents northern-most region (T_1), green for mid-latitude (T_2), and red for southern-most region (T_3). Stars for field condition, squares for incubation day 9 (t_9), and diamonds for incubation day 84 (t_{84}).

Supplementary information

1. Exo-enzyme assays

Each exo-enzyme was paired with fluorescence-tagged substrate to assess the rate of activities: 4-methylumbelliferyl beta-D-glucopyranoside (M3633, Sigma-aldrich), 4-methylumbelliferyl beta-D-cellobioside (M6018, Sigma-aldrich), 4-methylumbelliferyl N-acetyl-beta-D-glucosaminide (M2133, Sigma-aldrich), L-leucine-7-amino-4-methylcoumarin hydrochloride (L2800, Biosynth), and 4-methylumbelliferyl phosphate (M8883, Sigma-aldrich) as substrates for BG, CB, NAG, LAP, and AP, respectively. As a corresponding standard for correcting fluorescence, we used 4-methylumbelliferone (M1381, Sigma-aldrich) for BG, CB, NAG, and AP and 7-amino-4-methylcoumarin (M9891, Sigma-aldrich) for LAP. We prepared soil slurries by mixing 125 ml of 50 mM sodium acetate buffer at pH 4.5 (soil pH in NL-BELT) with 1 g of soil from each reconstructed soil core. In 96-well black plates, we mixed 200 µl of soil slurry with 50 µl of 400 µM substrate solution with corresponding soil control (50 µl of 50 mM sodium acetate buffer + 200 µl of soil slurry), quench control (50 µl of 10 uM standard), substrate control (50 ul of 400 µM substrate + 200 µl of 50 mM sodium acetate buffer), and standard (50 µl of 10uM standard + 200 ul of 50 mM sodium acetate buffer).

2. Sequencing microbial community composition

Amplicon PCR was performed with Q5® High Fidelity DNA Polymerase (New England BioLabs) on an Eppendorf MasterCycler Gradient thermocycler. For bacterial community composition, the hypervariable regions of the 16S rRNA gene from V3-V4 region was targeted using primers 341F and 805R (Herlemann *et al*. 2011) under the following conditions: initial

denaturation at 98°C for 3 min, then 22 cycles of 30s at 98°C, 30s at 55°C, and 30s at 72°C. The last step was 7 min at 72°C after which the samples were held at 4°C. For fungi, ITS2 region was PCR amplified with fungal-specific primers ITS1F and ITS4 (Manter & Vivanco 2007). We purified PCR products from both bacterial and fungal amplicons using the Agencourt Ampure XP-PCR purification system (Beckman Coulter). We generated dual indexed libraries from the amplicons using the Illumina Nextera® XT index kit and quantified the concentration of the PCR products with Qubit® dsDNA HS Assay Kit (Life Technologies) using Qubit® 2.0 Fluorometer. Following library preparation and pooling (multiplexed n=124), a paired-end 300 cycle sequence run was carried out on the libraries on an Illumina MiSeq sequencer (Illumina) at the Integrated Genomic Facility at Kansas State University.

3. Processing of Sequence Data.

The sequences were processed using the Quantitative Insights into Microbial Ecology (Qiime v1.9.0) pipeline (Caporaso *et al*. 2010) for bacterial and fungal sequence. The two index files produced by the MiSeq sequencer containing the i5 and i7 Nextera indexes were merged using the extract_barcodes.py script on Qiime, which resulted in the generation of a unique 16bp index for each sequenced sample. This unique 16bp indexes was then used for demultiplexing the fastq file containing the forward reads. The reads were demultiplexed to trim the barcode, primer and to remove low quality sequence reads less than 25 Phred score, truncate end sequence (end trimming) with low quality score and all sequences containing ambiguous bases. The resulting quality filtered sequence were then separated for bacterial and fungal communities and analyzed separately. Both bacterial and fungal sequences were clustered using open-reference OTU picking in Qiime which further denoised the sequences and removed singleton OTUs. In short,

sequences were clustered into operational taxonomic units (OTUs) using uclust (Edgar 2010) with 97% sequence identity threshold. Representative sequences from each OTU were aligned using PyNAST (Caporaso *et al*. 2010) and taxonomic identity was assigned using Greengenes 13_8 database and Unite database (Abarenkov *et al*. 2010) for bacteria and fungi, respectively. For bacteria, a total of 5589199 reads passed this QA/QC step encompassing 353345 OTUs. To compare all samples at equal sequencing depth, samples were normalized to the minimum number of sequences (i.e., 17597 reads/sample) by random subsampling (without replacement). For fungi, a total of 4008134 reads generated 53752 OTUs. The phylogenic diversity of abundant phyla (>0.1%) was visualized in a heatmap using R 'gplots' program.

4. community dissimilarity

To estimate sampling completeness and calculate the probability that randomly selected amplicon sequence from a sample has already been sequenced; good's coverage and rarefaction analysis was performed on the resulting OTU table. Rarefaction curves based on 97% similarity of sequence reached a plateau for most of the samples, suggesting that diversity of microbial community was captured in most of the samples. This was further confirmed by average 86±4 % Good's coverage indicating that these libraries represented the majority of bacterial and fungal sequence present in each sample. Community dissimilarity in each category was estimated with weighted and unweighted UniFrac distance for bacteria and Bray Curtis distance for fungi. The distance matrix was visualized by Canonical Analysis of Principal Coordinates (CAP) using the statistical software PRIMER 7 (version 7.0.5) and PERMANOVA+ add on (version 1.0.3)

References for SI

1. Herlemann, D.P., Labrenz, M., Jürgens, K., Bertilsson, S., Waniek, J.J. and Andersson, A.F. (2011). Transitions in bacterial communities along the 2000 km salinity gradient of the Baltic Sea. *The ISME*, 5, 1571-1579.

2. Manter, D.K. & Vivanco, J.M. (2007). Use of the ITS primers, ITS1F and ITS4, to characterize fungal abundance and diversity in mixed-template samples by qPCR and length heterogeneity analysis. *J. Microbiol. Methods*, 71, 7-14.

3. Caporaso, J.G., Kuczynski, J., Stombaugh, J., Bittinger, K., Bushman, F.D., Costello, E.K., *et al.* (2010). QIIME allows analysis of high-throughput community sequencing data. *Nat. Methods*, 7, 335-336.

4. Abarenkov, K., Henrik Nilsson, R., Larsson, K.H., Alexander, I.J., Eberhardt, U., Erland, S., *et al*. (2010). The UNITE database for molecular identification of fungi–recent updates and future perspectives. *New Phytologist*, 186, 281-285.

5. Edgar, R.C. (2010). Search and clustering orders of magnitude faster than BLAST, *Bioinformatics* 26, 2460-2461.

Table S1.

Table S1. Location and climate of the Newfoundland and Labrador Boreal Ecosystem Latitude Transect.

region	forest ID	latitude	longitude	closest weather station †	latitude	longitude	mean annual precipitation (mm)	mean annual PET ‡ (mm)	mean annual temperature (°C)
northern-most	Harry's Pond	53°35'N	56°53'W	Cartwright	53°42'N	57°02'W	1073.5	432.9	0.0
	Sheppard's Ridge	53°33'N	56°56'W						
	Muddy Pond	53°33'N	56°59'W						
mid-latitude	Hare Bay	51°15'N	56° 8'W	Main Brook	51°11'N	56°01'W	1223.9	489.1	2.0
	Tuckamore	51° 9'N	56° 0'W						
	Catch-A-Feeder	51° 5'N	56°12'W						
southern-most	Slug Hill	48° 0'N	58°54'W	Doyles	47°51'N	59°15'W	1504.6	608.1	5.2
	Maple Ridge	48° 0'N	58°55'W						
	O'Regans	47°53'N	59°10'W						

† Climate normal data between 1981 and 2000 were retrieved at the weather stations near the three replicated forests at each region (http://climate.weather.gc.ca/climate_normals/index_e.html).

‡ PET, potential evapotranspiration

Table S2. The most parsimonious model for biomass-specific CO_2 rates

```
Linear mixed model fit by REML
t-tests use  Satterthwaite approximations to degrees of freedom ['lmerMod']
Formula: LogSpecificFlux * (-0.008314) ~ InverseTemp + (1 | id)
   Data: CO2

REML criterion at convergence: -479.5

Scaled residuals:
    Min      1Q  Median      3Q     Max
-2.2742 -0.5766 -0.0401  0.4868  4.3135

Random effects:
 Groups   Name        Variance  Std.Dev.
 id       (Intercept) 1.129e-05 0.003360
 Residual             9.296e-05 0.009642
Number of obs: 76, groups:  id, 27

Fixed effects:
            Estimate Std. Error       df t value Pr(>|t|)
(Intercept) -0.23867    0.04587 22.52600  -5.203 3.01e-05 ***
InverseTemp 74.38942   13.22141 22.63200   5.626 1.06e-05 ***
---
Signif. codes:  0 ‘***’ 0.001 ‘**’ 0.01 ‘*’ 0.05 ‘.’ 0.1 ‘ ’ 1
```

Table S3. The most parsimonious model for soil mass-specific CO_2 rates

```
Linear mixed model fit by REML
t-tests use  Satterthwaite approximations to degrees of freedom ['lmerMod']
Formula: LogFlux * (-0.008314) ~ InverseTemp + (1 | id)
   Data: CO2

REML criterion at convergence: -499.5

Scaled residuals:
    Min      1Q  Median      3Q     Max
-1.8445 -0.6622 -0.0223  0.5757  5.3514

Random effects:
 Groups   Name        Variance  Std.Dev.
 id       (Intercept) 3.288e-18 1.813e-09
 Residual             9.310e-05 9.649e-03
Number of obs: 78, groups:  id, 27

Fixed effects:
             Estimate Std. Error       df t value Pr(>|t|)
(Intercept) -0.21283    0.03867 76.02000  -5.504 4.82e-07 ***
InverseTemp 53.22687   11.15883 76.02000   4.770 8.71e-06 ***
---
Signif. codes:  0 ‘***’ 0.001 ‘**’ 0.01 ‘*’ 0.05 ‘.’ 0.1 ‘ ’ 1
```

Table S4. The most parsimonious model for biomass-specific BG activities

```
Linear mixed model fit by REML
t-tests use  Satterthwaite approximations to degrees of freedom ['lmerMod']
Formula: LogSpecificActivity * (-0.008314) ~ InverseTemp + (1 | id)
   Data: BGdata

REML criterion at convergence: -744.8

Scaled residuals:
    Min      1Q  Median      3Q     Max
-2.75282 -0.77354  0.03755  0.85626  1.85026

Random effects:
 Groups   Name        Variance  Std.Dev.
 id       (Intercept) 0.000e+00 0.000000
 Residual             4.633e-05 0.006806
Number of obs: 105, groups:  id, 27

Fixed effects:
             Estimate Std. Error        df t value Pr(>|t|)
(Intercept)  -0.20419    0.02361 103.05000  -8.647 7.42e-14 ***
InverseTemp  70.27595    6.79543 103.05000  10.342  < 2e-16 ***
---
Signif. codes:  0 ‘***’ 0.001 ‘**’ 0.01 ‘*’ 0.05 ‘.’ 0.1 ‘ ’ 1
```

Table S5. The most parsimonious model for biomass-specific NAG activities

```
Linear mixed model fit by REML
t-tests use  Satterthwaite approximations to degrees of freedom ['lmerMod']
Formula: LogSpecificActivity * (-0.008314) ~ InverseTemp + (1 | id)
   Data: NAGdata

REML criterion at convergence: -747.4

Scaled residuals:
    Min      1Q  Median      3Q     Max
-2.79017 -0.71727 -0.03788  0.72639  1.86066

Random effects:
 Groups   Name        Variance  Std.Dev.
 id       (Intercept) 2.185e-06 0.001478
 Residual             4.021e-05 0.006341
Number of obs: 104, groups:  id, 27

Fixed effects:
            Estimate Std. Error       df t value Pr(>|t|)
(Intercept) -0.18550    0.02435 24.90900  -7.620 5.78e-08 ***
InverseTemp 66.66222    7.00794 24.91000   9.512 9.02e-10 ***
---
Signif. codes:  0 ‘***’ 0.001 ‘**’ 0.01 ‘*’ 0.05 ‘.’ 0.1 ‘ ’ 1
```

Table S6. The most parsimonious model for biomass-specific LAP activities

```
Linear mixed model fit by REML
t-tests use  Satterthwaite approximations to degrees of freedom ['lmerMod']
Formula: LogSpecificActivity * (-0.008314) ~ InverseTemp + (1 | id)
   Data: LAPdata

REML criterion at convergence: -671

Scaled residuals:
    Min      1Q  Median      3Q     Max
-2.0831 -0.6093  0.1159  0.6927  2.1155

Random effects:
 Groups   Name        Variance  Std.Dev.
 id       (Intercept) 3.177e-05 0.005636
 Residual             5.472e-05 0.007397
Number of obs: 101, groups:  id, 27

Fixed effects:
             Estimate Std. Error       df t value Pr(>|t|)
(Intercept) -0.07907    0.04637 24.43000  -1.705  0.10088
InverseTemp 41.51614   13.35029 24.44200   3.110  0.00471 **
---
Signif. codes:  0 ‘***’ 0.001 ‘**’ 0.01 ‘*’ 0.05 ‘.’ 0.1 ‘ ’ 1
```

Table S7. The most parsimonious model for biomass-specific AP activities

```
Linear mixed model fit by REML
t-tests use  Satterthwaite approximations to degrees of freedom ['lmerMod']
Formula: LogSpecificActivity * (-0.008314) ~ InverseTemp + (1 | id)
   Data: APdata

REML criterion at convergence: -729.3

Scaled residuals:
    Min      1Q  Median      3Q     Max
-2.3987 -0.7528  0.0657  0.6332  2.0236

Random effects:
 Groups   Name        Variance  Std.Dev.
 id       (Intercept) 0.000e+00 0.000000
 Residual             5.385e-05 0.007338
Number of obs: 105, groups:  id, 27

Fixed effects:
             Estimate Std. Error        df t value Pr(>|t|)
(Intercept)  -0.16414    0.02546 103.04000  -6.447 3.74e-09 ***
InverseTemp  56.56139    7.32640 103.04000   7.720 7.81e-12 ***
---
Signif. codes:  0 ‘***’ 0.001 ‘**’ 0.01 ‘*’ 0.05 ‘.’ 0.1 ‘ ’ 1
```

Table S8. The most parsimonious model for biomass-specific CB activities

```
Linear mixed model fit by REML
t-tests use  Satterthwaite approximations to degrees of freedom ['lmerMod']
Formula: LogSpecificActivity * (-0.008314) ~ InverseTemp + (1 | id)
   Data: CBdata

REML criterion at convergence: -654.8

Scaled residuals:
    Min      1Q  Median      3Q     Max
-2.51823 -0.69432  0.05411  0.74956  2.40686

Random effects:
 Groups   Name        Variance  Std.Dev.
 id       (Intercept) 0.000e+00 0.000000
 Residual             7.033e-05 0.008387
Number of obs: 98, groups:  id, 27

Fixed effects:
            Estimate Std. Error       df t value Pr(>|t|)
(Intercept) -0.23068    0.02998 96.03000  -7.695 1.25e-11 ***
InverseTemp 81.80714    8.63862 96.03000   9.470 2.00e-15 ***
---
Signif. codes:  0 ‘***’ 0.001 ‘**’ 0.01 ‘*’ 0.05 ‘.’ 0.1 ‘ ’ 1
```

Table S9. The most parsimonious model for soil mass-specific BG activities

```
Analysis of Variance Table of type III  with  Satterthwaite
approximation for degrees of freedom
                     Sum Sq    Mean Sq NumDF  DenDF F.value    Pr(>F)
InverseTemp          0.001285  0.001285     1 25.284 139.195  8.88E-12 ***
Sampling              0.00014  4.67E-05     3 74.635   5.06  0.003033 **
InverseTemp:Sampling 0.000156  5.19E-05     3  74.65  5.621  0.001575 **
---
Signif. codes:  0 ‘***’ 0.001 ‘**’ 0.01 ‘*’ 0.05 ‘.’ 0.1 ‘ ’ 1
```

```
Linear mixed model fit by REML
t-tests use  Satterthwaite approximations to degrees of freedom ['lmerMod']
Formula: LogActivity * (-0.008314) ~ InverseTemp * Sampling + (1 | id)
   Data: BGdata

REML criterion at convergence: -893.7

Scaled residuals:
    Min      1Q  Median      3Q     Max
-1.9305 -0.5961  0.1243  0.3749  3.5962

Random effects:
 Groups   Name        Variance  Std.Dev.
 id       (Intercept) 2.976e-06 0.001725
 Residual             9.235e-06 0.003039
Number of obs: 107, groups:  id, 27

Fixed effects:
                     Estimate Std. Error       df t value Pr(>|t|)
(Intercept)          -0.12305    0.02373 84.44000  -5.185 1.46e-06 ***
InverseTemp          32.34450    6.83148 84.44000   4.735 8.75e-06 ***
Sampling2            -0.10226    0.02919 74.32000  -3.504 0.000781 ***
Sampling3            -0.08624    0.02969 74.96000  -2.904 0.004831 **
Sampling4            -0.08692    0.02919 74.32000  -2.978 0.003917 **
InverseTemp:Sampling2 31.04807    8.40165 74.32000   3.695 0.000417 ***
InverseTemp:Sampling3 26.34966    8.55358 74.99000   3.081 0.002888 **
InverseTemp:Sampling4 26.16460    8.40165 74.32000   3.114 0.002619 **
---
Signif. codes:  0 ‘***’ 0.001 ‘**’ 0.01 ‘*’ 0.05 ‘.’ 0.1 ‘ ’ 1
```

Table S10. The most parsimonious model for soil mass-specific NAG activities

Analysis of Variance Table of type III with Satterthwaite approximation for degrees of freedom

	Sum Sq	Mean Sq	NumDF	DenDF	F.value	Pr(>F)	
InverseTemp	0.001995	0.001995	1	22.867	129.16	6.98E-11	***

Signif. codes: 0 ‘***’ 0.001 ‘**’ 0.01 ‘*’ 0.05 ‘.’ 0.1 ‘ ’ 1

```
Linear mixed model fit by REML
t-tests use  Satterthwaite approximations to degrees of freedom ['lmerMod']
Formula: LogActivity * (-0.008314) ~ InverseTemp + (1 | id)
   Data: NAGdata

REML criterion at convergence: -860.5

Scaled residuals:
    Min      1Q  Median      3Q     Max
-2.4018 -0.7042  0.1223  0.7409  2.3947

Random effects:
 Groups   Name        Variance  Std.Dev.
 id       (Intercept) 9.847e-07 0.0009923
 Residual             1.545e-05 0.0039302
Number of obs: 106, groups:  id, 27

Fixed effects:
            Estimate Std. Error       df t value Pr(>|t|)
(Intercept) -0.17296    0.01513 22.82400  -11.43 6.35e-11 ***
InverseTemp 49.51461    4.35688 22.86700   11.37 6.98e-11 ***
---
Signif. codes:  0 ‘***’ 0.001 ‘**’ 0.01 ‘*’ 0.05 ‘.’ 0.1 ‘ ’ 1
```

Table S11. The most parsimonious model for soil mass-specific LAP activities

```
Analysis of Variance Table of type III  with  Satterthwaite
approximation for degrees of freedom
                Sum Sq    Mean Sq NumDF   DenDF F.value  Pr(>F)
InverseTemp   6.61E-05   6.61E-05     1  25.221  3.6993 0.04579 *
---
Signif. codes:  0 ‘***’ 0.001 ‘**’ 0.01 ‘*’ 0.05 ‘.’ 0.1 ‘ ’ 1
```

```
Linear mixed model fit by REML
t-tests use  Satterthwaite approximations to degrees of freedom ['lmerMod']
Formula: LogActivity * (-0.008314) ~ InverseTemp + (1 | id)
   Data: LAPdata

REML criterion at convergence: -773

Scaled residuals:
    Min      1Q  Median      3Q     Max
-1.8418 -0.5805 -0.1354  0.6538  2.1748

Random effects:
 Groups   Name        Variance  Std.Dev.
 id       (Intercept) 3.578e-05 0.005982
 Residual             1.786e-05 0.004226
Number of obs: 103, groups:  id, 27

Fixed effects:
            Estimate Std. Error       df t value Pr(>|t|)
(Intercept) -0.06520    0.04321 25.20700  -1.509   0.1438
InverseTemp 23.92663   12.44002 25.22100   1.923   0.04579 *
---
Signif. codes:  0 ‘***’ 0.001 ‘**’ 0.01 ‘*’ 0.05 ‘.’ 0.1 ‘ ’ 1
```

Table S12. The most parsimonious model for soil mass-specific AP activities

Analysis of Variance Table of type III with Satterthwaite approximation for degrees of freedom

	Sum Sq	Mean Sq	NumDF	DenDF	F.value	Pr(>F)	
InverseTemp	0.000554	0.000554	1	25.245	56.205	7.06E-08	***

Signif. codes: 0 ‘***’ 0.001 ‘**’ 0.01 ‘*’ 0.05 ‘.’ 0.1 ‘ ’ 1

```
Linear mixed model fit by REML
t-tests use  Satterthwaite approximations to degrees of freedom ['lmerMod']
Formula: LogActivity * (-0.008314) ~ InverseTemp + (1 | id)
   Data: APdata

REML criterion at convergence: -897

Scaled residuals:
    Min      1Q  Median      3Q     Max
-2.2872 -0.7146  0.1025  0.7822  1.6829

Random effects:
 Groups   Name        Variance  Std.Dev.
 id       (Intercept) 4.170e-06 0.002042
 Residual             9.851e-06 0.003139
Number of obs: 107, groups:  id, 27

Fixed effects:
            Estimate Std. Error       df t value Pr(>|t|)
(Intercept) -0.14613    0.01754 25.23200  -8.330 1.04e-08 ***
InverseTemp 37.86466    5.05063 25.24600   7.497 7.06e-08 ***
---
Signif. codes:  0 ‘***’ 0.001 ‘**’ 0.01 ‘*’ 0.05 ‘.’ 0.1 ‘ ’ 1
```

Table S13. The most parsimonious model for soil mass-specific CB activities

Analysis of Variance Table of type III with Satterthwaite approximation for degrees of freedom

	Sum Sq	Mean Sq	NumDF	DenDF	F.value	Pr(>F)	
InverseTemp	0.002075	0.002075	1	32.305	139.034	3.04E-13	***
Region:Sampling	0.000432	3.93E-05	11	55.122	2.631	0.008929	**
InverseTemp:Region:Sampling	0.000453	4.12E-05	11	55.377	2.763	0.006301	**

Signif. codes: 0 ‘***’ 0.001 ‘**’ 0.01 ‘*’ 0.05 ‘.’ 0.1 ‘ ’ 1

```
Linear mixed model fit by REML
t-tests use  Satterthwaite approximations to degrees of freedom ['lmerMod']
Formula: LogActivity * (-0.008314) ~ InverseTemp + Region:Sampling + InverseT
emp:Region:Sampling +
    (1 | id)
   Data: CBdata

REML criterion at convergence: -797.5

Scaled residuals:
     Min       1Q   Median       3Q      Max
-2.24426 -0.49253 -0.07447  0.51083  1.95666

Random effects:
 Groups   Name        Variance  Std.Dev.
 id       (Intercept) 8.177e-07 0.0009042
 Residual             1.492e-05 0.0038631
Number of obs: 100, groups:  id, 27

Fixed effects:
                            Estimate Std. Error       df t value Pr(>|t|)
(Intercept)                -0.02975    0.05170 75.79000  -0.575 0.566689
InverseTemp                 8.60083   14.95491 75.80000   0.575 0.566915
RegionER:Sampling1         -0.17365    0.06965 75.67000  -2.493 0.014848
*
RegionGC:Sampling1         -0.16416    0.06965 75.67000  -2.357 0.021012
*
RegionSR:Sampling1         -0.16150    0.06801 57.37000  -2.375 0.020926
*
RegionER:Sampling2         -0.21251    0.06965 75.67000  -3.051 0.003143
**
RegionGC:Sampling2         -0.13922    0.07308 75.84000  -1.905 0.060564
.
RegionSR:Sampling2         -0.28082    0.06801 57.37000  -4.129 0.000119
***
RegionER:Sampling3         -0.25239    0.06965 75.67000  -3.624 0.000523
***
RegionGC:Sampling3         -0.25920    0.06965 75.67000  -3.721 0.000378
***
RegionSR:Sampling3         -0.06104    0.14152 72.20000  -0.431 0.667512
```

```
RegionER:Sampling4              -0.28033    0.06965 75.67000  -4.025 0.000134
***
RegionGC:Sampling4              -0.15783    0.06965 75.67000  -2.266 0.026308
*
InverseTemp:RegionER:Sampling1 50.64068   20.10300 75.68000   2.519 0.013877
*
InverseTemp:RegionGC:Sampling1 48.56297   20.10300 75.68000   2.416 0.018117
*
InverseTemp:RegionSR:Sampling1 47.46483   19.63111 57.52000   2.418 0.018803
*
InverseTemp:RegionER:Sampling2 63.02279   20.10300 75.68000   3.135 0.002447
**
InverseTemp:RegionGC:Sampling2 42.15824   21.13395 75.85000   1.995 0.049656
*
InverseTemp:RegionSR:Sampling2 84.11782   19.63111 57.52000   4.285 7.04e-05
***
InverseTemp:RegionER:Sampling3 74.37963   20.10300 75.68000   3.700 0.000407
***
InverseTemp:RegionGC:Sampling3 77.31452   20.10300 75.68000   3.846 0.000249
***
InverseTemp:RegionSR:Sampling3 20.62020   41.72545 72.37000   0.494 0.622671
InverseTemp:RegionER:Sampling4 82.28966   20.10300 75.68000   4.093 0.000105
***
InverseTemp:RegionGC:Sampling4 47.54319   20.10300 75.68000   2.365 0.020595
*
---
Signif. codes:  0 ‘***’ 0.001 ‘**’ 0.01 ‘*’ 0.05 ‘.’ 0.1 ‘ ’ 1
```

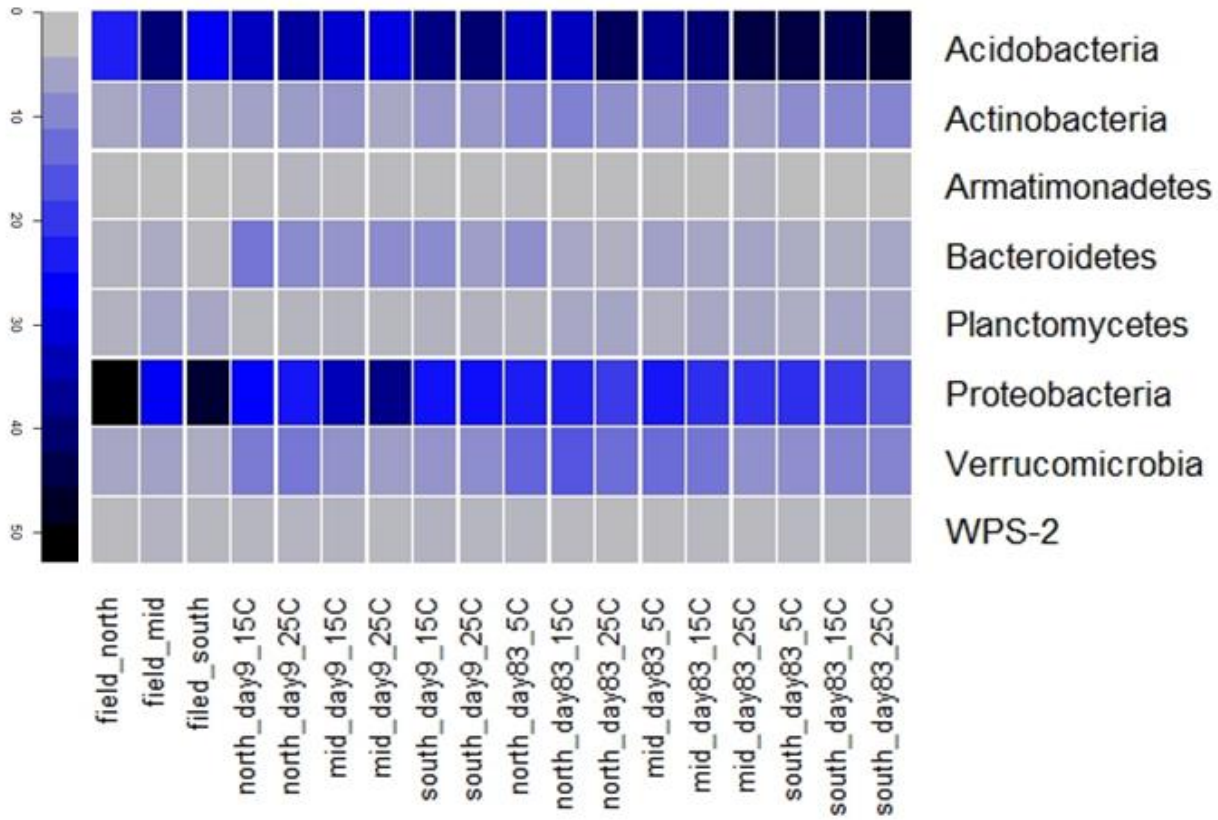

Figure S1. Heatmap distribution of dominant phyla (>0.1 % of total reads) for pooled replicate samples. The color intensity in each cell shows the percentage of phylum in the corresponding sample.

REFERENCES

1.Allison, S.D. & Martiny, J.B.H. (2008). Resistance, resilience, and redundancy in microbial communities. *Proc. Natl. Acad. Sci.*, 105, 11512–11519

2.Anderson, M.J. & Willis, T.J. (2003). Canonical Analysis of Principle Coordinates: A useful method of constrined ordination for ecology. *Ecology*, 84, 511–525

3.Baldrian, P., Šnajdr, J., Merhautová, V., Dobiášová, P., Cajthaml, T. & Valášková, V. (2013). Responses of the extracellular enzyme activities in hardwood forest to soil temperature and seasonality and the potential effects of climate change. *Soil Biol. Biochem.*, 56, 60–68

4.Bradford, M.A. (2013). Thermal adaptation of decomposer communities in warming soils. *Front. Microbiol.*, 4, 1–16

5.Bradford, M.A., Davies, C.A., Frey, S.D., Maddox, T.R., Melillo, J.M., Mohan, J.E., *et al.* (2008). Thermal adaptation of soil microbial respiration to elevated temperature. *Ecol. Lett.*, 11, 1316–1327

6.Bradford, M.A., Watts, B.W. & Davies, C.A. (2010). Thermal adaptation of heterotrophic soil respiration in laboratory microcosms. *Glob. Chang. Biol.*, 16, 1576–1588

7.Craine, J.M., Fierer, N., McLauchlan, K.K. & Elmore, A.J. (2013). Reduction of the temperature sensitivity of soil organic matter decomposition with sustained temperature increase. *Biogeochemistry*, 113, 359–368

8.Davidson, E.A. & Janssens, I.A. (2006). Temperature sensitivity of soil carbon decomposition and feedbacks to climate change. *Nature*, 440, 165–173

9.German, D.P., Marcelo, K.R.B., Stone, M.M. & Allison, S.D. (2012). The Michaelis–Menten kinetics of soil extracellular enzymes in response to temperature: a cross-latitudinal study. *Glob. Chang. Biol.*, 18, 1468–1479

10.Graham, E.B., Knelman, J.E., Schindlbacher, A., Siciliano, S., Breulmann, M., Yannarell, A., *et al.* (2016). Microbes as engines of ecosystem function: When does community structure enhance predictions of ecosystem processes? *Front. Microbiol.*, 7, 214

11.Hartley, I.P., Heinemeyer, A. & Ineson, P. (2007). Effects of three years of soil warming and shading on the rate of soil respiration : substrate availability and not thermal acclimation mediates observed response. *Glob. Chang. Biol.*, 13, 1761–1770

12.Heskel, M.A., O'Sullivan, O.S., Reich, P.B., Tjoelker, M.G., Weerasinghe, L.K., Penillard, A., *et al.* (2016). Convergence in the temperature response of leaf respiration across biomes and plant functional types. *Proc. Natl. Acad. Sci.*, 113, 3832–3837

13.Jing, X., Wang, Y., Chung, H., Mi, Z., Wang, S., Zeng, H., *et al.* (2014). No temperature acclimation of soil extracellular enzymes to experimental warming in an alpine grassland ecosystem on the Tibetan Plateau. *Biogeochemistry*, 117, 39–54

14.Joergensen, R.G., Brookes, P.C. & Jenkinson, D.S. (1990). Survival of the soil microbial biomass at elevated temperatures. *Soil Biol. Biochem.*, 22, 1129–1136

15.Khalili, B., Nourbakhsh, F., Nili, N., Khademi, H. & Sharifnabi, B. (2011). Diversity of soil cellulase isoenzymes is associated with soil cellulase kinetic and thermodynamic parameters. *Soil Biol. Biochem.*, 43, 1639–1648

16.Kirschbaum, M.U.F. (2004). Soil respiration under prolonged soil warming: are rate reductions caused by acclimation or substrate loss? *Glob. Chang. Biol.*, 10, 1870–1877

17.Knorr, W., Prentice, I.C., House, J.I. & Holland, E.A. (2005). Long-term sensitivity of soil carbon turnover to warming. *Nature*, 433, 298–301

18.Laganière, J., Podrebarac, F., Billings, S.A., Edwards, K.A. & Ziegler, S.E. (2015). A warmer climate reduces the bioreactivity of isolated boreal forest soil horizons without increasing the temperature sensitivity of respiratory CO2 loss. *Soil Biol. Biochem.*, 84, 177–188

19.Lehmeier, C.A., Ballantyne IV, F., Min, K. & Billings, S.A. (2016). Temperature-mediated

changes in microbial carbon use efficiency and 13C discrimination. *Biogeosciences*, 13, 3319–3329

20.Lehmeier, C.A., Min, K., Niehues, N.D., Ballantyne IV, F. & Billings, S.A. (2013). Temperature-mediated changes of exoenzyme-substrate reaction rates and their consequences for the carbon to nitrogen flow ratio of liberated resources. *Soil Biol. Biochem.*, 57, 374–382

21.Luo, Y., Wan, S., Hui, D. & Wallace, L.L. (2001). Acclimatization of soil respiration to warming in a tall grass prairie. *Nature*, 413, 622–625

22.Machmuller, M.B., Mohan, J.E., Minucci, J.M., Phillips, C.A. & Wurzburger, N. (2016). Season , but not experimental warming , affects the activity and temperature sensitivity of extracellular enzymes. *Biogeochemistry*, 131, 255–265

23.Malcolm, G.M., López-Gutiérrez, J.C. & Koide, R.T. (2009). Little evidence for respiratory acclimation by microbial communities to short-term shifts in temperature in red pine (Pinus resinosa) litter. *Glob. Chang. Biol.*, 15, 2485–2492

24.Min, K., Lehmeier, C.A., Ballantyne, F., Tatarko, A. & Billings, S.A. (2014). Differential effects of pH on temperature sensitivity of organic carbon and nitrogen decay. *Soil Biol. Biochem.*, 76, 193–200

25.Pimm, S. (1984). The complexity and stability of ecosystems. *Nature*, 307, 321–326

26.Podrebarac, F.A., Laganière, J., Billings, S.A., Edwards, K.A. & Ziegler, S.E. (2016). Soils isolated during incubation underestimate temperature sensitivity of respiration and its response to climate history. *Soil Biol. Biochem.*, 93, 60–68

27.Robinson, J.M., O'Neill, T.A., Ryburn, J., Liang, L.L., Arcus, V.L. & Schipper, L.A. (2017). Rapid laboratory measurement of the temperature dependence of soil respiration and application to seasonal changes in three diverse soils. *Biogeochemistry*, 133, 101–112

28.Romero-olivares, A.L., Allison, S.D. & Treseder, K.K. (2017). Soil Biology & Biochemistry Soil microbes and their response to experimental warming over time : A meta-analysis of fi eld studies. *Soil Biol. Biochem.*, 107, 32–40

29.Rustad, L.E., Campbell, J.L., Marion, G.M., Norby, R.J., Mitchell, M.J., Hartley, A.E., *et al.* (2001). A meta-analysis of the response of soil respiration, net nitrogen mineralization, and aboveground plant growth to experimental ecosystem warming. *Oecologia*, 126, 543–562

30.Schimel, D.S. (1995). Terrestrial ecosystems and the carbon cycle, 77–91

31.Schimel, J.P. & Schaeffer, S.M. (2012). Microbial control over carbon cycling in soil. *Front. Microbiol.*, 3, 348

32.Schindlbacher, A., Schnecker, J., Takriti, M., Borken, W. & Wanek, W. (2015). Microbial

physiology and soil CO 2 efflux after 9 years of soil warming in a temperate forest – no indications for thermal adaptations. *Glob. Chang. Biol.*, 21, 4265–4277

33.Shade, A., Peter, H., Allison, S.D., Baho, D.L., Berga, M., Bürgmann, H., *et al.* (2012). Fundamentals of microbial community resistance and resilience. *Front. Microbiol.*, 3, 1–19

34.Sierra, C.A. (2011). Temperature sensitivity of organic matter decomposition in the Arrhenius equation: some theoretical considerations. *Biogeochemistry*, 108, 1–15

35.Sihi, D., Gerber, S., Inglett, P.W. & Inglett, K.S. (2016). Comparing models of microbial-substrate interactions and their response to warming. *Biogeosciences*, 13, 1733–1752

36.Subke, J., Inglima, I. & Francesca Cotrufo, M. (2006). Trends and methodological impacts in soil CO2 efflux partitioning: a metaanalytical review. *Glob. Chang. Biol.*, 12, 921–943

37.Vance, E.D., Brookes, P.C. & Jenkinson, D.S. (1987). An extraction method for measuring soil microbial biomass C. *Soil Biol. Biochem.*, 19

38.Wallenstein, M. & Hall, E. (2012). A trait-based framework for predicting when and where microbial adaptation to climate change will affect ecosystem functioning. *Biogeochemistry*, 109, 35–47

39.Wallenstein, M.D., McMahon, S.K. & Schimel, J.P. (2009). Seasonal variation in enzyme activities and temperature sensitivities in Arctic tundra soils. *Glob. Chang. Biol.*, 15, 1631–1639

40.Ziegler, S.E., Benner, R., Billings, S.A., Edwards, K., Philben, M., Zhu, X., *et al.* (2017). Climate warming can accelerate carbon fluxes without changing soil carbon stocks. *Front. Earth Sci.*, 5, 2

41.Zogg, G.P., Zak, D.R., Ringelberg, D.B., White, D.C., MacDonald, N.W. & Pregitzer, K.S. (1997). Compositional and functional shifts in microbial communities due to soil warming. *Soil Sci. Soc. Am. J.*, 61, 475

GENERAL CONCLUSIONS

The overarching goal of my dissertation was to better understand the effects of temperature on microbial decomposition of organic matter and resultant CO_2 losses from soils with little concern of confounding factors. To obtain a mechanistic understanding of microbial temperature responses, I investigated microbial activities at various scales, ranging from isolated microbial exo-enzymes, to populations in controlled laboratory environments, and to communities in their natural environments.

In chapter 1, I excluded soil microorganisms and quantified temperature responses of exo-enzyme activities at varying pH. I did this by employing commercially available, purified exo-enzymes similar to those exuded by microbes and assessing their activities at various temperature and pH. I found that different exo-enzymes responsible for microbial C and N acquisition exhibit distinct responses to temperature and pH, and that these differences may lead to changes in the relative abundance of C and N available to microorganisms. At acidic conditions, warming can induce relatively higher availability of C compared to N, while at alkaline conditions N becomes more available than C with increasing temperature. These findings on pure molecular responses of exo-enzyme activities have direct ecological implications for predicting microbial behavior in a warmer world. Because microorganisms exude exo-enzymes to obtain nutrients from soil organic matter, when relative availability of C becomes greater with warming at acidic conditions, microorganisms may become less efficient at using C and respire more CO_2. In contrast, at alkaline conditions, it is likely that N losses from

soils via volatilization and ammonification increase with warming due to relatively greater N availability.

In chapter 2, I assessed the effects of temperature and substrate availability on C pools and fluxes of populations of *Pseudomonas fluorescens*, a Gram-negative bacterium common to many soils and aquatic systems. I coupled a chemostat (a continuous liquid culture of microorganisms) with a stable C isotope analyzer to determine microbial C transformations at steady state. I demonstrated that temperature and substrate availability interactively influence microbial C transformations: temperature increased biomass-C specific respiration rates and C uptake affinity at lower C availability, but did not influence those parameters at higher C availability. Carbon use efficiency (CUE) decreased non-linearly with increasing temperature. The non-linear, negative relationship between CUE and temperature was more pronounced under lower C availability than under relatively high C availability. Microbial discrimination against ^{13}C-containing cellobiose during C uptake was influenced by temperature and C availability, while discrimination during respiration was only influenced by C availability. This work highlights that microorganisms can adjust the flow of C into and out of their biomass in response to temperature and substrate availability. These microbial responses assessed at biomass-C specific rates can help improve parameterization of microbially-explicit Earth-system models.

In the final chapter, I investigated how temperature responses of microbial exo-enzyme activities and respiration vary across diverse timescales in boreal forest soils. Microbial process rates were quantified at soil mass-specific and biomass-specific rates. Also, I assessed microbial community composition across time along their functions. For exo-enzymes BGase, NAGase, acid

phosphase, leucine aminopeptidase, cellobiohydrolase, and respiration, temperature sensitivities as biomass-specific rates exhibited resistance across diverse timescales, indicating consistent relative enhancements in reaction rates with increasing temperature. In contrast, temperature sensitivities as soil mass-specific rates showed resilience (changes in temperature sensitivity and returns back to its original value) for NAGase and cellobiohydrolase, and resistance for BGase, acid phosphatase, leucine aminopeptidase, and respiration. Microbial community composition varied across diverse timescales regardless of their functional responses. Resistant temperature sensitivity at a biomass-specific rate despite varying community composition implies a generalizable relationship between temperature and microbial physiology at a fundamental level. The results also highlight how the unit of observation can drive the diverse narratives describing microbial temperature responses in literature.

Taken together, my dissertation demonstrates how temperature influences soil microbial function and structure at scales ranging from exo-enzymes to populations and to communities. However, even though reductionist approaches I employed here are helpful to tease apart microbial temperature responses from confounding factor-driven dynamics, it still needs to be explored how microbial temperature responses at different scales can be combined to reflect their functions in soils. Therefore, we need to find a way to reconcile microbial dynamics at diverse scales to advance our understanding of microbial feedbacks to climate change.